

<b>The Analysis of Beam-Column Joint Reinforced with Cross Bars according to SK SK T-15-1991-03</b>	<b>01</b>
<i>Zardan Araby, Samsul Rizal, Abdullah, Mochammad Afifuddin</i>	
<b>The Low Flow Assessment of Padma River in Bangladesh</b>	<b>11</b>
<i>Md. Abu Sayed, Aysha Akter</i>	
<b>Finite Element Modelling of Prestressed Concrete Piles in Soft Soils: Case Study Northern Jakarta, Indonesia</b>	<b>21</b>
<i>Aswin Lim, Varian Harwin Batistuta, Yiska Vivian Christensen Wijaya</i>	
<b>The Building Information Modelling (BIM)-Based System Framework to Implement Circular Economy in Construction Waste Management</b>	<b>31</b>
<i>Tantri N. Handayani, Kartika N. R. Putri, Nurul A. Istiqomah, Veerasak Likhitruangsilp</i>	
<b>Seismic Ground Response Analysis of Input Earthquake Motion and Site Amplification Factor at KUET</b>	<b>45</b>
<i>Sonia Akter</i>	
<b>The Use of Drop-Structure to Increase the Dissolved Oxygen Level along the Cibarani Channel</b>	<b>55</b>
<i>Jonathan Wijaya, Doddi Yudianto, Finna Fitriana</i>	
<b>Optimizing The Functional Performance of Road Network using Vulnerability Assessment to Cope with Unforeseen Road Incidents</b>	<b>67</b>
<i>Mukhammad Rizka Fahmi Amrozi, Raihan Pasha Isheka</i>	
<b>Analysis of Spatial Distribution of The Drought Hazard Index (DHI) by Integration AHP-GIS-Remote Sensing in Gorontalo Regency</b>	<b>81</b>
<i>Muhammad Ramdhan Oliy, Aleks Oliy, Ririn Pakaya</i>	
<b>Organic Removal Treatment Using Microbubble Generator (MBG) in Eutrophic Disorder Condition</b>	<b>97</b>
<i>Tri Yulianti, Sri Puji Saraswati, Johan Syafri Mahathir Ahmad, Wiratni Budhijanto</i>	
<b>Factors Affecting Cyclist Behaviours in the Special Region of Yogyakarta</b>	<b>105</b>
<i>Danang Febrianto, Dewanti, Imam Muthohar</i>	

# JOURNAL OF THE CIVIL ENGINEERING FORUM

Vol. 8 No. 1 (January 2022)

ISSN 2089-5631 (print)  
ISSN 2549-5925 (online)

## Editor in Chief

Ali Awaludin Structural Engineering, Universitas Gadjah Mada, Indonesia

## Associate (Handling) Editors

Djoko Legono Hydraulics Laboratory, Universitas Gadjah Mada, Indonesia  
Lindung Zalbuin Mase Geotechnical Engineering, Universitas Bengkulu, Indonesia  
Ni Nyoman Nepi Marleni Environmental Engineering, Universitas Gadjah Mada, Indonesia  
Suprpto Siswosukarto Structural Engineering, Universitas Gadjah Mada, Indonesia  
Suryani Eka Wijaya Department of Transportation, West Nusa Tenggara Province, Indonesia

## International Editorial Boards

Dimuth Navaratna Environmental Engineering, Victoria University, Australia  
Edwin K. Kanda Hydraulics and Water Resources Engineering, Masinde Muliro University of Science and Technology, Kenya  
Endita Prima Ari Pratiwi Hydraulic and Water Resources Engineering, Rice husk biochar application, Water Saving Irrigation, Universitas Gadjah Mada, Indonesia  
Evi Anggraheni Civil Engineering Department, Universitas Indonesia, Indonesia  
Fikri Faris Geo-technics/Soil Mechanics Engineering, Universitas Gadjah Mada, Indonesia  
Frank Dehn Structural Engineering, Karlsruhe Institute of Technology, Germany  
G M Sadiqul Islam Structural Engineering, Professor, Department of Civil Engineering, Chittagong University of Engineering and Technology (CUET), Bangladesh  
Imam Muthohar Transportation Laboratory, Universitas Gadjah Mada, Indonesia  
Othman Jaafar Hydraulics and Water Resources Engineering, Universiti Kebangsaan Malaysia, Malaysia  
Rini Kusumawardani Geotechnical Engineering, Universitas Negeri Semarang, Indonesia  
Sugianto, S. Associate Professor in Transport Planning, Policies and Travel Behavior Analysis. Department of Civil Engineering. Universitas Syiah Kuala, Indonesia  
Teerapong Senjutichai Structural Engineering, Chulalongkorn University, Thailand  
Tri Joko Wahyu Adi Construction Management, Institut Teknologi Sepuluh Nopember, Indonesia  
Yutaka Gonda Erosion Control Engineering, Faculty of Agriculture, Niigata University, Japan  
Benazir Coastal Engineering, Universitas Gadjah Mada

## Ethics Advisory Board

Istadi Universitas Diponegoro, Indonesia  
Nyoman Suwartha Universitas Indonesia, Indonesia  
Radianta Triatmadja Universitas Gadjah Mada, Indonesia

## Assistant Editors

Guntur Triatmaja Universitas Gadjah Mada, Indonesia  
Urwatul Wusqo Universitas Gadjah Mada, Indonesia  
Afaf Nadiyah Rifa Protomo Universitas Gadjah Mada, Indonesia  
Davina Daudina Universitas Gadjah Mada, Indonesia

## Web Administrator

Idham Muhammad Irfani Universitas Gadjah Mada, Indonesia

## Administration

Shinta Wardani Universitas Gadjah Mada, Indonesia

Journal of the Civil Engineering Forum (JCEF) is a four-monthly journal on Civil Engineering and Environmental related sciences. The JCEF is publish and disseminate research in the fields of structural engineering, geotechnical engineering, water resources engineering, environmental engineering, transportation engineering, and construction management, with particular emphasis on disaster risk reduction including socio-engineering approach for the countermeasures. JCEF publishes four categories of paper, i.e. Research Articles, Technical Notes, Editorial Notes, and Review Articles between 6 - 12 pages per paper, 6 - 10 papers per issue, reviewed by selected peer-reviewers. Currently, the JCEF is indexed by the Google Scholar (January 2016), Indonesia One Search (January 2016), DOAJ (September 2017), Crossref (December 2017), GARUDA (December 2017), WorldCat (December 2017), SINTA (July 2018).

# The Analysis of Beam-Column Joint Reinforced with Cross Bars according to SK SNI T-15-1991-03 on Cyclic Loads

Zardan Araby<sup>\*1</sup>, Samsul Rizal<sup>2</sup>, Abdullah<sup>3</sup>, Mochammad Afifuddin<sup>3</sup>

<sup>1</sup>Doctoral Program, Faculty of Engineering, Postgraduate Program, Faculty of Engineering, Syiah Kuala University  
Jalan Teuku Nyak Arief No. 441, Kopelma Darussalam, Syiah Kuala, Banda Aceh 23111, Indonesia

<sup>2</sup>Department of Mechanical Engineering, Faculty of Engineering, Syiah Kuala University  
Jalan Teuku Nyak Arief No. 441, Kopelma Darussalam, Syiah Kuala, Banda Aceh, 23111, Indonesia

<sup>3</sup>Department of Civil Engineering, Faculty of Engineering, Syiah Kuala University  
Jalan Teuku Nyak Arief No. 441, Kopelma Darussalam, Syiah Kuala, Banda Aceh, 23111, Indonesia

\*Corresponding authors: [zardan\\_araby@unsyiah.ac.id](mailto:zardan_araby@unsyiah.ac.id)

SUBMITTED 21 May 2021 REVISED 22 July 2021 ACCEPTED 14 August 2021

**ABSTRACT** The primary structural component supporting the other structural loads in a building is the beam-column joint. It is considered a critical area of a building which needs to be accurately designed to ensure energy is dissipated properly during the occurrence of an earthquake. Beam-column joint has the ability to offer a proper structure required to transform cyclic loads in the inelastic region but also has a direct impact on the components connected to it during the occurrence of any failure. This is one of the reasons the beam-column connection needs to be designed carefully. Therefore, this study focused on designing a beam-column joint with reinforcement according to SK SNI T-15-1991 in order to withstand cyclic loads. The test specimen used was observed to have a concrete compressive strength of 19.17 MPa while the dimension of the beam was 120 x 30 x 40 cm and the column was 30 x 30 x 200 cm, having 8Ø13.4 mm bars with 310.03 MPa yield strength ( $f_y$ ) as well as Ø9.8-100 mm stirrup reinforcement with ( $f_y$ ) 374.59 MPa. The test was initiated through the provision of 0.75 mm, 1.5 mm, 3 mm, 6 mm, 12 mm, 24 mm monotonic cyclic loads at the end of the beam up to the moment the specimen cracked. A maximum load of 68.35 kN for the compression and 49.92 kN for the tension was required to attain the cyclic load capacity. The maximum load was attained at 50.98 mm displacement. Furthermore, beam-column with 23.93 mm displacement caused a reduction in capacity. Meanwhile, the load at 24 mm produced the cycle's highest dissipation energy of 13.25 but this can be increased through the addition of stirrups to provide stiffness in the joint. The stiffness value was also observed to have increased after the structural repairs.

**KEYWORDS** Beam-Column Joint; Cyclic Load; Ductility; Monotonic Loading; Building Structure.

© The Author(s) 2022. This article is distributed under a Creative Commons Attribution-ShareAlike 4.0 International license.

## 1 INTRODUCTION

Indonesia is a country located between three tectonic plates and this increases its vulnerability to natural disasters, specifically earthquakes. Therefore, the buildings in the country require to be earthquake-resistant to prevent any damage during these disasters. This means the beam-column joint also needs to be designed to sustain the building and provide higher strength capability for the other structural components during earthquake occurrence to avoid damages. Therefore, the purpose of this study was to determine the ability of building structures constructed using

reinforced beam-column joint according to SK SNI T-15-1991 to withstand cyclic loads.

Previous studies only analyzed the behavior of columns and beams subjected to cyclic loading under ductile conditions and discovered that there are no repairs which conducted on these elements without destroying their structure. Moreover, Abdullah & Takiguchi (2003) examined the behavior and strength of concrete columns reinforced with ferrocement using 6 columns covered with square ferrocement as the test specimen. The result showed that the use of ferrocement along the column was able to increase ductility significantly. Soebandono *et al.*

(2011) also showed the improvement made by the ferrocement jacketing method using exterior beams with cyclic loads up to the level of damage caused to the ultimate load. Furthermore, Venkatesan & Ilangoan (2016) also evaluated the ability of retrofitting techniques to strengthen beam-column joints.

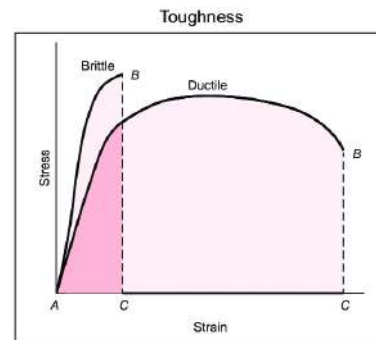
Literature studies involve reviewing several books, standardization documents such as SK SNI T-15-1991, and the findings of previous study in order to obtain information required to complete a particular study. This method was applied in this study while data were also collected from the laboratory tests conducted in the Construction and Building Materials Laboratory in Syiah Kuala University. The findings are expected to be applied to old buildings constructed using the SK SNI T-15-1991 standard and which are experiencing damages in their joints to provide the best method to repair these buildings without destroying them.

### 1.1 Ductility

Rodrigues *et al.* (2010) showed that ductility detailing is very important during the design process of new and existing buildings. Meanwhile, one important topic which was not referenced in the current situation is the impact of the masonry infill panels on the structural response and this has the ability to cause a brittle failure, even in structural design with a higher ductility degree.

According to Elghazouli (2017), ductility is the capability to resist large deformations of a structure beyond its yield point without causing any lead on the fracture. In earthquake engineering, the term is normally used to define a building's capability to endure large lateral displacements imposed by ground shaking. Some of the advantages of a ductile-reinforced concrete structure include: (1) the ability to resist overloads, reversals of the load, and the differential foundations settlement caused by the impact and secondary stresses in the ground, (2) provision of enough time for the occupants to vacate the structure by indicating large

deformations before the final collapse, and (3) the ductility property of the material allows the absorption of dynamic loads, thereby reducing the failure risk during an earthquake (Raghucharan & Prasad, 2015). Ductility has also been defined as the ability of a structure or sub-structure to hold the response provided by a dominant inelastic structure in carrying a load to prevent it from collapsing.



Toughness = the ability to absorb energy up to fracture  
= the total area under the strain-stress curve up to fracture

Figure 1. Typical stress versus strain curves for brittle and ductile materials

Source: (Sudha *et al.*, 2015)

Mathematically, the ductility value ( $\mu$ ) of a structure is defined as the ratio between the structure deformation parameter ( $\delta_u$ ) and the deformation at the time of the first meeting in the structure under review ( $\delta_y$ ). Figure 1 shows the common deformation parameters include curvature, rotational angle, strain, and displacement. Moreover, the amount of ductility is usually represented as a displacement ductility factor  $\mu$  which was calculated using the Equation (1).

$$\mu = \frac{\delta_u}{\delta_y} \quad (1)$$

### 1.2 Design Planning for Beams-Column Shear Reinforcement According to SK-SNI-T15-1991

Design planning, according to Schodek (1998), uses the ultimate strength design method and this involves planning the cross-section of the structure by considering the condition of the inelastic strain when it reaches its boundary conditions (the condition of the stable structure before collapse). In this plan, the workload was multiplied by a load factor called the factor load

and this was further used to plan the structural dimensions to ensure a smaller size of collapsed cross-section compared to the actual collapse strength. It is also important to note that the strength at the time of collapse is normally called a strong ultimate limit while the load that is occurring, is known as an ultimate load. Moreover, the strength of the cross-sectional plane is usually calculated by multiplying the nominal/theoretical strength with a capacity factor.

### 1.2.1 Beam Shear Reinforcement Design

According to SK-SNI-T15-1991-03 (1991), shear reinforcement is designed to prevent failure in shear, increase beam ductility, and subsequently reduce the likelihood of sudden failure. The ability of the concrete produced with shear-resisting structural components to withstand shear forces can be calculated using the Equation (2).

$$V_c = \left(\frac{1}{6} \sqrt{f_c'}\right) \cdot b_w \cdot d \quad (2)$$

The multiplier limit and  $V_c$  can be calculated as describe in Equation (3).

$$V_c \leq \left(0.30 \sqrt{f_c'}\right) \cdot b_w \cdot d \quad (3)$$

The shear strength provided by the shear stress can be using the Equation (4) and (5).

$$V_s \leq \frac{A_v \cdot f_y \cdot d}{s} \quad (4)$$

$$V_s \leq 0.66 \sqrt{f_c'} \cdot b_w \cdot d \quad (5)$$

The basics of shear reinforcement planning are as described in Equation (6), (7), and (8).

$$V_u \leq \phi V_n \quad (6)$$

$$V_n = V_c + V_s \quad (7)$$

$$V_u \leq \phi (V_c + V_s) \quad (8)$$

The distance of the shear reinforcement can be calculated as describes in Equation (9) and (10).

For vertical cross bar

$$S_{req} = \frac{A_v \cdot f_y \cdot d}{V_s} \quad (9)$$

For horizontal cross bar

$$S_{req} = (1.414) \frac{A_v \cdot f_y \cdot d}{V_s} \quad (10)$$

Where  $V_c$  is the nominal shear strength,  $f_c'$  is the compressive strength of concrete (MPa),  $b_w$  is the beam width (mm),  $d$  is the distance from the outer compression part to the center of gravity of the longitudinal tension reinforcement and it is expected not to be less than  $0.80h$  for practical elements (mm),  $A_v$  is the area of shear reinforcement in the range  $s$  or area of vertical shear reinforcement perpendicular to the tensile flexural reinforcement in a region with a distance  $s$  in the component for the high bending structure ( $\text{mm}^2$ ),  $V_u$  is the shear force with a factor on the cross-section,  $V_n$  is nominal shear strength,  $V_s$  is nominal shear strength provided by shear reinforcement,  $f_y$  is yield point (MPa), and  $s$  is transversal reinforcement spacing measured along the longitudinal axis of the structural member (mm).

### 1.2.2 Column Shear Reinforcement Plan

Schodek (1998) showed that the spacing of the stirrup reinforcement is not more than 16 times the length of the reinforcement base lengthwise, 48 times the diameter of the stirrup reinforcement, and the smallest dimension of the column. Moreover, the stirrup bar is required to be installed and arranged to ensure the angles do not bend at a value greater than  $135^\circ$  while the minimum shear reinforcement diameter is usually 10 mm.

### 1.2.3 Bond Requirement

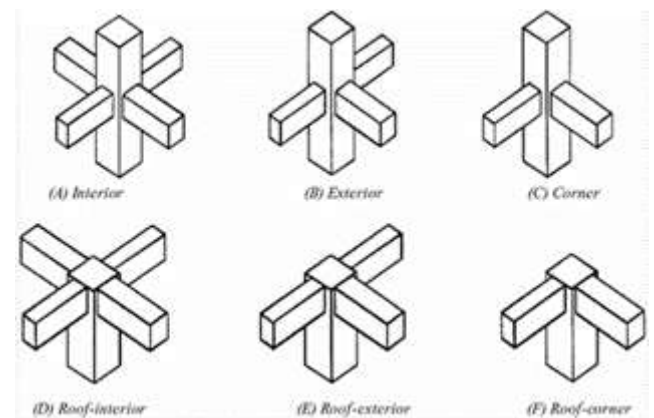


Figure 2. Beam-Column Joint Connection Types  
Source: (Elmasry et al., 2017)

Flexural forces in beams and columns cause tension or compressive forces on the longitudinal reinforcement through the joint. Moreover, the magnitude of the tensile force at the plastic joint is transmitted through bonds. It is important to note that the types of connection or bond between columns and beams can be described as indicated in Figure 2.

#### 1.2.4 Beam-Column Joint Failure

The first crack of the beam-column joint usually occurs when the concrete has exceeded its maximum tensile strain due to loading and this usually reduces the concrete tensile and shear strength to zero, thereby allowing the longitudinal and stirrup reinforcement to take over the concrete's ability to withstand tensile and shear forces. Therefore, the failure pattern of the beam-column connection is presented in the Figure 3.

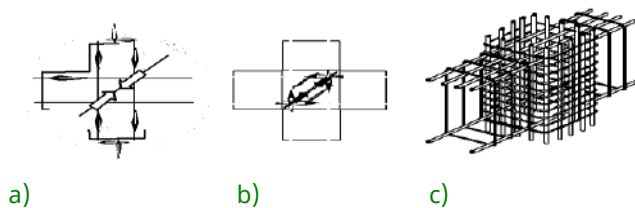


Figure 3. Beam-Column Connections Pattern: a). Forces to Joint, b). Crack on Joint, c). Shear Reinforcement Joint Source: (Wang and Salmon, 1991)

Figure 3 shows that the initial crack pattern in the concrete beam-column joint specimen starts with hair fracture in the joint followed by the shear crack attacking the joint. This has the tendency of causing damage in the joint, thereby leading to its structural failure. Therefore, it is necessary to have appropriate restraints in the joint area of the connection.

## 2 STUDY METHOD

### 2.2 Details of Beam-Column Joint Specimen

The specimens tested were reinforced concrete beams and columns designed based on SK SNI T-15-1991 with the dimension of the column designed to be 300 x 300 x 2000 mm while the beam was 300 x 400 x 1200 mm. Moreover, the cyclic load capacity testing required reinforced concrete column joints and this led to the use of

8Ø14 mm primary reinforcement and Ø10-100 mm stirrup as indicated in the detailed beam-column joint shape presented in Figure 4.

### 2.3 The Process of Making and Maintaining Specimens

The maximum aggregate used was 19.1 mm in diameter as indicated by the physical property tests conducted on filter analysis, specific gravity, volume weight, and water absorption. The process involved connecting the test object to an iron plate measuring 300 x 300 x 15 mm which was fastened to the frame beam and other supporting loads with bolts. The assembled specimens were placed on the three cylindrical formworks prepared for casting to ensure quality. Moreover, during the process of casting, fresh concrete was poured into the formwork and vibrated to ensure it is evenly distributed and solid. After 24 hours of casting, the formwork was opened and treated with wet burlap up to the moment the concrete was 28 days old.

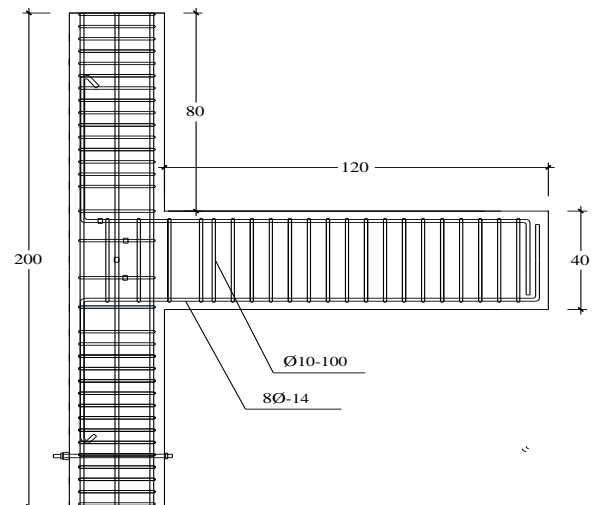


Figure 4. Specimen Shape

### 2.4 Procedure of Beam-Column Joint Test Objects

The test was conducted on the 28 days old test specimens using both the beam-column and cylindrical specimens with the focus on the compressive strength of the load which is part of the cyclic load capacity. Moreover, the surface of the cylindrical specimen was painted white before the test and placed on the grid to ensure a clearer crack pattern after which it was firmly installed on the frame beam. A two-way steel plate was attached to the surface of the beam

connected to a bolt while the plate to the load cell was fastened as the desired cyclic load was provided. It is also important to note that the load was applied horizontally on the end of the beam through the hydraulic jack connected to the load cell and transferred to the beam-column specimen. Furthermore, the load provided was controlled by reading the dial in the data logger to determine the cycle and associated crack patterns. The load was provided continuously up to the moment the specimen was destroyed. A transducer was also installed to measure the deflection in the lateral direction on the side of the beam. These configurations and procedures are presented in the test kits series and specimen installation on steel frames presented in the Figure 5.

A Portable Data Logger was used to measure the strain in the beam-column joint connected to the strain gauge. It was discovered that the loading value also stopped when the load stopped

increasing and this is associated with the inability of the specimens to receive more loads, thereby leading to cracking and failure. The crack development pattern observed on the image of the column is related to the load provided over time as indicated in the Figure 6.

### 2.5 Data Processing

The data obtained from the cyclic load test of reinforced beam-column joints include the beam-column joint crack pattern, beam-column joint cyclic load capacity, concrete strain and displacement, primary reinforcement strain in the stirrups, and the beam-column joint area were processed. The results presented in the form of tables and graphs showed the capacity of the beam-column joint under cyclic load and it was discovered that the repair efforts can be planned for the joint without having to knock down the building in case of insufficient capacity or occurrence of any damage.

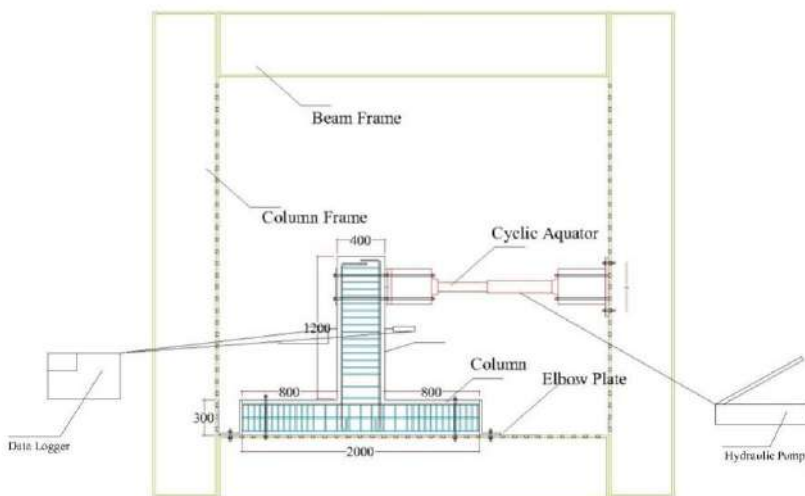


Figure 5. Set-Up for the Beam-Column Joint Test



Figure 6. Load Cycle Pattern

### 3 RESULTS AND DISCUSSION

#### 3.2 Cyclic Load

The maximum load achieved by the beam-column joint specimen was found to be 68.35 kN, the compressive load was discovered to have occurred at 24 mm displacement, and the tensile load was recorded to be 49.92 kN as presented in the graph of the cyclic load placed on the test object at 24 mm, 12 mm, 6 mm, 3 mm, 1.5 mm, and 0.75 mm. Figure 6 shows that the load continues to increase as the displacement increased, and the joint area was observed to have broken and cracked at the maximum conditions, thereby leading to a reduction of the load during the displacement. Moreover, the beam-column joint specimens showed a relatively horizontal crack pattern on the pedestal as indicated in Figures 7 and 8.



Figure 7. Crack Pattern of the Compressive Load (-), 24 mm

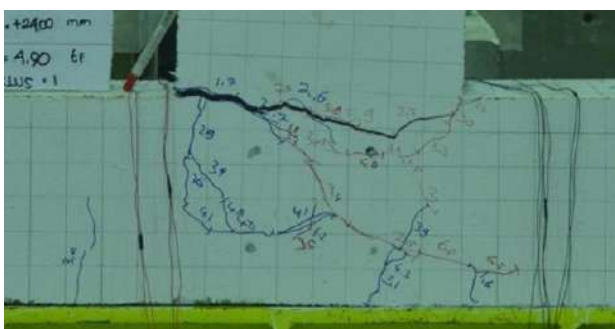


Figure 8. Crack Pattern of the Tensile Load (+), 24 mm

#### 3.3 Monotonic Loading

The cracking discovered to be occurring continuously and widening in the beam-column joint was due to monotonic loading. The most significant crack in the connected beams became wider as the load increased, and the different

kinds of patterns observed due to the monotonic loading are indicated in the Figure 9.

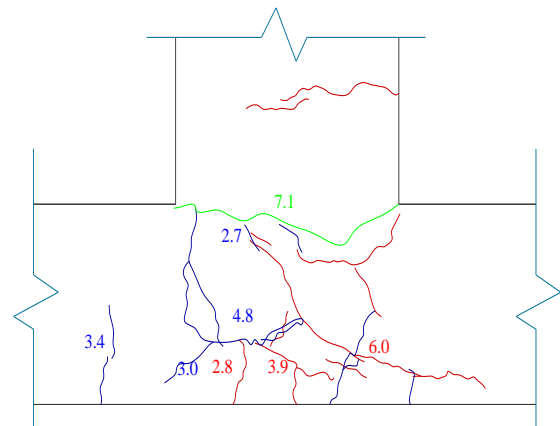


Figure 9. Monotonic Loading Crack Patterns

Larger cracks were observed to have occurred at the connection point of the beam-column. This was associated with the sliding capacity of the column beam and the reinforcement provided for the connection through the stirrup which led to a reduction in the flexural capacity and serves as the weak point.

#### 3.4 Load and Lateral Displacement of the Beams and Columns Specimens

The load and displacement relationship graphs were obtained from the results of the cyclic lateral test conducted on the joint. The maximum lateral displacement value was found to be 50.98 mm which was recorded from the LVDT 1 located at the middle of the beam's left side. Moreover, the graph of the structural behavior towards the cyclic load is presented in Figure 10.

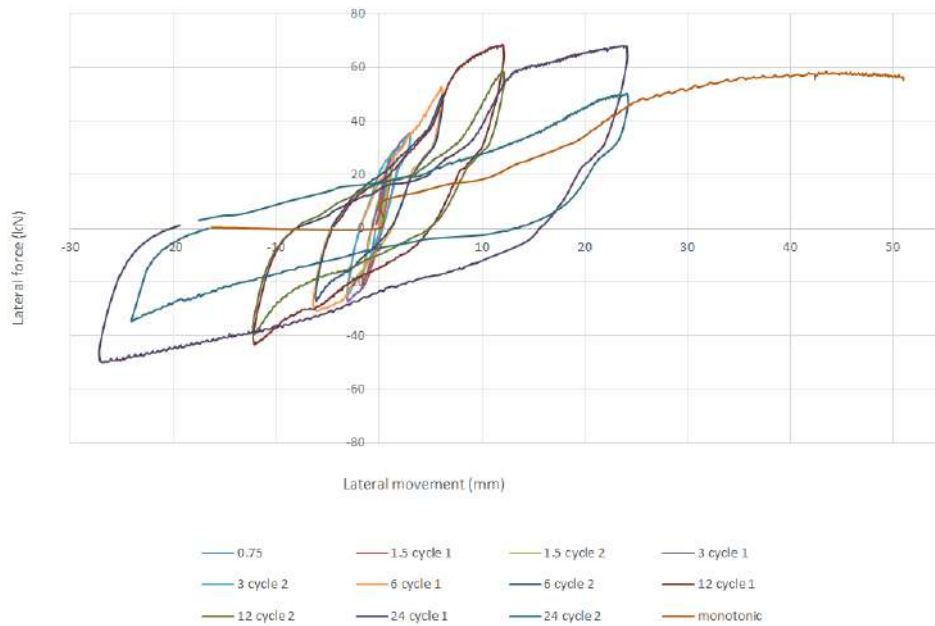


Figure 10. Hysterical Curves of Structural Behavior Against Cyclic Load

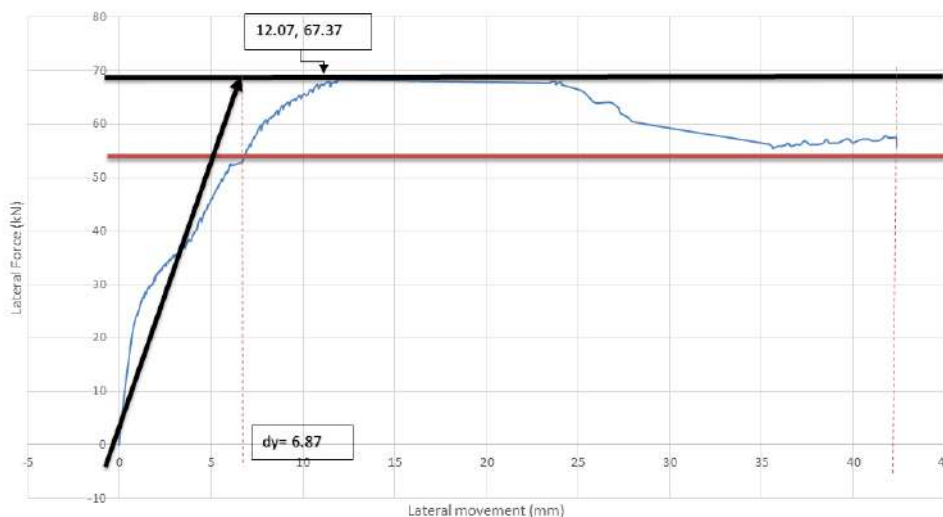


Figure 11. Graph of load and displacement envelopes

### 3.5 Structural Ductility

Structural ductility was obtained from the graph of envelope load and displacement as shown in Figure 11. It was used to determine the ability of the whole structure or a structural member to resist large deformations after exceeding the yield point without having any fracture. The term is normally used in earthquake engineering

to designate the capacity of a building to resist large lateral displacements imposed by ground movement. The load envelope and displacement graph can be seen in Figure 11. The graph showed the ultimate displacement ( $d_u$ ) was obtained at 50.99 mm, the yield displacement ( $d_y$ ) value was 6.87 mm, and the ductility values of the test objects are presented in the Table 1.

Table 1. Ductility Value on the Specimens

Specimen	Max. Displacement $d_{maks}$ (mm)	Ultimate Displacement $d_u$ (mm)	Yield Displacement $d_y$ (mm)	Ductility $d_u/d_y$
SNI91	50.99	50.99	12.07	4.22

#### 4 CONCLUSIONS AND REKOMENDATION

The seismic design focuses on the resilience of a framework, which serves as the main structure, to resist lateral forces using some structural elements such as beams and columns. This means there is a need for the connection between the elements to be ductile until they reach their load capacity. Therefore, this study discovered that the capacity of cyclic load value increased by the beam-column joint area of the reinforcement of stirrup replenishment. A maximum load of 68.35 kN for the compression and 49.92 kN for the tension was required to attain the cyclic load capacity. The maximum load was attained at 50.98 mm displacement.

Furthermore, beam-column with 0.09 secant stiffness and 23.93 mm displacement caused a reduction in capacity. Meanwhile, the load at 24 mm produced the cycle's highest dissipation energy of 13.25 but this can be increased through the addition of stirrups to provide stiffness in the joint. The stiffness value was also observed to have increased after the structural repairs.

Hence, it is important to increase the load capacity that can be carried by SNI 1991 test objects through structural repairs as indicated in the background information and problem formulated in the introductory section of this study. Some types of structural repair materials observed to be efficient and can be used as an easy alternative were discovered in this study. Cyclic load is a repetitive loading such as the exertion of regular repetitive pressure on a part which sometimes causes fatigue fractures. Therefore, it is possible to conduct a refinement effort through treatments such as reinforcement or additive materials. This study is recommended to be further developed by analyzing the treatment of beam-column joints based on the reinforcement channel length for failed

specimens. In this regard, there is a need to repair the damaged part of the beam-column joints and to ensure proper application of the data obtained from these studies in order to provide better results.

#### DISCLAIMER

The authors declare no conflict of interest.

#### AVAILABILITY OF DATA AND MATERIALS

All data are available from the authors.

#### AUTHOR CONTRIBUTION STATEMENTS

Zardan A conducted data testing in the laboratory and processed the test results data. Samsul R observed and supervised the data processing process. Abdullah A and Affifuddin helped supervise the testing in the laboratory. All authors took a substantial contribution in discussing the result and drafting the manuscript.

#### ACKNOWLEDGEMENT

We thank Maulana, Jovan, Rizki and Delfian and Laboratory of Construction and Building Materials assistants in Civil Engineering at Syiah Kuala University for their assistance in laboratory testing and data processing.

#### REFERENCES

- Abdullah & Takiguchi, K., 2003. An Investigation Into The Behavior and Strength of Reinforced Concrete Columns Strengthened With Ferrocement Jackets. *Cement and Concrete Composites*, 25 , pp. 233-242.
- Departemen Pekerjaan Umum RI, 1991. *Standar SK SNI T-15-1991-03, Tata Cara Penghitungan Struktur Beton untuk Bangunan Gedung*. Bandung: LPMB Departemen Pekerjaan Umum RI.

Elghazouli, A.Y., 2017. *Seismic design of buildings to Eurocode 8*. Boca Raton: CRC Press/Taylor & Francis Group.

Elmasry, M.I., Abdelkader, A.M., & Elkordy, E.A., 2017. *An Analytical Study of Improving Beam-Column Joints Behavior Under Earthquakes, South Sinai: GeoMEast 2017*.

Raghucharan, M. & Prasad, D., 2015. How to Make Concrete More Ductile - A State of Art, *International Journal of Engineering and Technical Study (IJETR)*, 3(5), 2321-0869.

Rodrigues, H., Varum, H., & Costa, A., 2010. Simplified Macro-Model for Infill Masonry Panels, *Journal Earthquake Engineering*, 14(3), pp. 390–416.

Schodek, D.L., 1998. *Struktur*. Terjemahan Bambang Suryoatmono. Bandung: Refika Aditama.

Soebandono, B., Triwiyono, A., & Muslikh, 2011. Perbaikan Balok Beton Bertulang dengan Metode Jacketing dengan Bahan Ferosemen Akibat Beban Siklik pada Beban Ultimit, *Jurnal Ilmiah Semesta*, 1(2), pp. 166-176.

Sudha, Kuncham & Sadiku, Rotimi & Jayaramudu, Tippabattini & K.Sudhakar, & Moropeng, Mapula, 2015. Chapter-16 “Mechanism of toughening in nanostructured polymer blends.. 10.1016/B978-0-323-39408-6.00015-7.

Venkatesan, B. & Ilangovan, R., 2016. Structural Behaviour of Beam Column Joint Retrofitted with Ferrocement Laminates, *International Journal of Advanced Engineering Technology*, VII, pp.1272-1280.

Wang, C. K. & Salmon, C.G., 1991. *Desain Beton Bertulang*. Jilid I, Jakarta : Erlangga.

[This page is intentionally left blank]

## The Low Flow Assessment of Padma River in Bangladesh

Md. Abu Sayed, A. Akter\*

Department of Civil Engineering, Chittagong University of Engineering & Technology (CUET), Chittagong 4349, BANGLADESH  
Parhatoli, Raozan, Chittagong – 4349, Bangladesh

\*Corresponding authors: [aysha\\_akter@cueta.ac.bd](mailto:aysha_akter@cueta.ac.bd)

SUBMITTED 13 May 2021 REVISED 9 September 2021 ACCEPTED 19 September 2021

**ABSTRACT** Low flow or Environmental Flow (EF) assessment is vital to ensure the river and ecosystem remain healthy. Both natural and human interventions might alter a river. Therefore, this study presents EF requirements of the famous Hilsa breeding center in the Padma River, Bangladesh, by applying the Hydrologic Engineering Centers River Analysis System (HEC-RAS) for discharge and water surface levels simulations at different stations. The frequency analysis of 20 years of historical data, spanning 2000-2019, used the Log-Pearson Type III (LP-III) distribution method, while the one-dimensional unsteady flow simulation was performed for the last 10 years (i.e., 2012-2019). Subsequently, the HEC-RAS simulated water level values reasonably correlated with the field observations at four stations, namely Baruria Transit, Mawa, Tarpasha, Sureswar, with Coefficient of determination  $R^2=0.86, 0.83, 0.92,$  and  $0.74,$  alongside simulated minimum water surface levels of 1.57 m, 0.37 m, 0.30 m, and 0.27 m, respectively. Also, the Baruria Transit and Mawa had simulated flows that reasonably correlated with the field observations at  $R^2=0.70$  and  $0.61,$  with a simulated minimum flow of  $3849.51 \text{ m}^3/\text{s}$  and  $3789.14 \text{ m}^3/\text{s},$  respectively. The minimum flow according to the frequency analysis was  $4017 \text{ m}^3/\text{s}, 3685 \text{ m}^3/\text{s}, 3449 \text{ m}^3/\text{s}, 3229 \text{ m}^3/\text{s},$  and  $3113 \text{ m}^3/\text{s}$  at Baruria Transit and  $3304 \text{ m}^3/\text{s}, 2781 \text{ m}^3/\text{s}, 2438 \text{ m}^3/\text{s}, 2141 \text{ m}^3/\text{s}, 1992 \text{ m}^3/\text{s}$  at Mawa station in 5, 10, 20, 50 and 100 years return periods, respectively. This study overlooked to report the ongoing investigations into the water quality issues. Thus, this study is expected to guide the required EF quantity towards a healthy Hilsha fish habitat and surface water source for drinking purposes in this studied river. The stated method is also applicable to other similar rivers around the world.

**KEYWORDS** Environmental Flow; HEC-RAS; Log-Pearson Type-III; Hilsha Breeding, Return Period.

© The Author(s) 2022. This article is distributed under a Creative Commons Attribution-ShareAlike 4.0 International license.

### 1 INTRODUCTION

The harm to the entire ecosystem caused by 'low flow' below a certain level of a stream can be addressed and resolved by Environmental Flow (EF) assessments. Thus, EF describes the required quantity, quality, and timing of water flow to sustain the river ecosystem and maintain stakeholders' livelihood. In the late 1940s EF assessment methodologies were initiated in the United States of America, while the implementation occurred later in the 1970s. Besides the USA, methods for developing and implementing Environmental Flow Assessment (EFA) were executed around the 1980s or later. Generally, EFAs deal with the minimum flow required in any river flow regime without negative impacts on the river's ecosystem. Tharme (2003) found that most developed or advanced countries, particularly Australia and South Africa, were concerned with the development and application of EFAs. Based on

the global literature on EFAs, Tharme (2003) recorded 207 different EFA methodologies used within 44 countries (Pusey and Arthington, 1991; Pusey *et al.*, 1993; and Arthington & Zalucki, 1998). Meanwhile, many EFA methods have been applied in Australia and occasionally modified based on the circumstances.

In Bangladesh, the applied EFA methods are mostly the Indicator of Hydraulic Alteration (IHA), Building Block Method (BBM), Mean Annual Flow (MAF), Flow Duration Curve (FDC), Range of Variability Approach (RVA), and the Tennant or Montana Method. Akter (2010) used the Indicator of Hydraulic Alteration (IHA) for analyzing hydrologic data and used RVA and BBM to assess the EF of the Ganges River after the construction of Farakka Barrage. The study also employed the Building Block Method (BBM) to estimate the fisheries and ecological demand, Sundarban's requirement, flushing flow, and

morphological equilibrium (Akter, 2010). Jahid (2016) used the Flow Duration Exceedance Percentile (FDEP) Method for Kobadak River, while Akter and Ali (2012) used the Building Block Methodology (BBM) and Log-Pearson Type III (LPIII) for the Halada River. In addition, the MAF, FDC, and Constant Yield (CY) method were utilized for the Gorai and Turag Rivers (Moly *et al.*, 2015; Rahman *et al.*, 2013), while the Tennant, FDC, and Range of Variability Approach (RVA) methods were used for the Teesta River (Mullick *et al.*, 2010). The Tennant or Montana Method, Flow Duration Curve (FDC) Analysis, Aquatic Base Flow, and RVA methods have also been applied on the North-West Zone of Bangladesh (Rahman *et al.*, 2019). These techniques are often carried out on wetland, riparian vegetation, geomorphology, channel morphology, aquatic vibrates, freshwater, estuarine areas, water quality, and water-dependent wildlife. Hence, increasing awareness is necessary to continue the smooth ecological process, provide better services to the community, and maintain biodiversity (Smakhtin *et al.*, 2004). There is currently no single method that can provide the solutions for all the EFA needs and requirements (Saha, 2007). However, “minimum low flow” is the key term to assess the EF of a regime, which is generally complex due to a shortage of flow monitoring data (Akter and Tanim, 2018). Hydraulic modeling also serves as a solution to determine the hydraulic parameters through the stream.

Meanwhile, Padma River plays an essential role for its diverse stakeholders, including a river ecosystem, drinking water supply, irrigation, industries, and navigation. It is also famous as the habitat of the Bangladeshi national fish, Hilsha. As shown in Figure 1, the Dhaka Water Supply and Sewerage Authority (DWASA) recently constructed a 450 million liters/day water treatment plant at Mawa to supply the drinking water (Khan and Uddin, 2019). However, the Farakka Barrage constructed in 1975 over River Ganges in West Bengal, India, has possibly reduced the Padma River's mean flows (Islam, 2006). This alteration has caused many problems to the river's ecosystem, including the loss of fish

species, the drying of distributaries, saltwater water intrusion from the Bay of Bengal, and damage to the most extensive Sundarbans mangrove forests (Islam, 2006; Baten and Titumir, 2016). Also, the low flow has severely impacted the geomorphology, ecology, fish, and fisheries of Padma River, its branches, and surroundings (Rahman *et al.*, 2003).

Padma river is well known for Hilsha breeding, as about 60% of this fish is available in Bangladesh. Hilsha contributes 11% of the total national production and 1% of Gross Domestic Products (GDP) (Sunny *et al.*, 2003). Although Hilsha fish can pass through comparatively lower depth (Average 10 m) in the winter season, 20 m above water column is suitable for easy movement, migration, and pre-breeding congregation (Ahsan *et al.*, 2014). Hence, reducing the Padma River flow restricts navigation, creates a disturbance in fish habitat, decreases soil moisture, lowers the groundwater table, and ultimately threatens the economic livelihood. The reduced freshwater flow also results in landward salinity intrusion, posing threats to the ecosystem.

Therefore, the main objective of this study is to assess the EF requirements of the Padma river using HEC-RAS to conduct intensive hydraulic modeling. The lowest discharge and water level at different return periods were also predicted using the Log-Pearson Type III (LPIII) distribution method.

## 2 MATERIALS AND METHOD

### 2.1 Study Area

Bangladesh has a highly dynamic river system with a comprehensive seasonal fluctuation in discharge, which peaks during the monsoon from July to September and is lowest from January to March. It comprises the Ganges River, which originates from the Gongotri Glacier and runs through India and Bangladesh. At the confluence with Jamuna River near Goalundo, this river is known as the Padma and runs approximately 120 km with the Meghna River near the Bay of Bengal (Sultana and Alam, 2016). As shown in Figure 1, the Padma River started from the Ganges-Jamuna

confluence to the Padma-Meghna confluence. It has a straight, whole course toward the southeast and holds some great islands.

## 2.2 Methodology

A river analysis computer program, HEC-RAS, was used to estimate the hydraulic parameters of the Padma River and assess the EF requirements. Meanwhile, the determination of low flow frequency was conducted using the Log-Pearson Type III (LPIII) distribution. Figure 2 presents the adopted methodology in this study.

## 2.3 Data Preparation

The long-term monthly water level data were collected between 2000 and 2019 from the Bangladesh Water Development Board (BWDB) for four gauging stations, namely Baruria Transit, Mawa, Tarpasha, Sureswar, depicted in Figure 1. Also, the discharge data of Baruria Transit and Mawa during this period were assembled. The minimum discharges from the observed long-term monthly dataset were 2540 m<sup>3</sup>/s and 1817 m<sup>3</sup>/s at Baruria Transit and Mawa stations, while the minimum water levels were 1.48m, 0.84m,

0.39m, and 0.26m at Baruria Transit, Mawa, Tarpasha, and Sureswar stations, respectively. Meanwhile, the lowest flow duration and water level were recorded between December and April each year in the datasets.

Figure 3 shows the measured data for the 14 Padma River cross-sections collected from the BWDB in 2019 and the river bed elevations acquired from the 30m Digital Elevation Model (DEM) by the United States Geological Survey (USGS).

## 2.4 Low Flow Frequency Analysis

Log-Pearson Type III, the Gumbel distribution method, and lognormal distributions are the most used streamflow frequency analysis techniques. The Gumbel distribution method has been used for designing flood control developments in Bangladesh (Ferdows and Hossain 2005). Subsequently, the minimum extreme values were selected from the yearly datasets, and the frequency analysis was conducted using the LPIII distribution following US WRC (USGS, 2019) recommendation.

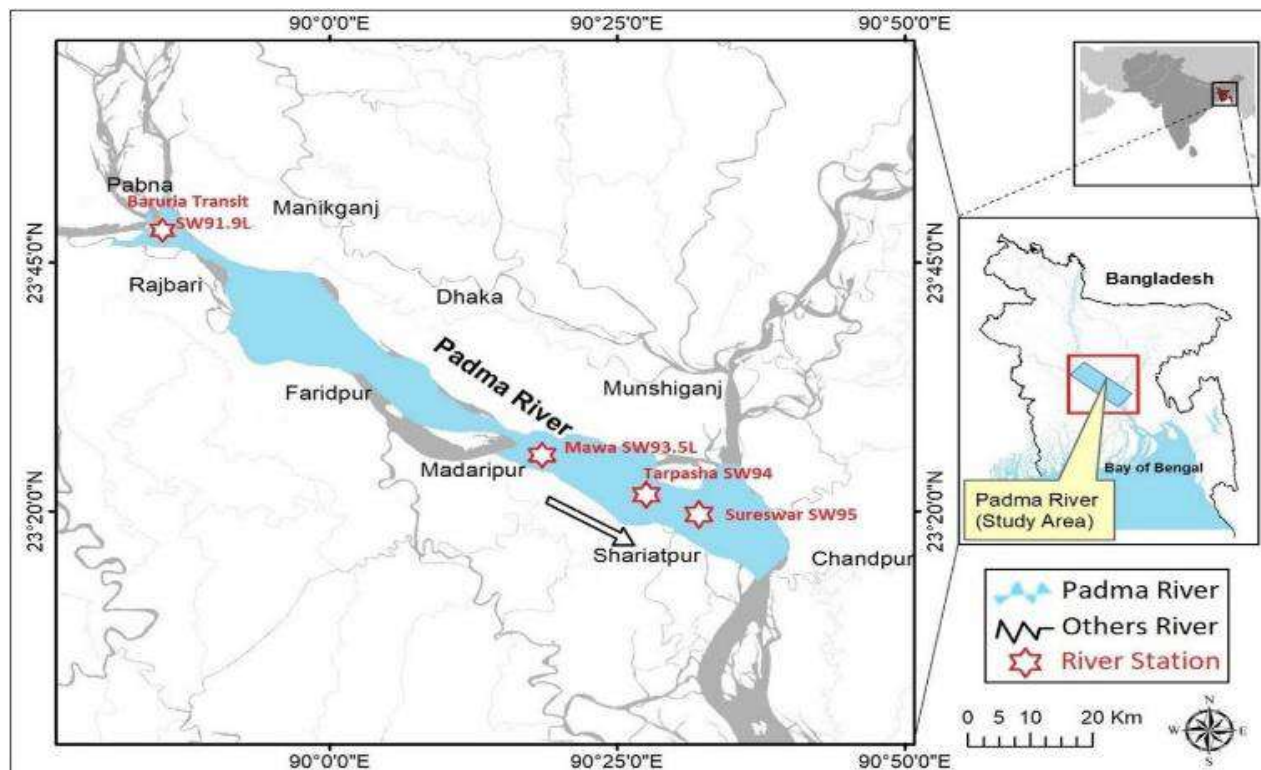


Figure 1. Location Map of the Study Area.

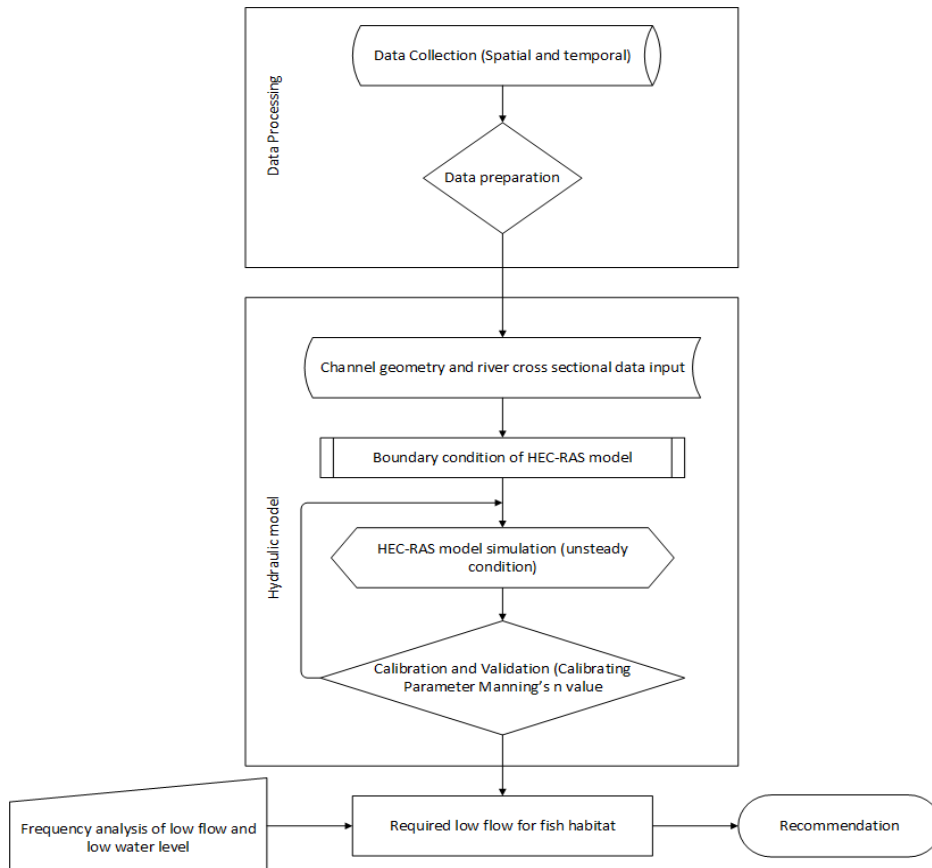


Figure 2. Flow chart of the adopted method.

The logarithms of the hydrological data,  $y = \text{Log } x$ , were used to calculate the mean, standard deviation, coefficient of skewness of the LPIII distribution. The frequency factor depends on the return period and coefficient of skewness and is equal to the standard normal variable when this coefficient is zero.

Here,  $y_m$  is Average,  $s$  is Standard Deviation,  $C_s$  is the coefficient of skewness,  $K_T$  is Frequency Factor,  $T$  is Return Period,  $z$  is Standard normal variable

When  $C_s$  is 0,  $K_T$  is approximated (Kite, 1977) as:

$$K_T = z + (z^2 - 1)k + \frac{1}{3} (z^3 - 6z)k^2 - (z^2 - 1)k^3 + zk^4 + \frac{1}{3}k^5 \quad (1)$$

Where  $k$  is  $C_s/6$  and  $C_s$  are given by

$$C_s = \frac{n \sum_{i=1}^n (y - y_m)^3}{(n-1)(n-2)s^3} \quad (2)$$

And  $s$  is given by

$$s = \left[ \frac{1}{n-1} \sum_{i=1}^n (y - y_m)^2 \right]^{1/2} \quad (3)$$

The value of  $z$  corresponding to a non-exceedance probability of  $1-p$  ( $p = 1/T$ ) can be calculated by finding the value of an intermediate variable,  $w$  is

$$w = \left[ \ln \left( \frac{1}{(1-p)^2} \right) \right]^{1/2} \quad (0 < p \leq 0.5) \quad (4)$$

Then, calculating  $z$  using the approximation:

$$z = w - \frac{2.515517 + 0.802853w + 0.010328w^2}{1 + 1.432788w + 0.189269w^2 + 0.001308w^3} \quad (5)$$

When  $p > 0.5$ ,  $1 - p$  can replace  $p$  in equation (4), and the  $z$  value obtained by equation (5) provides a '-ve' sign. The obtained error is lower than 0.00045 following Abramowitz and Stegun (Abramowitz, M. and Stegun, 1965).

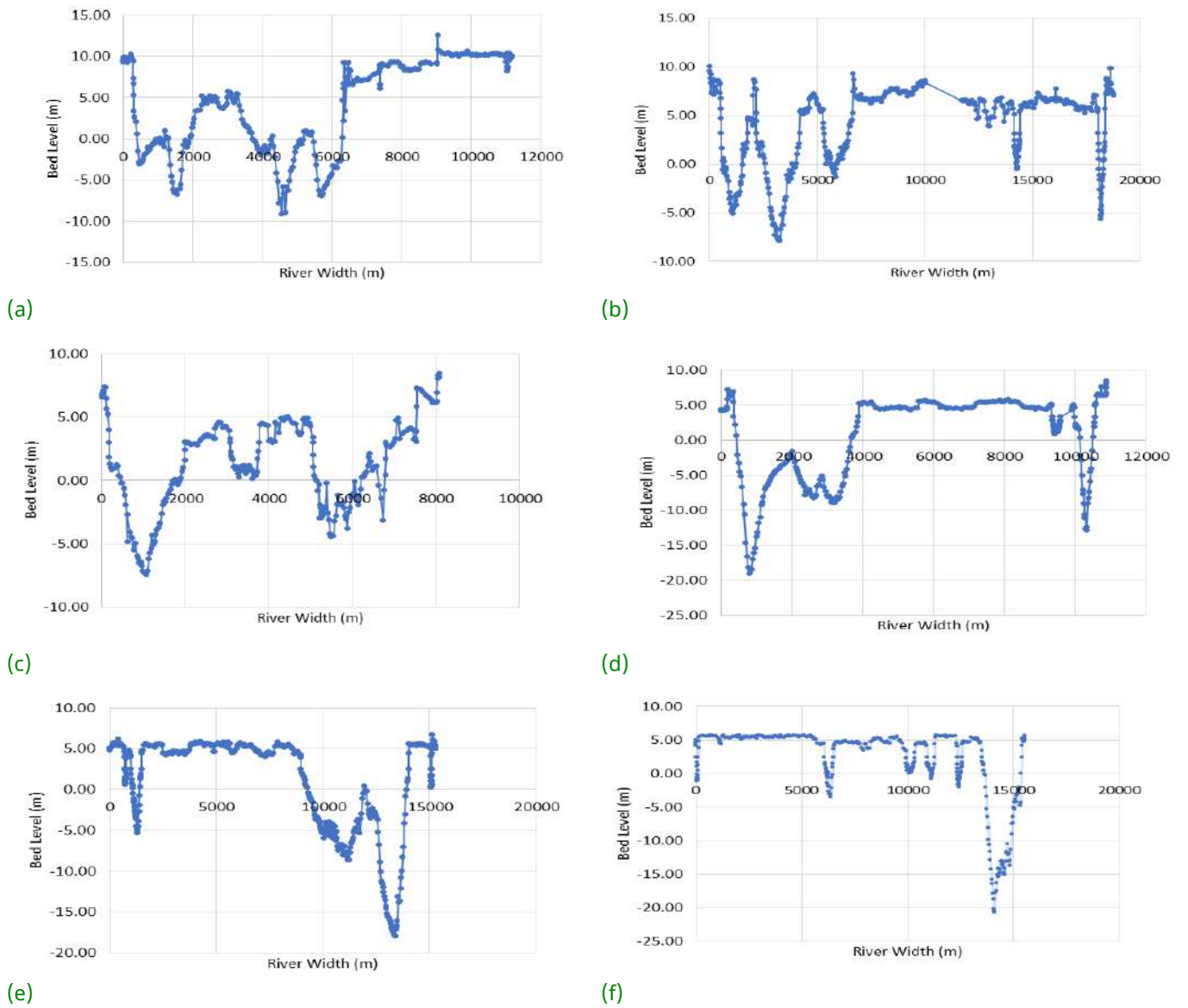


Figure 3. Riverbed level at each cross-section (marked on Figure 4) (a) Cross-section RMP8, (b) Cross-section RMP6, (c) Cross-section RMP4.1, (d) Cross-section RMP3, (e) Cross-section RMP1, (f) Cross-section RMP0.1

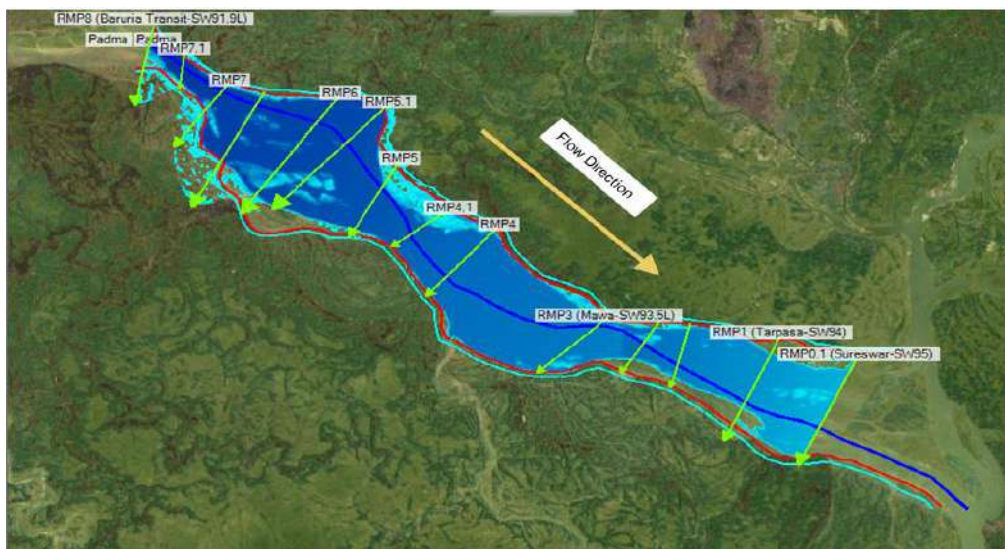


Figure 4. Padma River in the HEC-RAS Model.

### 3 MODEL SETUP

#### 3.1 Input Parameters

The Hydrologic Engineering Centre's River Analysis System (HEC-RAS, version 5.0.7) is a 1-D hydraulic-flow model that requires hydraulic parameters for the stream channel geometry and water flow analysis. As shown in Figure 4, the stream comprises 14 cross-sections, and each consists of a left and right floodway and the main channel. The relevant input parameters are:

- I. Geometric Data: The cross-section profiles consist of two components, i.e., the elevation data and properties. The cross-section has been located as GPS coordinates in the RAS Mapper and stored as geometric data. This RAS Mapper consists of and draws the stream centerline, cross-sectional cut lines, main channel bank lines, flow path lines, bridge/culverts, etc. In this study, the stream centerline and cross-sectional cut lines were taken as the fundamental data for the cross-section, while the main channel bank and flow path lines were the optional data. Then, the river bed elevation data at each cross-section has considered for subsequent editing.
- II. DEM File: For the study, the 30m DEMs were acquired from the USGS.
- III. Manning's roughness coefficients (n): The value of 'n' for Padma River ranges from 0.04 to 0.015 from the low to bankfull stage (Neill, Hotopp, and Hunter, 2013). In this study, Manning's n value was 0.04 in the main channel and 0.015 at the left and right overbank.
- IV. Following Brunner and CEIWR-HEC, the selected Contraction and Expansion coefficients were 0.1 and 0.3, respectively (Brunner and CEIWR-HEC, 2016).

The model setup was based on two assumptions, (a) the constant energy head exists within the cross-section, and (b) the velocity vector is perpendicular to the cross-section. For the hydraulic computations in which the iterative calculation of the energy equation plays a vital

role, the initial input consisted of channel geometry and river flow. Then, the rest of the analysis used the standard step method based on the secondary flow and the associated water surface elevation at each cross-section.

#### 3.2 Boundary Condition

The Padma River flow simulation used the HEC-RAS unsteady flow analysis, as steady river flow conditions are unusual. The observed minimum flow hydrograph was an upstream boundary condition used at river station RMP8 (Baruria Transit SW91.9L). Furthermore, a low water level stage hydrograph measurement was employed as a downstream boundary condition at river station RMP0.1 (Sureswar SW95). The HEC-RAS model simulations of the unsteady state were computed at an hourly interval from Jan 2012 to Dec 2019.

#### 3.3 Statistical Analysis of the Model Outcome

The hydrologic and hydraulic model performances were evaluated using a matrix of error statistics, namely Efficiency Index (*EI*), Root Mean Square Error (*RMSE*), *MPE* (Mean Percentage Error) and *MAPE* (Mean Absolute Percentage Error), and  $R^2$  (Coefficient of Determination) as follows:

$$EI = 1 - \frac{\sum_{i=1}^N (X_i - Y_i)^2}{\sum_{i=1}^N (X_i - X_i^m)^2} \quad (6)$$

$$RMSE = \sqrt{\frac{1}{N} \sum_{i=1}^N (X_i - Y_i)^2} \quad (7)$$

$$MPE = \frac{1}{N} \sum_{i=1}^N \left( \frac{X_i - Y_i}{X_i} \right) \times 100 \quad (8)$$

$$MAPE = \frac{1}{N} \sum_{i=1}^N \left( \frac{ABS(X_i - Y_i)}{X_i} \right) \times 100 \quad (9)$$

$$R^2 = \frac{(\sum_{i=1}^N (X_i - X_i^m)(Y_i - Y_i^m))^2}{\sum_{i=1}^N (X_i - X_i^m)^2 \sum_{i=1}^N (Y_i - Y_i^m)^2} \quad (10)$$

Here, the mean observed value,  $X_i^m = \frac{1}{N} \sum_{i=1}^N X_i$   
And mean predicted value,  $Y_i^m = \frac{1}{N} \sum_{i=1}^N Y_i$

$N$  is the number of field observations.  $Y_i$  is the model Predicted value, and  $X_i$  is the observed value; a mean error below zero signifies that the model under-predicted the water level.

The Efficiency Index ( $EI$ ) value ranges from  $-\infty$  to 1, while 1 is the best fit. An  $EI$  value of approximately “0” refers to the model parameter following an accurate trend as an observed mean. Another statistical index is the coefficient of determination ( $R^2$ ), which shows the correlation between observed and simulated information.

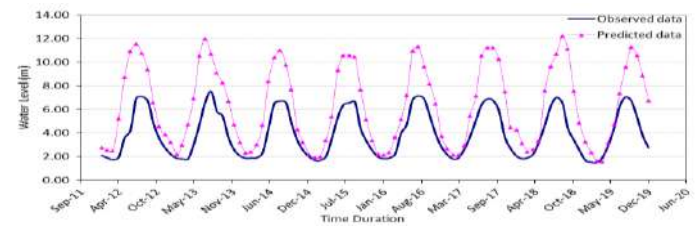
### 3.4 Frequency Analysis

The frequency analysis showed the minimum water surface level (Reduced Level, RL) as 1.49 m, 1.42 m, 1.37 m, 1.32 m, 1.30 m at Baruria Transit and 0.91 m, 0.87 m, 0.84 m, 0.82 m, 0.80 m at Mawa in 5, 10, 20, 50, and 100 years return periods, respectively. It also gave results of 0.67 m, 0.61 m, 0.57 m, 0.53 m, 0.51 m at Tarpasha, 0.22 m, 0.17 m, 0.14 m, 0.12 m, 0.11 m at Sureswar. The minimum flow was estimated as 4017  $m^3/s$ , 3685  $m^3/s$ , 3449  $m^3/s$ , 3229  $m^3/s$ , 3113  $m^3/s$  at Baruria Transit and 3304  $m^3/s$ , 2781  $m^3/s$ , 2438  $m^3/s$ , 2141  $m^3/s$ , 1992  $m^3/s$  at Mawa station in 5, 10, 20, 50, and 100 years return periods, respectively. Meanwhile, the water level and flow appeared at a minimum magnitude between December to April each year.

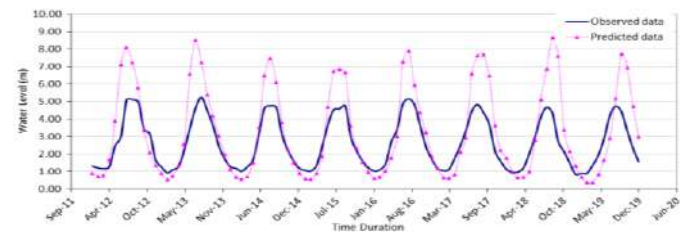
## 4 MODEL CALIBRATION AND VALIDATION

Model simulations were conducted monthly during 2012-2019, 2019 was selected as the calibrating year, and the findings were validated between 2016 to 2018. The calibrating parameter was Manning’s  $n$  value (0.04), and the historical dataset was compared with the simulated / predicted water level data. As shown in Figure 5a, the minimum observed water level from 2012 to 2019 at river station RMP8 (Baruria Transit SW91.9L) was recorded as 1.48 m in March 2019, while the simulated water level was 1.57 m in April 2019. During the simulation period presented in Figure 5b, river station RMP3 (Mawa SW93.5L) had a minimum observed water level of 0.84 m in January 2019, while the simulated water level was 0.37 m in March 2019. This period at the downstream river station recorded a minimum recorded observed water level of 0.74 m for RMP1 (Tarpasha SW94) in February 2013 and 0.26 m for RMP0.1 (Sureswar SW95) in February 2019. The simulated water levels at these two stations were

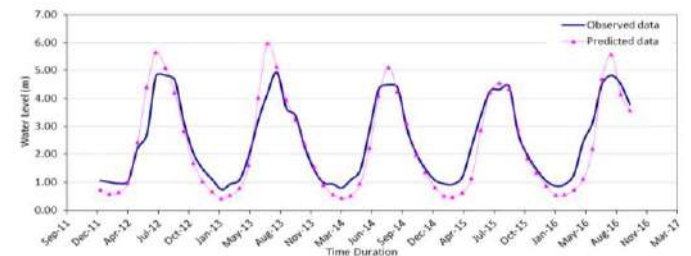
0.30 m and 0.27 m in March 2019, respectively, as shown in Figures 5c and d.



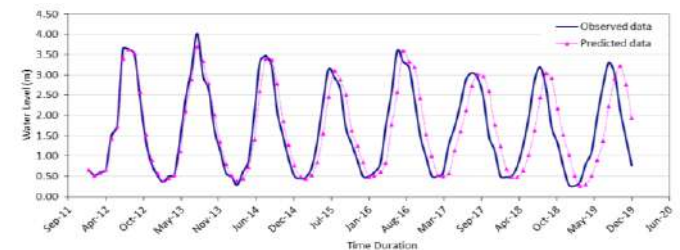
(a).



(b).



(c).



(d).

Figure 5. Simulated and observed water level comparisons at station (a) RMP8 (Baruria Transit SW91.9L). (b) RMP3 (Mawa SW93.5L). (c) RMP1 (Tarpasha SW94). (d) RMP0.1 (Sureswar SW95).

According to Figure 6a, the minimum observed flow from 2012 to 2019 at Baruria Transit was recorded at 2540  $m^3/s$  in March 2019, while the simulated minimum flow was 3849  $m^3/s$  in April 2019. During this period, the minimum observed flow was 1974  $m^3/s$  in February 2016, with a simulated minimum flow of 3789  $m^3/s$  in April 2019 at river station Mawa, as shown in Figure 6b.

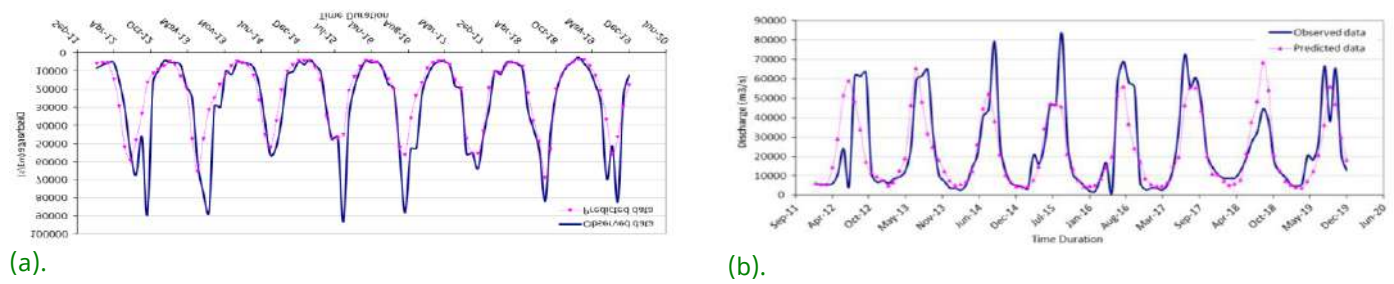


Figure 6. Simulated and observed flow comparisons at Station (a) RMP8 (Baruria Transit SW91.9L). (b) RMP3 (Mawa SW93.5L).

Table 1. Model Calibration Statistics

Statistical Parameters	Baruria Transit		Mawa		Tarpasha	Sureswar
	Monthly Water level	Monthly Flow	Monthly Water level	Monthly Flow	Monthly Water Level	Monthly Water Level
EI	-1.12	0.69	-0.66	0.63	-	0.26
RMSE	2.91	14419.41	1.77	12729.99	-	0.90
MPE	-54.91	5.82	-13.54	11.02	-	-32.37
MAPE	57.88	28.91	60.54	32.99	-	79.13
R2	0.74	0.78	0.58	0.66	-	0.39

Table 2. Model Validation Statistics

Statistical Parameters	Baruria Transit		Mawa		Tarpasha	Sureswar
	Monthly Water level	Monthly Flow	Monthly Water level	Monthly Flow	Monthly Water Level	Monthly Water Level
EI	-1.42	0.85	-0.52	0.76	0.83	0.58
RMSE	2.94	8972.17	1.71	10670.27	0.64	0.66
MPE	-53.15	10.41	-16.85	-19.56	21.76	-11.89
MAPE	53.15	14.23	42.59	41.76	25.75	40.63
R2	0.89	0.90	0.82	0.76	0.93	0.62

### 4.1 Model Performance

The low flow year, which was 2019, was selected as the calibration period. The statistical index in Table 1 shows that the *EI* values against water levels at Baruria Transit and Mawa station were close to 0, indicating the model parameter followed an accurate trend as an observed mean. Conversely, the *EI* values against the flow at these stations were close to 1, signifying that the model and observed parameters matched perfectly. The coefficient of determination ( $R^2$ ) at all the stations was close to 1, denoting the reasonable correlation between the model and observed parameters. However, statistical parameter values were calculated at Tarpasha Station because of the unavailability of the observed values. From the validation conducted from 2016 to 2018, the statistical index in Table 2 shows that the *EI* values at all the stations were close to 1. Also, the coefficients of determination ( $R^2$ ) were close to 1, and the *MPE* value showed minor

errors, indicating that the model and observed parameters matched.

### 5 CONCLUSION

This study aimed at assessing the EF of the Padma River using with HEC-RAS computer program HEC-RAS and low flow frequency analysis. Although fish, especially Hilsha, can pass through comparatively lower depth at a 10 m average in the winter season, 20 m above water depth is suitable for easy movement, migration, and pre-breeding congregation. Hence, this 20 m water or channel depth maintenance required the water surface level (Reduced Level, RL) at Baruria Transit, Mawa, Tarpasha, and Sureswar stations to be at 10.83 m 1.0 m, 2.09 m, and -0.75 m, respectively. The simulation found 1.57m, 0.37 m, 0.30 m, and 0.27 m monthly minimum water surface levels at Baruria Transit, Mawa, Tarpasha, and Sureswar stations. Conversely, the frequency analysis showed 1.30 m, 0.80 m, 0.51 m, and 0.11

m water surface level, respectively, in a 100-year return period. These analytical techniques also discovered that the lowest water levels occurred between December and April each year.

Therefore, Baruria Transit to Tarpasha is unsuitable for the easy movement, migration, and pre-breeding congregation of the Hilsha Fish, while Sureswar station is suitable for breeding. The December to April period was also revealed a difficult time for the movement of Hilsha Fish in the Padma River.

Generally, Padma River plays an essential role in supplying domestic water to Dhaka city through the Padma Jashaldia Water Treatment Plant, which currently has the highest capacity (450 MLD) in Bangladesh and an intake channel close to Station RMP3 (Mawa SW93.5L). Subsequently, the simulated result found that the minimum water surface level was 0.37 m in March 2019, while the frequency analysis showed a minimum water level of 0.80 m in the 100-year return period. The simulated minimum flow was recorded at 3789 m<sup>3</sup>/s, and frequency analysis showed a minimum flow of 1992 m<sup>3</sup>/s at Mawa.

#### DISCLAIMER

The authors declare no conflict of interest.

#### AVAILABILITY OF DATA AND MATERIALS

All data are available from the author

#### AUTHOR CONTRIBUTION STATEMENTS

Md. Abu S. developed the numerical and analytical model set up under the supervision of Aysha A. Both the authors made a substantial contribution in discussing the result and drafting the manuscript.

#### ACKNOWLEDGMENTS

The author is grateful to the Department of Civil Engineering, Chittagong University of Engineering and Technology (CUET) in Bangladesh, for providing the funds for the acquisition of a Master's of Science degree. The author is also grateful to BWDB for providing hydrological and hydraulic data during the study.

#### REFERENCES

- Abramowitz, M. and Stegun, I.A., 1965. *Handbook of mathematical functions*. New York: Dover.
- Ahsan, D.A., Naser, M.N., Bhaumik, U., Hazra, S. and Bhattacharya, S.B., 2014. *Migration, Spawning Patterns and Conservation of Hilsa Shad (Tenulosa ilisha) in Bangladesh and India*.
- Akter, A. and Ali, M.H., 2012. Environmental flow requirements assessment in the Halda River, Bangladesh. *Hydrological Sciences Journal*.
- Akter, A. and Tanim, A.H., 2018. A modeling approach to establish environmental flow threshold in ungauged semidiurnal tidal river. *Journal of Hydrology*, [online] 558, pp.442–459. Available at: <<https://doi.org/10.1016/j.jhydrol.2018.01.061>>.
- Akter, J., 2010. Environmental flow assessment for the Ganges river. (March), p.158.
- Arthington, A.H. and Zalucki, J.M., 1998. Comparative evaluation of environmental flow assessment techniques: Review of methods. *LWRRDC Occasional Paper Series 27/98*.
- Baten, M.A. and Titumir, R.A.M., 2016. Environmental challenges of trans-boundary water resources management: the case of Bangladesh. *Sustainable Water Resources Management*, 2(1), pp.13–27.
- Brunner, G.W. and CEIWR-HEC, 2016. HEC-RAS River Analysis System User's Manual. US Army Corps of Engineers–Hydrologic Engineering Center. [online] (January), pp.1–790. Available at: <[https://www.hec.usace.army.mil/software/hecras/documentation/HEC-RAS\\_5.0\\_Users\\_Manual.pdf](https://www.hec.usace.army.mil/software/hecras/documentation/HEC-RAS_5.0_Users_Manual.pdf)>.
- Editor Engr Taqsem Khan, C.A., Editor, E. and Shahid Uddin Director, A., 2019. *DEWASA Annual Report 2018-19*.
- Ferdows, M., and Hossain, M., 2005. Flood frequency Analysis at Different Rivers in Bangladesh: A Comparison Study on Probability Distribution Functions. *Thammasat International Journal of Science and Technology*, 10 (3), pp.53–

- 62.
- Islam, N., 2006. IRLP or the Ecological Approach to Rivers? *Economic and Political Weekly*, [online] 41(17), pp.1693–1702. Available at: <<http://www.jstor.org/stable/4418148>>.
- Jahid, S.A., 2016. Assessing Environmental Flow for the Kobadak River and Developing a Framework for Its Maintenance Assessing Environmental Flow for the Kobadak River and Developing a Framework for Its Maintenance. (February).
- Kite, G.W., 1977. Frequency and risk analysis in hydrology. *Fort Collins, CO: Water Resources Publications*.
- Moly, S.H., Rahman, M.A.T.M. and Saadat, A.H.M., 2015. Environmental Flow Characteristics of the Gorai River, Bangladesh. *International Journal of Scientific Research in Environmental Sciences*.
- Mullick, M., Babel, M. and Perret, S., 2010. Flow characteristics and environmental flow requirements for the Teesta River, Bangladesh. *Proceedings of International Conference on ...*, [online] pp.105–114. Available at: <[http://scholar.google.co.in/scholar?q=mullick+2010+teesta&btnG=&hl=en&as\\_sdt=0%2C5#0](http://scholar.google.co.in/scholar?q=mullick+2010+teesta&btnG=&hl=en&as_sdt=0%2C5#0)>.
- Neill, C., Hotopp, D. and Hunter, B., 2013. Some hydrotechnical features of Padma River, Bangladesh. pp.1–11.
- Pusey, B.J. and Arthington, A.H., 1991. The utility and applicability of the in-stream flow incremental methodology (IFIM) for Australian lotic environments. *SIL Proceedings, 1922-2010*.
- Pusey, B.J., Arthington, A.H. and Read, M.G., 1993. Spatial and temporal variation in fish assemblage structure in the Mary River, south-eastern Queensland: the influence of habitat structure. *Environmental Biology of Fishes*.
- Rahman, A., Roy C., Rahman, A., Jamil, F., and Islam, M.S., 2019. Environmental Flow Assessment for the Main Rivers of the North-West Zone of Bangladesh. *North American Academic Research*, 2 (3), pp 81-101.
- Rahman, M.A.T.M.T., Moly, S.H. and Saadat, A.H.M., 2013. Environmental Flow Requirement and Comparative Study of the Turag River, Bangladesh. *International Journal of Scientific Research in Environmental Sciences*.
- Rahman, M.K., Akhter, J.N., Nima, A., Ahmed, S.U. and Mazid, M.A., 2003. Studies on geomorphology, ecology and fish production of the 92 rivers of Rajshahi Division , Bangladesh. *Bangladesh J. Fish. Res.*, 7(2), pp.141–150.
- Saha, P.P., 2007. As assessment of instream flow requirement of Gorai river considering salinity intrusion and fish habitat.
- Smakhtin, V., Revenga, C. and Döll, P., 2004. *Taking into Account Environmental Water Requirements in Global-scale Water Resources Assessments. Comprehensive Assessment of Water Management in Agriculture Research Report 2. IWMI, Colombo, Sri Lanka. Assessment*.
- Sultana, R. and Alam, S., 2016. HAZARD CHARACTERISTICS OF NATURAL FLOOD : A CASE STUDY OF PADMA RIVER. 4(12), pp.13–20.
- Sunny, A.R., Ahamed, G.S., Mithun, M.H., Islam, M.A., Das, B., Rahman, A., Rahman, T., Hasan, N. and Chowdhury, M.A., 2003. Livelihood Status of the Hilsa ( *Tenualosa ilisha* ) Fishers : The Case of Coastal Fishing Community of the Padma River , Bangladesh. *Journal of Coastal Zone Management*, 22(2), p.469.
- Tharme, R.E., 2003. A global perspective on environmental flow assessment: Emerging trends in the development and application of environmental flow methodologies for rivers. *River Research and Applications*.
- USGS, 2019. *Guidelines for Determining Flood Flow Frequency Bulletin 17C Book 4, Hydrologic Analysis and Interpretation*. [online] Book:, Available at: <<https://pubs.usgs.gov/tm/04/b05/tm4b5.pdf>>.

# Finite Element Modelling of Prestressed Concrete Piles in Soft Soils, Case Study: Northern Jakarta, Indonesia

Aswin Lim\*, Varian Harwin Batistuta, Yiska Vivian Christensen Wijaya

Department of Civil Engineering, Universitas Katolik Parahyangan, Bandung, INDONESIA  
Jalan Ciumbuleuit No 94, Bandung

\*Corresponding authors: [aswinlim@unpar.ac.id](mailto:aswinlim@unpar.ac.id)

SUBMITTED 20 July 2021 REVISED 14 September 2021 ACCEPTED 04 October 2021

**ABSTRACT** Jakarta is faced with limited land resources due to its position as the capital city of Indonesia. Therefore, numerous high-rise buildings are being constructed to solve this problem and provide accommodations for a large number of Jakarta residents. Studies have shown that prestressed concrete piles (spun piles) are commonly used as the foundations of high-rise buildings in metropolitan cities across Indonesia, especially in the Northern Jakarta Coastal area, which is predominant with deep soft soils deposit. To further assess and verify the ultimate capacity of the pile, a static loading test was conducted. However, not all results from the field test produced ideal, accurate, precise, and reliable load-settlement curve (until failure) results. Therefore, this study aims to determine the soil properties for the analysis of prestressed concrete spun piles with a diameter of 600 mm in the Northern Jakarta coastal area based on the standard penetration test values (SPT-N). It is a case study of a well-documented static pile load test using the kentledge system. Back analyses were performed by the finite element method to obtain the extrapolated load-settlement curve. Furthermore, the effect of interface strength between pile and soil on the load-settlement curve was also investigated. The results showed that a reduction of interface strength leads to a smaller load-settlement curve. In addition, several geotechnical engineering parameters of soil, such as the undrained shear strength and effective young's modulus, were established using data from an in-situ soil site investigation and empirical correlations with SPT-N.

**KEYWORDS** Finite Element Modeling; Axial Load Test; Load-Settlement Curve; Back Analysis; Prestressed Concrete Piles.

© The Author(s) 2022. This article is distributed under a Creative Commons Attribution-ShareAlike 4.0 International license.

## 1 INTRODUCTION

According to the Indonesian Central Bureau of Statistics, Jakarta has an estimated population of over 10.5 million people, and it is expected to keep growing yearly. Due to the shortage of land resources and the increase of urban population, many construction projects in Jakarta and several metropolitan cities worldwide choose to build high-rise buildings. Generally, prestressed concrete piles (spun piles) are used as the foundations for high-rise buildings, especially in the Northern Jakarta Coastal area, predominantly with deep soft soil deposits. There are several advantages associated with spun piles, such as durability, cost-effectiveness, and being less prone to cracking during the driving process.

Numerous studies have been conducted on numerical modeling analyses to investigate the soil-structure interaction problem of the pile

foundation. Most of these studies examined the behavior of piles when subjected to axial compression (Rojas *et al.*, 1999; Kitiyodom *et al.*, 2004; Lu *et al.*, 2005; Said *et al.*, 2009; Dijkstra *et al.*, 2011; Li *et al.*, 2012; Karlsrud, 2014; Mahmoud *et al.*, 2014; Dias & Bezuijen, 2018). The result showed that numerical modelings can properly reproduce the load-settlement curves, such as the finite element model. Furthermore, Zhou *et al.* (2013) simulated full-scale destructive field tests of static drill rooted nodular pile in soft soil areas and stated that the bearing capacity is approximately 8% to 10% higher than the bored pile. Moreover, studies on dynamic and static load testing of model piles driven into dense sand and in heterogeneous soil areas showed that the pile's capacity was in good agreement with the test results (Bruno & Randolph, 1999; Crispin *et al.*,

2018; Nasrollahzadeh & Hataf., 2019). Randolph (2003) stated that the most integral factors of pile analyses still depend on empirical correlations based on experimental observations from laboratory and full-scale in situ testing. Therefore, field soil investigations and laboratory testing need to be carried out to determine the soil properties from the assumptions validated with the initial load–settlement curve from the field loading test results. Unfortunately, there are limited studies on soil properties of Northern Jakarta Coastal area clay (Taqwa *et al.*, 2018; Hutabarat *et al.*, 2019). Therefore, this study aims to back-analysis the properties of soft soil, such as Undrained Shear Strength ( $S_u$ ) and Effective Soil Young's Modulus ( $E'$ ) for designing prestressed concrete piles at North Jakarta area based on the standard penetration test values (SPT-N). Besides, the effect of interface strength between pile and soil on the load-settlement curve was also investigated. A well-documented case study of apartment construction in the Northern Jakarta coastal area was selected to validate and verify the finite element analysis, namely PLAXIS 2D 2019. Finally, some empirical correlations to determine soil properties were proposed for further practice.

**2 METHODS**

**2.1 Project Description**

The apartment project has 11 towers located at the North Coast of Jakarta area, known as Dadap, and dominated by thick and soft soil, as shown in Figure 1. This study focused on the spun pile, namely A1204, embedded in the Tower 1 area and driven about 44.5 m below the ground level, with 600 mm of diameter and a compressive concrete ( $f_c'$ ) strength of 45 MPa.

**2.2 Soil Stratification**

In this project, Soil boring and Standard Penetration Tests (SPT-N) were carried out to accommodate soil samples and their stratification information. The SPT-N test was followed by ASTM-D1586, also known as Borehole 01 (BH-01), as shown in Figure 2. In general, the soil layers were divided into 5, dominated by medium to hard clays. From +0.0 to

-1.0, the soil was very soft silty clay soil, followed by a loose sand layer from -1.0 to -7.0. In addition, very soft silty clay was found from -7.0 to -31.0 and continued with a layer of dense sand from -31.0 to -39.0. Lastly, the hard silty clay soil layer was identified from -39.0 to -69.0, with the groundwater table located -0.5 m below the surface. The detail of the sub-soil stratifications is shown in Table 1 and Figure 3.



Figure 1. Location of tested prestressed concrete spun pile (Pile A1204 – Tower 1)



Figure 2. Location of Borehole 01 (BH-01)

Table 1. Soil stratification of BH – 01

Elevation Depth (m)	Soil Type	USCS Symbol	SPT-N
0.0 – 1.0	Very Soft – Silty Clay	CL	2
1.0 – 7.0	Loose – Sand	SW	8
7.0 – 31.0	Very Soft – Silty Clay	CL	2
31.0 – 39.0	Dense – Sand	SW	32
39.0 – 69.0	Hard – Silty Clay	CL	26
69.0 – 80.0	Dense – Sand	SW	27

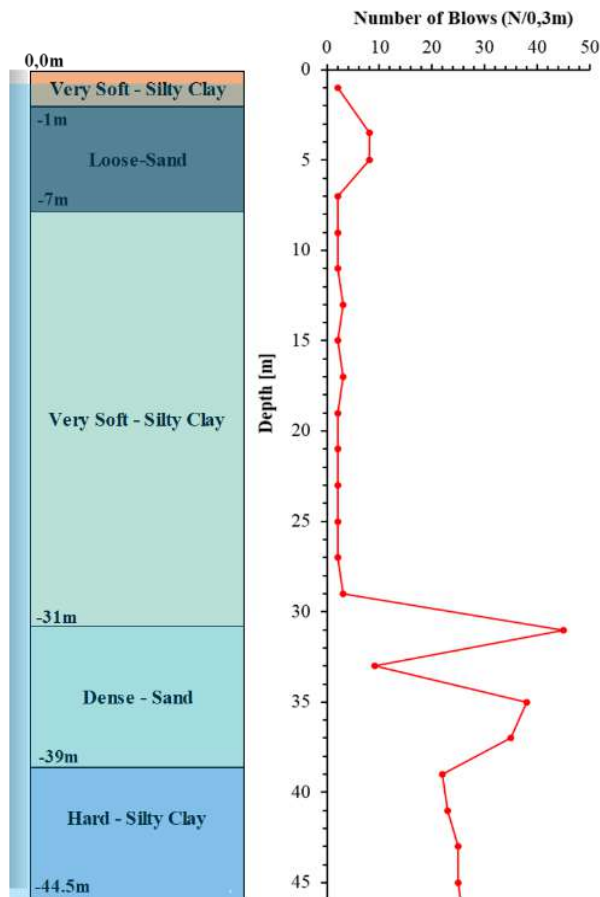


Figure 3. Soil stratification and SPT-N value of BH-01

### 2.3 Pile Loading Test

The acceptable axial load capacity is an important geotechnical requirement for the design of a deep foundation because it is used to support working loads. Therefore, this led to the development of various methods of assessing the axial load of the piles by geotechnical engineers, such as the full-static load test (Coduto, 2001). Generally, there are two types of pile loading tests, namely the constant rate of penetration (CRP) and the Maintained Load (ML) tests. This study focused on the ML test procedure, which requires accurate increment in loading data at constant periods. According to Tomlinson (1994), the rate of piling borders from ICE decreases when the movement is above 0.25 mm/h. This indicates that it is important to ensure the time at each load increases to obtain a similar degree of soil consolidation because the slower the rate of load increment, the smaller the ultimate failure. The sequence of this test includes loading, unloading, and reloading to the working level. Afterward, the

load was raised until the maximum axial pile capacity was achieved. In this case, the testing sequence incorporated an initial loading value of 700 kN (50% of Working Load (WL)), which is commonly known as cycle A1. This is followed by a second, third, fourth, and fifth loading and unloading cycle of 1400 kN (100% WL), 2100 kN (150% WL), 2800 kN (200% WL), and 3500 kN (250% WL) using cycles A2, A3, A4, and A5 to reach the maximum capacity of the hydraulic jacks.

Table 2. Pile A1204 – Tower 1 Loading test result

%	Load (kN)	Settlement (m)
0	0	0.00000
25	350	0.00163
50	700	0.00376
75	1050	0.00591
100	1400	0.00806
125	1750	0.01026
150	2100	0.01265
175	2450	0.01504
200	2800	0.01768
225	3150	0.02086
250	3500	0.02517

The balance deformation or the settlement of the pile depends on the period of each particular loading step. The benchmark to describe this condition was determined when the applied load for each loading step was maintained for one hour or the rate of settlement attained was lower than 0.25 mm/h. Figure 4 showed a schematic of the loading test system, which consists of multiple supports of concrete weights used to determine the reaction for a hydraulic jack, which is then used to provide the test load. The settlement of the top pile head was controlled by 4 different electronic displacement transducers attached to a rigid steel beam with an accuracy resolution of 0.001 mm. Therefore, to limit any further interaction effects, it is located far from the test piles.

The load pressure cell was used to organize the hydraulic pressure in the jacking system. Overall, this system is much more stable and less prone to collapse, although it is expensive and cumbersome.

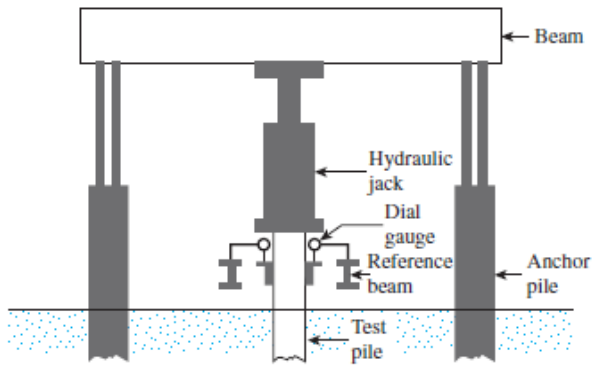


Figure 4. Schematic design of pile load test arrangement (Das, 2016)

For this study case, Pile A1204 was selected and installed on April 16<sup>th</sup>, 2019, before conducting the axial load test on May 28<sup>th</sup>, 2019. Furthermore, this study showed the behavior of the load–settlement curve obtained from this fifth cycle static pile load test result after it was numerically simulated through finite element analysis.

#### 2.4 Finite Element Model

The numerical simulation of the single pile load test was determined through the finite element method program, PLAXIS 2D. This finite element method (FEM) is a numerical strategy for solving accurate and precise solutions of partial differential and integral equations. The geometry of the generated mesh was parametrically delineated to grant the probability of geometrical variations when needed. This study used a model consisting of a 600 mm diameter pile with an embedded length of 44.5 m to determine the simulation of the single pile loaded with axial load until the load-settlement curve indicates failure.

The two-dimensional finite element geometry model between the soil-pile interaction systems is displayed in Figure 5(a). Meanwhile, Figure 5(b) portrays the finite difference mesh utilized in the pile test analysis consisting of 1359 elements and 11632 nodes. The soil was modeled using triangular elements with 15 nodes, with a total geometry of 12 m width and 80 m depth. Furthermore, the standard fixities were used to determine the boundaries condition, where both

sides of geometry used the roller conditions, and bottom boundaries were fixed.

The material behavior of the soil layers was used to simulate the perfectly elastic-plastic Mohr-Coulomb constitutive law. Afterward, the interaction between the pile structures with surrounding soil was determined using the interface factor ( $R_{int}$ ) along the pile's shaft. Interfaces are joined elements added to plates or geo-grids to allow proper modeling of soil-structure interaction. It is also used to simulate the thin zone of intensely sharing material at the contact between a plate and the surrounding soil (Dandagawhal, 2018).

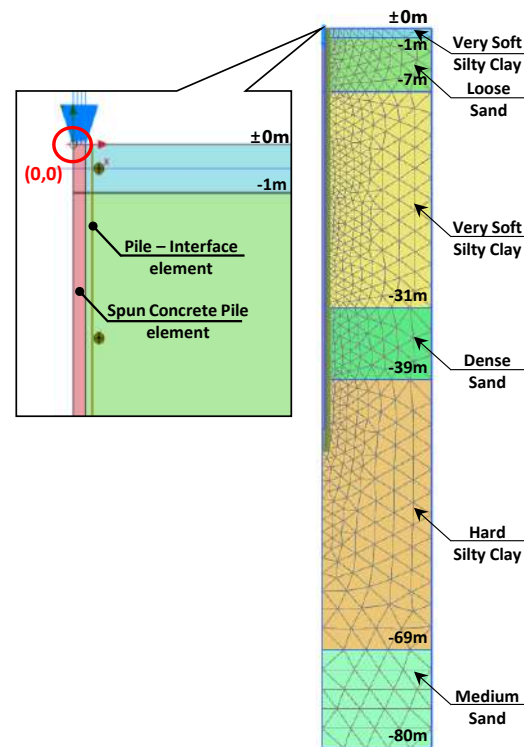


Figure 5. Finite Element Model for analysis (PLAXIS 2D 2019) Stage Construction

This project's finite element model simulation stage started with calculating the soil's initial stress to determine the  $K_0$  condition. This process was carried out using Jaky's formula, where  $K_0$  equals  $1 - \sin \phi'$ , then installed and activated the single pile at a groundwater level of 0.5 m below the ground. Furthermore, the initial displacements were reset to zero because the measured data were obtained without considering the installation effects. Lastly, the

interface element was activated, and additional axial loads were given until the pile failed with a total load of 5655 kN. The detailed construction stages are shown in Table 3.

**Table 3. Finite Element Method stage construction activities of the tested spun pile**

Orders	Stage Construction Activities
1	Initial phase
2	Installation of the prestressed tested spun pile
3	Reset displacement to zero activation
4	Activate of interface and apply maximum loads of 5655 kN

### 2.5 Soil Constitutive Model

The spun pile is considered a linear–elastic material, where the model represents Hooke's law of isotropic linear elasticity. According to the geotechnical field investigation, the groundwater table was located  $-0.5$  m below the ground level, while the spun pile used for this study was classified as class A1 concrete. Furthermore, the pile was modeled using a cluster, and the linear elastic material was applied to determine the rigidity of the concrete material, such as modulus of elasticity ( $E$ ), Poisson's ratio ( $\nu$ ), and the unit weight of concrete ( $\gamma_c$ ). Table 4 summarizes the input parameters for the tested spun pile elements.

The Mohr-Coulomb model, a commonly linear elastic perfectly plastic model as a first approximation of soil behavior, with a constant average stiffness was used to predict the soil layer. This model involves 4 main input soil parameters, namely Elastic modulus ( $E$ ),

Poisson's ratio ( $\nu$ ), friction angle ( $\phi$ ), and cohesion ( $c$ ). The clays and the sands were simulated following undrained and drained behavior, respectively. The main difference between those two behaviors was the generation of excess pore pressure due to loading. In the undrained condition, the excess pore pressure is generated, while in the drained condition, it remains zero.

In this analysis, the clay and silt adopted the Undrained B model consisting of effective stiffness parameters and undrained shear strength ( $S_u$ ). During this process, the consolidation analysis does not need to be performed after undrained calculation due to excess pore pressure generation. A more detailed explanation is shown in the Plaxis 2D 2019 manual. The detailed type of materials for the soil and structural element in this study is shown in Table 5. Meanwhile, the complete soil stratification and parameter input of the Finite Element Method (PLAXIS 2D, 2019) are summarized in Table 6.

**Table 4. Prestressed Concrete Spun Pile Input Materials**

Properties	Value
Unit Weight ( $\gamma$ )	24 kN/m <sup>3</sup>
Modulus of Elasticity ( $E$ )	3E+07 kN/m <sup>2</sup>
Poisson Ratio ( $\nu$ )	0.2

**Table 5. Type of Material Model in PLAXIS 2D 2019**

Material	Material Model	Type of Material
Concrete	Linear Elastic	Non-porous
Clay	Mohr-Coulomb	Undrained (B)
Silt	Mohr-Coulomb	Undrained (B)
Sand	Mohr-Coulomb	Drained

**Table 6. Input parameters for Mohr-Coulomb Model in PLAXIS 2D 2019**

Layer	Depth (m)	Soil Type	N <sub>SPT</sub>	USCS Symbol	$\phi$ (°)	$\gamma$ (kN/m <sup>2</sup> )	$\gamma_{sat}$ (kN/m <sup>2</sup> )	$S_u$ (kN/m <sup>2</sup> )	$E'$ (kN/m <sup>2</sup> )	$\nu'$	$R_{int}$
1	0.0 – 1.0	Very Soft – Silty Clay	2	CL	0	16	17	11	2700	0.35	1
2	1.0 – 7.0	Loose – Sand	8	SW	30	16	18	0	21000	0.25	1
3	7.0 – 31.0	Very Soft – Silty Clay	2	CL	0	16	17	11	3250	0.35	1
4	31.0 – 39.0	Dense – Sand	32	SW	37	19	21	0	50000	0.30	1
5	39.0 – 69.0	Hard – Silty Clay	26	CL	0	18	20	156	40000	0.30	1
6	69.0 – 80.0	Medium – Sand	27	SW	36	19	21	0	45000	0.30	1

### 3 RESULTS AND DISCUSSION

#### 3.1 Soil Modulus and Shear Strength Properties Correlation

Several trial-error processes were used to determine the correct input parameters for the curve-fitting process. This technique is known as the back analysis and consists of soil parameters with considerable effects on the load-settlement curve results, such as the Undrained Soil Strength ( $S_u$ ) and Effective Young's Modulus ( $E'$ ). Several iterations changed those 2 soil parameters based on back analysis until the computed results were close to the field measurement.

The clay's undrained shear strength ( $S_u$ ) was achieved from empirical correlation through back analysis, which correlates  $S_u$  with the  $N_{SPT}$ , as described in Equation (1) and (2).

$$S_u = 5.5 N_{SPT} (kPa) \tag{1}$$

$$S_u = 6 N_{SPT} (kPa) \tag{2}$$

The empirical equations (1) and (2) are used to forecast the  $S_u$  of the clay with very soft and stiff to hard clay consistencies. Figure 6 compares the  $S_u$  profile calculated from the above equation and actual soil profile depth. The  $S_u$  obtained from these 2 equations depends on the SPT-N value of each soil layer.

The effective soil modulus ( $E'$ ) is also a fundamental soil property for predicting its deformation characteristics. Due to the back analyses, the effective soil modulus for clay was estimated as  $E'=1350$  N (kPa) and  $E'=2625$  N (kPa) for sand. Figure 7 shows the comparison between the  $E'$  values with the actual soil profile stratification depth. Like the  $S_u$  values determination, the effective soil modulus ( $E'$ ) also relies on each layer's SPT-N value. For practical purposes, the suggested correlations equations between SPT-N values with Undrained Soil Strength ( $S_u$ ) and Effective Young's Modulus ( $E'$ ) used in the Mohr-Coulomb model are summarized in Table 7. This correlation could be used for future projects near the area, assuming the soil stratification is similar.

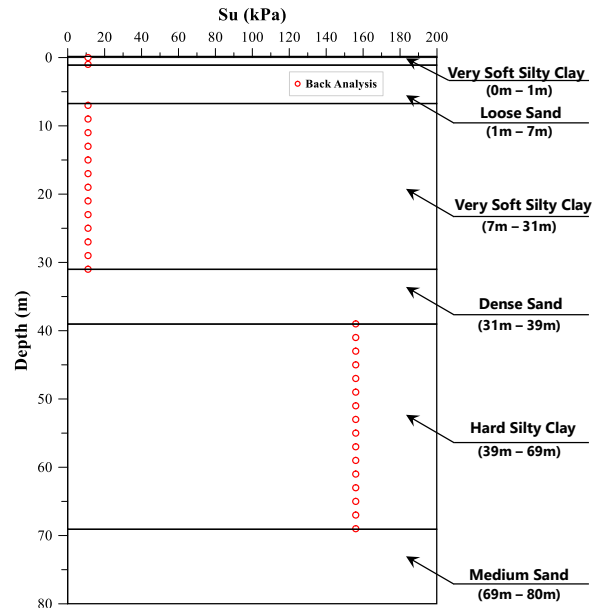


Figure 6. The profile of undrained shear strength with depth

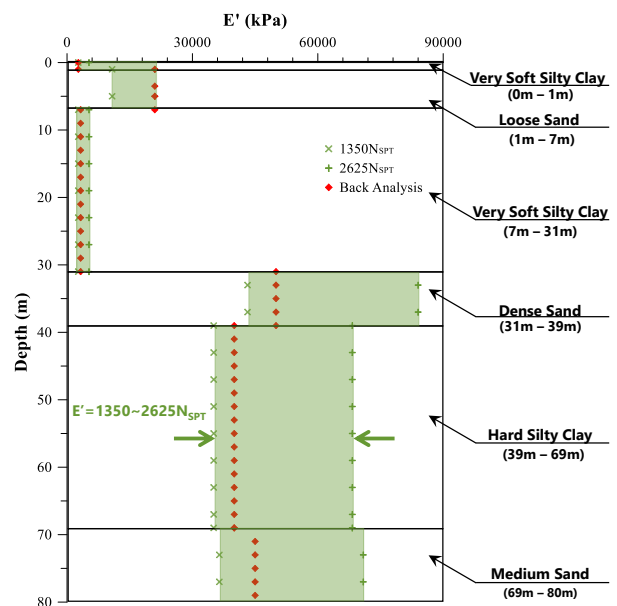


Figure 7. The profile of Effective Young's modulus with depth

Table 7.  $S_u$  and  $E'$  Correlation based on SPT-N Data Borehole 01

Layer	Soil Type	$S_u$ (kN/m <sup>2</sup> )	$E'$ (kN/m <sup>2</sup> )
1.	Very Soft – Silty Clay	$5.5 \times N_{SPT}$	$1350.0 \times N_{SPT}$
2.	Loose – Sand	-	$2625.0 \times N_{SPT}$
3.	Very Soft – Silty Clay	$5.5 \times N_{SPT}$	$1625.0 \times N_{SPT}$
4.	Dense – Sand	-	$1562.5 \times N_{SPT}$
5.	Hard – Silty Clay	$6 \times N_{SPT}$	$1538.5 \times N_{SPT}$
6.	Medium – Sand	-	$1666.7 \times N_{SPT}$

### 3.2 Load–Settlement Curve

The test results indicated that the spun pile was not tested until failure, while the finite element analysis was utilized to extrapolate the load-settlement curve to assess the maximum capacity of the tested pile. The pile is not tested until 200% of the design load is achieved because the cost of static pile testing is expensive, hence non-failure pile testing becomes common practice in the field. The load–settlement curve of the determined and computed finite element method analyses is shown in Figure 8. The results showed that the computed curve fitted properly with the measured data. Therefore, it can be concluded that the FE model and input parameters were valid and verified. According to Mazurkiewicz's theory, the ultimate pile capacity was 4110 kN.

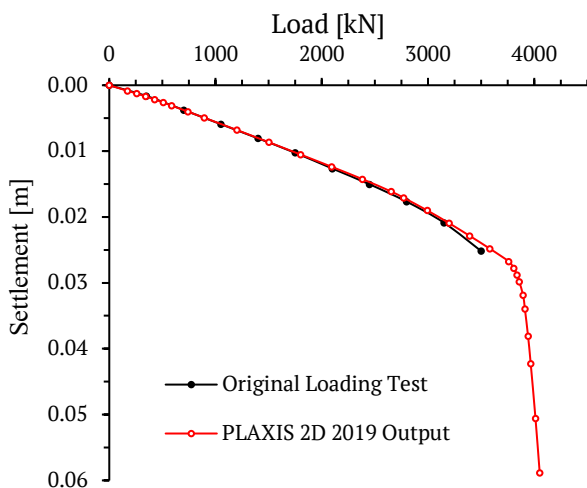
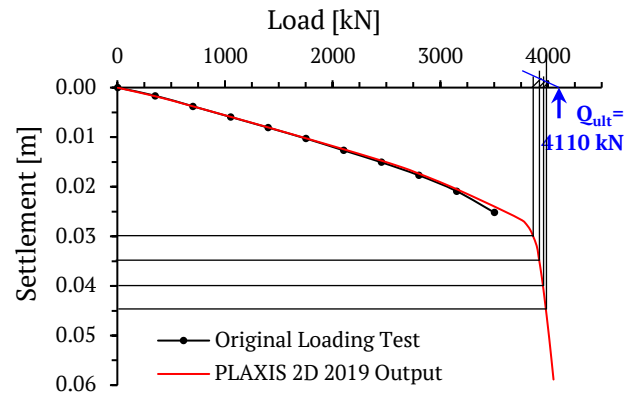
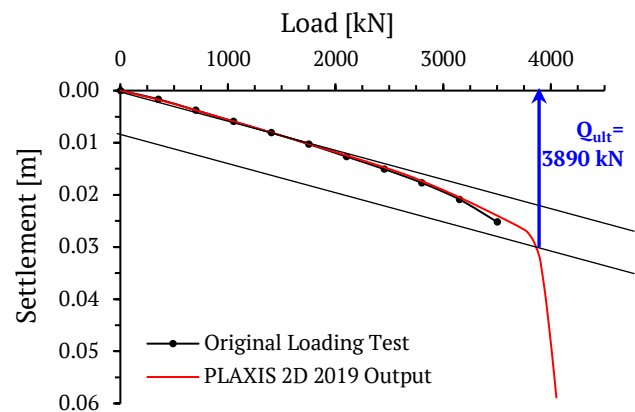


Figure 8. Comparison of measured and computed load-settlement curves

The interpretation of the pile ultimate capacity ( $R_{inter} = 1$ ) was carried out with Mazurkiewicz's and Davisson's Method after obtaining the extrapolated load-settlement curve with the PLAXIS 2D 2019 program. The calculation and determination of the ultimate capacity are shown in Figure 9. Davisson's method yields a smaller ultimate capacity than Mazurkiewicz, with a difference of approximately 5%.



a)



b)

Figure 9. Comparison of measured ultimate capacity value based on a different method: a). Mazurkiewicz's Method ( $Q_{ult} = 4110$  kN), b) Davisson's Method ( $Q_{ult} = 3890$  kN)

### 3.3 Influence of the Interface Coefficient ( $R_{inter}$ )

To study the influence of the interface values, the axially loaded single pile was modeled by various  $R_{inter}$  values, varying from 0.7 to 1. Therefore, the interface value is used to reduce the friction between the structure (pile foundation) and the adjacent soil was used to reduce the friction between the structures with sand or clay soil, according to Gouw (2014). Figure 10 shows experimental (trial and error) load–settlement curves with different  $R_{inter}$  values used to produce several forms of load-settlement curves. It shows that the variation of the soil-pile interface ( $R_{inter}$ ) influenced the changes and decreased the pile capacity before reaching failure conditions.

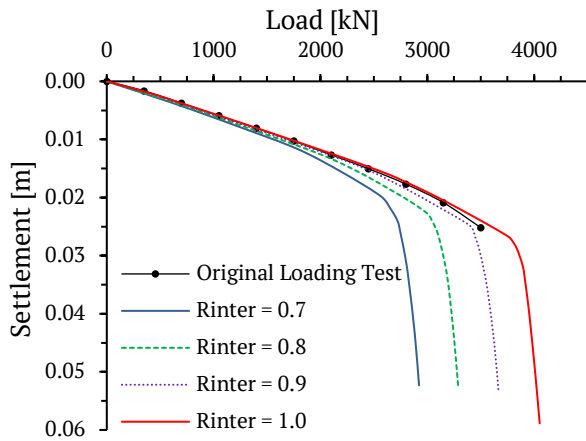


Figure 10. Load-Settlement Curves for A1204 pile with variations of  $R_{inter}$  values

### 3.4 Influence of the Pile Embedded Length

Another parametric study was also performed with the different lengths of embedment piles, such as 35 m and 47.50 m, with the load-settlement curve result shown in Figure 11. The ultimate capacity of the driven pile with an embedded length of 35 m is smaller by 47.5 m due to skin friction.

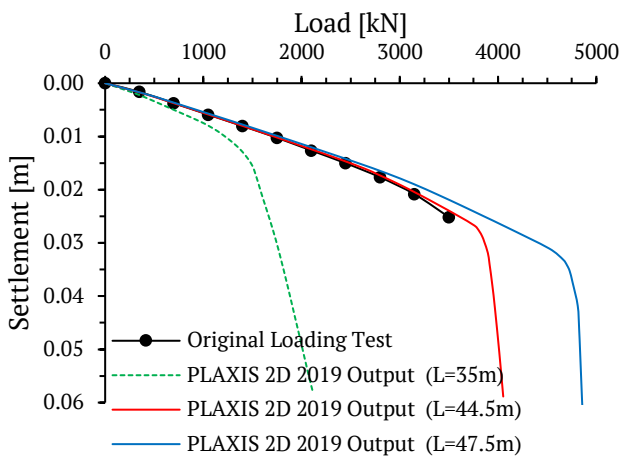


Figure 11. Load-Settlement Curves for A1204 pile with variations of pile length.

## 4 CONCLUSION

This study used a 2D finite element to analyze the pile foundation located in the Northern Jakarta Coastal Area, Indonesia. Furthermore, several geotechnical engineering parameters of soil, such as undrained shear strength and effective modulus, were achieved using data from an in-situ soil site investigation and empirical correlations with SPT-N. The simulation of the 2D

Finite Element model for forecasting the ultimate pile capacity was validated in this study. The results shows that the pile load test is successfully simulated using finite element analysis. The computed load settlement curve is generally close to the measured data. Furthermore, the empirical correlation according to SPT-N values is developed to obtain the Undrained Shear Strength and Effective Young's modulus. The effective soil modulus for clay was estimated as  $E' = 1350 N_{SPT}$  (kPa) and  $E' = 2625 N_{SPT}$  (kPa) for sand, while the Undrained Shear Strength ( $S_u$ ) was estimated at  $5.5 N_{SPT}$  and  $6 N_{SPT}$ . This empirical correlation is valid for the soil near the project. Meanwhile, further study needs to be carried out for other locations. The interpretation of ultimate pile capacity by Mazurkiewicz and Davisson's methods yielded a close result, with a 5% difference. Numerical results showed that reducing  $R_{inter}$  values leads to a smaller load-settlement curve with a decrease in load.

### DISCLAIMER

The authors declared no conflict of interest.

### AVAILABILITY OF DATA AND MATERIALS

All data are available from the author.

### AUTHOR CONTRIBUTION STATEMENTS

Aswin L contributes in conceptualization, writing-original draft, writing-review and editing, and supervision. Varian H. B carried out the FEM analysis, wrote- review and edited the manuscript, collected the field data, and plot figures. Yiska V. C. W performed the FEM analysis, wrote- review and edited the manuscript, and plot figures.

### ACKNOWLEDGMENTS

The authors are grateful to PT. Pakubumi Semesta, for providing detailed geotechnical information on this case study.

### REFERENCES

ASTM D1586-67, 1978. *Standard Method for Penetration Test and Split-Barrel Sampling of Soils*. United States of America: American Society for Testing and Materials.

- ASTM D1143, 2007. *Standard Test Methods for Deep Foundations Under Static Axial Compressive Load*. United States of America: American Society for Testing and Materials.
- Bruno, D., & Randolph, M., 1999. Dynamic and Static Load Testing of Model Piles Driven into Dense Sand. *Journal of Geotechnical and Geoenvironmental Engineering*, 125(11), pp. 988-998.
- Coduto, D.P., 2001. *Foundation Design Principles and Practices 2<sup>nd</sup> ed.* New Jersey: Prentice-Hall, Inc.
- Crispin, J., Leahy, C., & Mylonakis, G., 2018. Winkler Model for Axially-Loaded Piles in Inhomogeneous Soil. *Géotechnique Letters*, 8(4), pp. 290-297.
- Dandagawhal, S., 2018. Settlement Analysis of Pile Foundation using Plaxis 2D. *International Journal of Science and Research*, 8(9) pp. 1706-1714.
- Das, B.M., 2016. *Principles of Foundation Engineering*. Boston: Cengage Learning.
- Dias, T.G.S. & Bezuijen, A., 2018. Load-Transfer Method for Piles under Axial Loading and Unloading. *J. Geotech. Geoenviron. Eng.*, 144(1):04017096.
- Dijkstra, J., Broere, W., & Heeres, O.M., 2011. Numerical Simulation of Pile Installation. *Computers and Geotechnics*, 38 (5), pp. 612-622.
- Gouw, T.L., 2014. Common Mistakes on the Application of Plaxis 2D in Analyzing Excavation Problems. *International Journal of Applied Engineering Research*, 9(21) pp. 8291-8311.
- Hutabarat, L.E., Rainaldo, D., Ilyas, T., & Prakoso, W.A., 2019. Site Characterization of Marine Clay Consolidation Ratio on Kamal Muara Area, Northern Jakarta. *South Lampung: International Conference on Science, Infrastructure Technology and Regional Development*.
- Karlsruh, K., 2014. Ultimate Shaft Friction and Load-Displacement Response of Axially Loaded Piles in Clay Based on Instrumented Pile Tests. *Journal of Geotechnical and Geo-environmental Engineering*, 140 (12) : 04014074.
- Kitiyodom, P., Matsumoto, T., & Kanefusa, N., 2004. Influence of Reaction Piles on The Behaviour of a Test Pile in Static Load Testing. *Canadian Geotechnical Journal*, 41(3), pp. 408-420.
- Li, J., Tan, Y. & Liang, F., 2012. A Modified Analysis Method for the Nonlinear Load Transfer Behaviour of Axially Loaded Piles. *KSCE J. Civ. Eng*, 16 (3), 325-333.
- Lu, X., Li, P., Chen, B., & Chen, Y., 2005. Computer Simulation of The Dynamic Layered Soil-Pile-Structure Interaction System. *Canadian Geotechnical Journal*, 42(3), pp. 742-751.
- Mahmoud, H.N., Tetsuo, T., Susumu, I., & Mourad, K., 2014. On the Influence of Vertical Loads on the Lateral Response of Pile Foundation. *Computers and Geotechnics*, 55, pp. 392-403.
- Nasrollahzadeh, E. & Hataf, N., 2019. Experimental and Numerical Study on The Bearing Capacity of Single and Groups of Tapered and Cylindrical Piles in Sand. *International Journal of Geotechnical Engineering*. pp. 1-12.
- PLAXIS. 2019. *Manual Tutorial Plaxis 2D 2019*. Netherlands: Delft University of Technology & PLAXIS.
- Randolph, M.F., 2003. Science and Empiricism in Pile Foundation Design. *Geotechnique*, 53(10), pp. 847-875.
- Rojas, E., Valle, C., & Romo, M. P., 1999. Soil-pile Interface Model for Axially Loaded Single Piles. *Soils and Foundations*, 39(4), pp. 35-45.
- Said, I., Gennaro, V.D., & Frank, R., 2009. Axisymmetric Finite Element Analysis of Pile Loading Tests. *Computers and Geotechnics*, 36 (1-2), pp. 6-19.
- Taqwa, F.M.L, Hutabarat, L.E., Ilyas, T., & Prakoso, W.A., 2019. *Estimation of Settlement Induced Land Subsidence of Marine Clay on Kamal Muara Area, Northern Jakarta, Based on the Change of Pore Water Pressure. Lampung: 2018*

*International Conference on Engineering, Technologies, and Applied Sciences.*

Tomlinson, M., 1994. *Pile Design and Construction Practice*. Fourth Edition. London: E & F N Spon.

Zhou, J.J., Wang, K.H., Gong, X.N., & Zhang, R.H., 2013. Bearing Capacity and Load Transfer Mechanism of a Static Drill Rooted Nodular Pile in Soft Soil Areas. *Journal of Zhejiang University-Science A.*, 14, pp. 705–719.

# The Building Information Modeling (BIM)-Based System Framework to Implement Circular Economy in Construction Waste Management

Tantri N. Handayani<sup>1\*</sup>, Kartika N. R. Putri<sup>1</sup>, Nurul A. Istiqomah<sup>1</sup>, Veerasak Likhitrungsilp<sup>2</sup>

<sup>1</sup>Department of Civil and Environmental Engineering, Universitas Gadjah Mada, Yogyakarta, INDONESIA  
Jalan Grafika No 2 Yogyakarta

<sup>2</sup>Department of Civil Engineering, Faculty of Engineering, Chulalongkorn University, Bangkok, THAILAND  
254 Phayathai Road, Wangmai, Pathumwan, Bangkok

\*Corresponding authors: [tantri.n.h@ugm.ac.id](mailto:tantri.n.h@ugm.ac.id)

SUBMITTED 30 July 2021 REVISED 16 September 2021 ACCEPTED 4 October 2021

**ABSTRACT** The tremendous quantity of waste produced from construction and demolition is a major cause of environmental degradation. This quantity tends to increase due to the rapid growth of building development and renovation. Meanwhile, construction waste management is a complex and costly process due to the fact that it requires different kinds of resources such as money, land, and technology. It is often ignored by all project participants even though it is an essential element of construction project management. However, it has been discovered that modern construction waste management is structured based on the concept of circular economy which focuses on eliminating construction waste and maximizing the value of materials. Therefore, this research proposes an innovative framework to implement the circular economy using building information modeling (BIM) in order to improve the construction waste management process. This involved a thorough review of past literature to identify the implementation of the concept of circular economy, waste management, and the application of BIM, also the research gaps observed were used to develop the functionality of the proposed framework. The five functionalities include (1) visualization and data integration, (2) direct construction waste quantity take-off, (3) BIM-based sorting system and selection of appropriate disposal parties, (4) estimating cost and schedule of waste disposal, and (5) simulation and monitoring report. This BIM system was designed to analyze material waste, quantity, disposal time, and waste treatment based on project conditions, material quantities, and schedule. It can also be used to plan and monitor the construction waste process, thereby making it possible to avoid the disruption of productivity and project time usually caused by unplanned waste management activities. Moreover, the proposed on-site sorting system also has the ability to facilitate the adoption of the circular economy concept during the construction phase.

**KEYWORDS** BIM-Based System; Waste Management Planning; Construction Project Management; Circular Economy; Quantity Take-off; Construction Materials Recycle.

© The Author(s) 2022. This article is distributed under a Creative Commons Attribution-ShareAlike 4.0 International license.

## 1 INTRODUCTION

The construction industry is growing rapidly worldwide and also serves as a pillar of the global economy. However, it was discovered to be contributing a significant amount of waste, thereby causing environmental degradation. These construction wastes are associated with the solid waste generated from construction and demolition projects such as concrete, wood products, drywall and plasters, steel, brick and clay tile, asphalt shingles, and asphalt concrete (EPA, 2020). In 2018, a total of 600 million tons of these wastes was generated in the US (EPA, 2020) while 67.8 million tons in the UK (DEFRA, 2021). These numbers reflect the urgency to manage waste accordingly due to the fact that

the use of landfills has been discovered to be causing subsequent problems such as social impacts and environmental degradation.

The circular economy is a modern concept designed to minimize the impact of operations on the environment. It was used to transform the traditional linear economy which involves "make, use, and dispose" to a new paradigm that minimizes input, waste, emission, and energy leakage by keeping a product in use for as long as possible and recreating new resources at the end of its service life (Geissdoerfer *et al.*, 2017). The concept is mainly associated with the 3R principles of reduce, reuse, and recycle to

achieve a more sustainable economy (Anastasiades *et al.*, 2020). Several attempts have been made to develop reused materials such as brick materials (Fořt and Āerný, 2020) and sewage sludge ash (Smol *et al.*, 2015a). Moreover, circular economy in construction is associated with technical solutions, user behavior and ownership, bio-based construction, and circularity assessments (Anastasiades *et al.*, 2020). Meanwhile, the efficiency of the design, assembling the reused materials, and minimization of waste have been investigated to support the technical solution aspect. Another potential implementation of circular economy in construction is to improve waste management by changing the current strategies, which are focused on the management after generation, to the aspect related to the prevention (Ajayi *et al.*, 2015). This process requires estimating the amount of waste, scheduling its disposal, quantifying its cost, and collaborating with the parties with the ability to recycle the waste materials. However, there is a need to apply digital technology to ensure the waste management plan is efficiently implemented without expanding the scope of work during the pre-construction process.

Building Information Modeling (BIM) is a virtual representation of building conditions which allows the integration of information to support different aspects of project management throughout the project life cycle. Several BIM-based systems have been proposed to implement a circular economy towards managing construction waste. For example, the disassembly and deconstruction analytics system (D-DAS) introduced to support building design by determining energy costs and waste output indexes (Akanbi *et al.*, 2019). Another is the BIM-based waste management designed to develop waste management plans (Won and Cheng, 2016). However, these systems were discovered to lack coordination and collaboration to support the recycling process.

This research was conducted to thoroughly analyze the current waste management processes and synthesize the findings to develop

a BIM-based waste management system with the ability to address the problem more comprehensively. The process involved exploring the potential of BIM to implement the circular economy in construction waste management, analyze the concept based on its implementation in construction projects, as well as evaluate several strategies designed to accelerate its implementation to identify the gaps and potentials. Moreover, the current waste management practices in construction projects were investigated using BIM and the findings were integrated with past literature to establish the framework for a BIM-based circular economy to plan waste management in construction projects by minimizing wastes and maximizing the value of materials.

## 2 METHOD OF THE RESEARCH

A semi-systematic literature review was conducted by gathering relevant literature using designated keywords such as circular economy, waste management, and BIM. The state-of-the-art issues from these researches were examined and categorized into three main groups which are circular economy in construction, current construction waste practices, and BIM implementation in waste management with each sub-categorized based on the object of the research or project life cycle. Moreover, potential future research works were also investigated. It is important to note that the circular economy group was the point of departure to ensure the implementation of BIM in construction waste management, while the waste management and current BIM implementation groups were the references to develop the functionality of the proposed framework which was further elaborated to fill the research gap.

## 3 CIRCULAR ECONOMY IN CONSTRUCTION

Circular economy challenges the end-of-life concept by ensuring the prolonged use of materials through reuse, reduce, recover, and recycle principles (Kirchherr *et al.*, 2017). It embraces a regenerative and restorative concept to maximize both value and utility of the products, elements, and materials during their

service life (Geissdoerfer *et al.*, 2017). The concept has been discovered to be enabling economic growth as indicated by its implementation in several countries. Nevertheless, the implementation process requires certain changes and innovations associated with systems, policies, and organizations.

The actualization of the circular economy is being resisted by some individuals and more severely at the industrial level (Adams *et al.*, 2017). This is observed to be related to the limited knowledge regarding its adoption and the lack of incentive to accelerate the process. Moreover, there is limited discussion on the universal measurement model for the circular economy transition which makes it impossible to track the progress of the implementation process (Jones and Comfort, 2018). These issues persist despite the possibility of using the concept in five important phases including the design, production of materials, construction, maintenance, and the end-of-life (Núñez-Cacho *et al.*, 2018).

There is a need for a paradigm shift from the traditional “linear” design to a “circular” economy through the selection of a suitable project delivery system involving several concepts such as green-field construction, adaptive reuse, and closed-loop cycle construction (Sanchez and Haas, 2018). Therefore, an innovative procurement system was proposed which involves adopting a relational type of contract associated with winning the trust of different parties in order to stem emerging problems through sustainable development of circular economy (Bao *et al.*, 2019). It was also argued that the use of a design tool such as BIM can be a solution in terms of the design (Hossain *et al.*, 2020; Núñez-Cacho *et al.*, 2018).

Defining the supply chain method to be used during the construction phase is essential in designing a circular material supply chain which involves transportation of reused materials and production of lower carbon emission (Nasi *et al.*,

2017). Another research proposed a strategy to design a waste minimization method during the pre-construction phase by prioritizing recovery strategies over landfilling (Ruiz *et al.*, 2020). Gínga *et al.* (2020) also showed similar findings which promote eliminating construction wastes observed to be threatening the environment. Meanwhile, ineffective waste deconstruction, sorting, and transportation are the main parts of the waste management practices considered to present the most crucial barrier to the adoption of a circular economy (Mahpour, 2018). These problems were addressed in this current research by proposing a functionality framework which focuses on waste management. The scope of the proposed framework encompasses waste treatment and collaboration among the relevant parties to expand the strategies required to implement the 3R principle.

Several researches on the circular economy focused on inventing new materials from the wastes to preserve the end-of-life of resources (Smol *et al.*, 2015; Osobajo *et al.*, 2020). Some other initiatives were also developed to reuse materials such as brick wastes as substitutes for Portland cement (Fořt and Černý, 2020) and sewage sludge ash in concretes (Smol *et al.*, 2015). Several materials have also been discovered to have the potential to be reused and recycled such as clay bricks, structural timber, structural steel, and concrete blocks (Iacovidou and Purnell, 2016). However, the process of recycling materials is also faced with some challenges associated with logistics (41%), cost (29%), time (12%), regulations (12%), and others (6%) (Ghaffar *et al.*, 2020).

It should be noted that the circular economy can be adopted throughout the project life cycle but this current research focuses primarily on project design in the pre-construction phase as well as the use of BIM technology in planning wastes before the construction process and selecting appropriate stakeholders to be included in the waste management system. Moreover, improving the current practices on circular economy such as the establishment of relevant waste plans is very important and this means

there is a need to examine the key areas of construction influencing its acceleration (Hossain *et al.*, 2020). The outline of the aforementioned circular economy concept is presented in the following Figure 1.

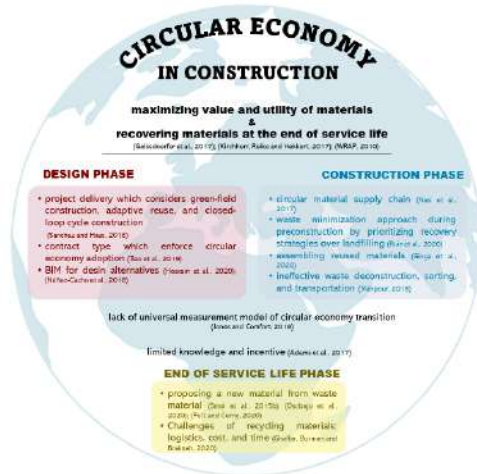


Figure 1. Outline of the circular economy concept in construction

#### 4 CURRENT CONSTRUCTION WASTE MANAGEMENT PRACTICES

Demolition is the construction process with the highest quantity of wastes followed by the civil and foundation works (Lu *et al.*, 2015). These processes generate the top three construction material wastes namely concrete, asphalt concrete, and wood products (EPA, 2020). The diversity in the properties of these materials and their waste management practices show there is a need to focus on each of them separately in preparing a waste management plan.

The impact of construction waste is not limited to the environmental pollutions and ecological damage, but also the cost overruns, project delays, economic losses, and social impact (Nagapan *et al.*, 2012). The current management practices are observed to be weakened by lack of regulation, low percentage of on-site waste sorting, poor waste reduction, and the lack of systematic planning such as recycling facilities (Yuan, 2013). Moreover, the previous research correlated waste management with social performances such as public satisfaction, public appeal to regulate dumping waste, new job opportunities, and physical working conditions

in addition to its effect on the environmental and project goals (Yuan, 2012).

Most architects do not consider waste minimization strategies during the design phase because the process is placed on a low priority (Osmani, *et al.* 2008) possibly due to the lack of appropriate policies for its enforcement and the absence of adequate incentives. The contractors also believe an appropriate waste management practice can reduce their profit due to the lack of incentives, practical tools, and guidelines (Papargyropoulou, 2011). This finding contrasts with another research where waste management practices were perceived to be beneficial in terms of cost savings and profit maximization, but the relationship between project characteristics and the benefits was not clarified (Hwang and Yeo, 2011). This simply shows that the perception of waste management systems varies in each case.

A waste management policy can be a supportive tool to achieve success. For example, Hong Kong's waste management policy designed using the 3R and "polluter pays" principles was perceived to be effective in reducing construction waste at landfills (Lu and Tam, 2013). Another research showed that the waste disposal charging scheme was perceived to be efficient by only 40% of the respondents due to the existence of some inevitable wastes and the fact that the cost was not high enough to raise awareness (Poon *et al.*, 2013). It is also possible to support waste minimization through the occasional imposition of penalties for poor waste management parties (Arif *et al.*, 2012).

The waste generation rate is a key performance index of waste management (Lu *et al.*, 2015) and this means that it is necessary to select an appropriate method to estimate the construction waste. This can be achieved based on the quantity of the work which is categorized by the type such as demolition, wreckage, and waste packaging (Solís-Guzmán *et al.*, 2009). The rate can also be influenced by policies, for example, the waste calculation method in Hong Kong was shifted from the gross floor area or total contract sum to the payment of contract sum for each

work (Poon *et al.*, 2013). This policy provides future opportunities to create an incentive for contractors that submit waste estimation during the tender process (Arif *et al.*, 2012). Therefore, it is necessary to adjust the waste calculation method, document the amount of waste, and monitor the actual waste generated. These features are addressed in this research to develop the framework for the proposed waste management system.

The process of disposing construction wastes varies from one country to another. This is observed from the findings of Hossain, *et al.* (2017) that the construction waste in Hong Kong is usually generated in the form of mixed wastes to be sorted at both on-site and off-site sorting areas. The non-inert wastes are normally processed to landfills while inert wastes are usually managed using the public fill. Meanwhile, an on-site sorting system was suggested to be adopted due to its effectiveness and ability to reduce environmental impacts. It also has the ability to promptly determine the next step for the recycled materials such as a direct reuse on-site, transportation to the recycled plants for processing, or transportation to landfills and public fill facilities. However, there is a lack of adequate information on the related parties despite the ability of this sorting system to separate the recycled materials effectively. It was also discovered that the wastes are usually moved directly to the landfill (Nagapan *et al.*, 2012) or burnt illegally (Papargyropoulou, 2011) in a situation where there is no waste management or sorting system, thereby endangering the environment. Therefore, these research findings and gaps indicate the need to include waste disposal plan destinations, specify waste carriers, and document recovery actions systematically in the waste management process. This proposition conforms with the findings of Saez *et al.* (2013) that it is possible to reduce construction waste by recruiting suppliers specialized in managing waste products and planning the sizes of the containers to match the construction activities. It is important to note that these aspects were

also considered in the development of the proposed framework.

Several innovative tools and technologies have been adopted to support the waste management process and these include the Waste Management Plan template and Designing Out Waste Tool Building which incorporate plans, outputs, and costs (WRAP, 2010). A similar tool, SMARTWaste, (BRE, 2021) was also developed to estimate the construction wastes to be generated but these technologies are limited by the lack of collaboration between related parties and the flexibility of waste calculation methods. The adoption of BIM is believed to have the ability to create a framework to address the current problems observed in waste management (Osmani and Villoria-Sáez, 2019). Therefore, a BIM-based framework was developed in this current research to address these problems systematically and efficiently.

## **5 BIM IMPLEMENTATION ON WASTE MANAGEMENT AND CIRCULAR ECONOMY**

BIM has been verified to have the ability to support waste management through design review, 3D coordination, quantity take-off, phase planning, site utilization planning, construction system design, digital fabrication, and 3D control and planning (Won and Cheng, 2017). It also accommodates the requirements of the stakeholders in its implementation and strengthens several features such as collaboration, waste-driven design, waste analysis during the whole project lifecycle, innovative analysis, and systematic documentation in the waste management process (Akinade *et al.*, 2018).

A BIM-Deconstructability Assessment Score (BIM-DAS) was proposed to assist the designer in selecting the best design among possible alternatives via an assessment score which considers the reusability, recyclability and secondary finishes, as well as the toxicity of the materials (Akinade *et al.*, 2015). This system can also simulate design alternatives and their assessment scores. Moreover, another waste management tool was proposed to accommodate

both design options and construction schemes through the automatic estimation of the wastes in each scenario considering the fact that the waste generated waste cannot be incorporated into the design (Lu *et al.*, 2017). Therefore, the waste generation was calculated by mapping the component on the database of the average waste generation level. Another research also showed the ability of BIM to support the design process with a specific focus on the processes involved in assembling and disassembling a building which consists of collaboration, visualization of deconstruction, quantification of recoverable materials, deconstruction plan, simulating end-of-life alternatives, and improving building lifecycle (Akinade *et al.*, 2017). It can be discovered that several BIM-based systems have been used to select, simulate, and optimize design alternatives, but they are not designed specifically to support waste management.

Several BIM-based systems are integrated into database systems such as the material & component bank which stores materials and components for basic waste management in order to ensure the efficiency of the systems (Jayasinghe and Waldmann, 2020). This concept was also adopted in this research to manage non-geometric information due to the fact that the 3D models primarily focus on geometrical information.

BIM is an efficient tool to perform quantity take-off of construction materials and can also be extended to the estimation of waste quantity. A BIM-based system was reported to have been used to estimate the wastes during the design review through clash detection and constructability review (Won *et al.*, 2016). This was conducted using a work breakdown structure provided in the BIM-based software and material classification standards (Kim *et al.*, 2017). Moreover, the accuracy of the process was enhanced through the integration of a linear BIM-based quantity take-off into the material purchasing database (Guerra *et al.*, 2019). It was observed that there was a lack of collaboration between the disposal parties and this is expected to be addressed through the proposed system

which was designed to estimate the amount of waste generated and the waste disposal charging fee based on the waste facilities available (Cheng and Ma, 2013). These findings were adopted in this current research to develop an extensive monitoring system for waste disposal practices.

This means the BIM has the capability to ensure the prolonged use of materials at the end of their service life. Previous research also showed that As-built BIM models can be used to develop a demolition plan in line with the preferred method and waste identification system (Ge *et al.*, 2017). They also serve as the tool to perform a cost-benefit analysis for demolition waste management (Hamidi *et al.*, 2014) even when the details of the framework have not been developed. However, the current framework of BIM implemented is based on local policies (Akbarieh *et al.*, 2020) without global coverage. Therefore, the proposed framework was designed to be flexible to ensure it can be easily implemented in any organization or country.

## 6 FUNCTIONALITY OF THE PROPOSED FRAMEWORK

The proposed framework is primarily designed to manage waste during construction with a focus on the quantity of waste, time of disposal, cost, as well as disposal parties and places. This is based on the fact that the integration of the BIM has the ability to plan waste management during the pre-construction phase and also to monitor the waste management process during the construction phase. The visualization of the BIM-based system allows the thorough understanding of the site conditions while the data integration system has the ability to create a systematic workflow, provide a high level of calculation accuracy, and support mutual collaboration works. Moreover, the use of quantity take-off by BIM leads to accurate waste estimates. The development of the framework functionality is presented in Figure 2.

Some of the uses of BIM in waste management include 4D simulation, quantity take-off, design review, 3D coordination, and site utilization planning (Won and Cheng, 2017). The proposed

framework only adopted the 4D simulation and quantity take-off to achieve the research objectives, but it is possible to extend these functionalities to a BIM-based platform in order

to ensure its actual implementation. Therefore, the features of the proposed BIM-based framework are presented in the following Figure 3.

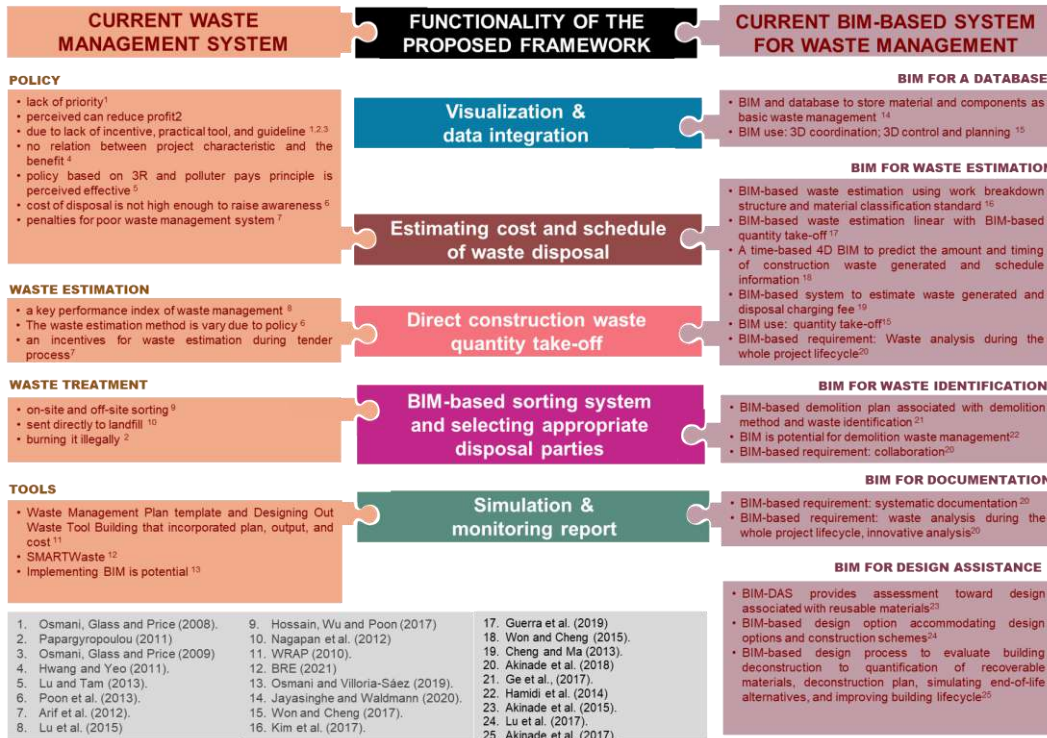


Figure 2. Research gaps and the proposed framework

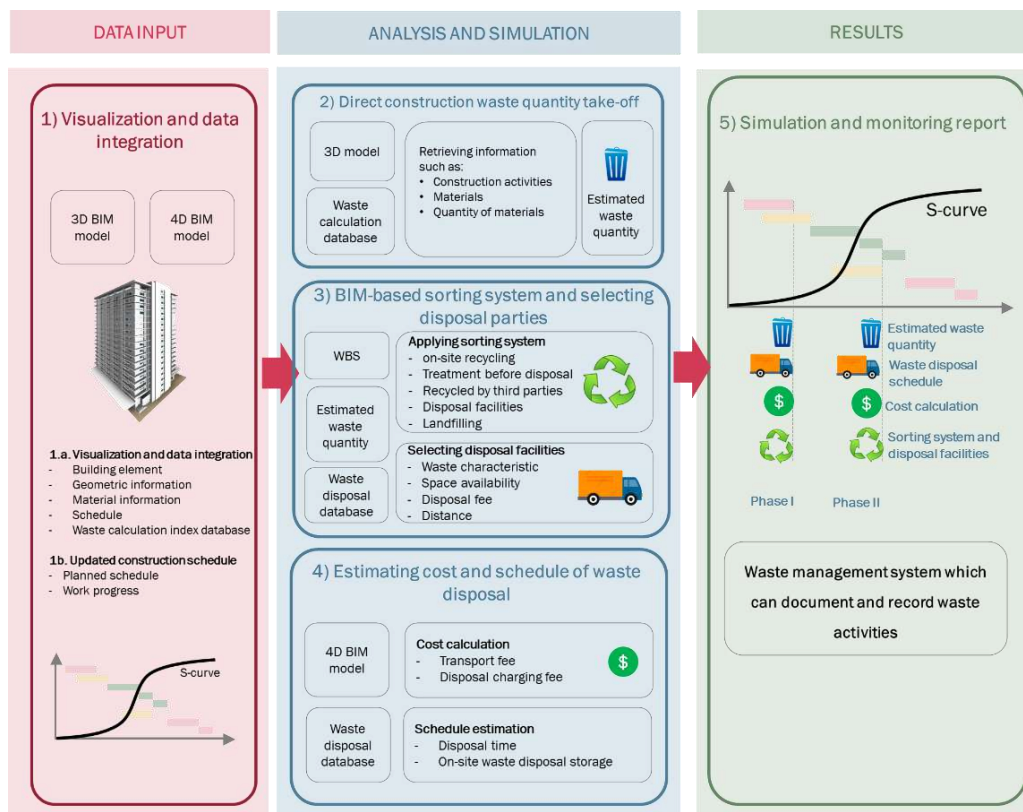


Figure 3. The functionality of the proposed framework

### 6.1 Visualization and data integration

The proposed system involves a 3D BIM model which was used as the central database consisting of the geometric information of the building elements such as the identity, size, shape, length, and material of each element. It is important to note that the BIM model has the same level of detail (LOD) as required in the construction phase to obtain an accurate estimate for the wastes. Moreover, the model includes every permanent part of the building elements in order to clearly present the actual building conditions.

The BIM model also contains important non-geometric information necessary for further analyses such as cost, schedule, and the database of disposal parties which are integrated by analyzing the work breakdown structure (WBS) of the model. The correlations between the non-geometric information and the building elements were later identified and represented by codes. It is important to note that the scope of the data integration encompasses the waste generation indexes to estimate the waste, schedule information, the sorting system for each material, and the disposal parties. Several methods have been proposed to integrate the geometric and non-geometric information and some of these include using the element ID and Dynamo program (Handayani *et al.*, 2019) and the WBS (Kang *et al.*, 2010). However, the ability of the model to simulate design alternatives using parametric modeling in order to determine the design with the minimum waste (Hang *et al.*, 2021; Likhitrungsilp *et al.*, 2019) was not included in this research.

### 6.2 Direct construction waste quantity take-off

Previous discussions showed the need for the system to be adjustable to different waste estimation methods due to the fact that the process of estimating waste is based on the amount of construction works conducted. This was achieved in the proposed system by extracting the quantity of the material from the 3D model along with the associated information. The data and information extracted are expected to be user-friendly in order to facilitate the

appropriate exchange of information and waste estimation. Moreover, the 3D model was observed to have yielded accurate estimation results and this can be applied to place orders for materials during the construction phase. This simply shows that the BIM model is adjustable to the change in the site condition during the construction process.

It is recommended that further research needs to be conducted to incorporate the waste estimation method as well as an integrated database for storing the parameters such as waste estimation indexes into the system. It is also advisable to organize the database based on materials, modular and non-modular types, and types of waste generated in order to automate the process and ensure it requires fewer inputs from the users. In addition, the system can also be extended through the addition of features relating to waste minimization for modular materials by optimizing construction methods and simulating alternative installment scenarios.

### 6.3 BIM-based sorting system and selecting appropriate disposal parties

The structure of the BIM-based sorting system module was based on the work breakdown structure (WBS) which consists of different activities involved in the construction, materials, and waste generated. The system was further sub-categorized into inert and non-inert waste, potential on-site recycling materials, potential recycling by third parties, public disposal facilities, free or non-free disposal facilities, and landfills. This hierarchical structure represents the 3R principle which is in line with the concept of circular economy formulated to minimize environmental degradation.

Most of the current waste management systems focus on estimating wastes and the disposal system was observed to be directly related to the design of construction waste management as previously discussed. However, these disposal methods need to be evaluated to determine whether the construction waste materials are causing environmental degradation or ensuring

the end-of-life of materials is prolonged in order to support the circular economy concept. This can be achieved by using the data integration system which allows the connection of each waste generated to disposal parties and also makes it possible for the sorting system to select the appropriate disposal facilities or recycling parties based on several parameters such as the waste characteristics, space availability, disposal/recycling fees, and distance. These outcomes aided the linkage of the disposed wastes to appropriate parties in order to minimize emissions usually caused by transportation.

#### 6.4 Estimating cost and schedule of waste disposal

The main results of integrating geometric and non-geometric data are 4D and 5D BIM models which allow the estimation of the waste quantity based on the values derived from the BIM model and waste calculation database. The estimates were used to determine the associated costs such as disposal charging fees and transportation costs which are usually obtained based on the sorting system and the selected disposal parties.

The 4D BIM model in the proposed system is required to be regularly updated in order to reflect the construction progress and actual schedule. This information and the estimated quantity of waste usually provide the contractor with an early warning concerning the disposal schedule. The proposed system also optimizes the time of waste disposal by considering the on-site storage and this allows the contractor to plan the resources to be used in managing wastes. Meanwhile, the possibility of preparing this estimation before the construction process is initiated makes it constructive for the contractor to submit the bidding documents with a detailed waste management plan.

#### 6.5 Simulation and monitoring report

The waste management plan prepared before the construction process can be used as a guideline during the construction. This is possible because the BIM-based system can be updated to reflect the change in the schedule information and

construction conditions. Moreover, it is necessary to record the quantity of wastes and the result of the sorting system, method of disposal, as well as the correlation of cost and time for each waste disposal activity. This is necessary to ensure that there is a systematic record of waste disposal activities for the project and which can be used later for further analyses.

## 7 CONCLUSION

This research was conducted to investigate the implementation of circular economy in the construction industry through the maximization of the construction materials value and recovery of these materials at the end of their service life. The major challenges observed with this concept include the lack of a universal measurement for the circular economy transition as well as limited knowledge and incentive. However, managing wastes and reusing construction materials were reported to have a major role in promoting circular economy in construction, but they were observed to be from perfect due to a lack of incentives, practical tools, and guidelines for waste quantification. Therefore, BIM is considered a potential innovation to improve the management process and this research examined the efficiency of its application in waste management.

The formulation of waste management plans involves estimating the quantity of waste, documenting waste disposal activities, and selecting the appropriate waste disposal alternatives with the ability to prolong the end-of-life of materials in order to achieve the goals of the circular economy concept. The gaps observed in the findings of these previous researches were synthesized with the BIM to develop a framework system for the circular economy. The functionality of this proposed BIM-based waste management system consists of five modules, namely: (1) visualization and data integration, (2) direct determination of construction waste quantity take-off, (3) BIM-based sorting system and selection of appropriate disposal parties, (4) estimation of cost and schedule of waste disposal, and (5)

simulation and preparation of monitoring report.

The visualization module used the BIM to represent the conditions of the facility effectively while the data integration concept was introduced to manage the geometric and non-geometric information of the facility. Moreover, the BIM was also used to estimate the waste and associated costs due to its ability to quantify materials accurately while the waste disposal schedule was established through the 4D BIM. It is also important to note that the work breakdown structure (WBS) in the BIM allowed the classification of the wastes to be disposed into suitable parties. Furthermore, the system has the ability to record and document waste activities based on the associated costs, schedule, and associated parties during the construction phase.

There are certain limitations observed with this proposed framework despite its numerous benefits in achieving the circular economy concept in construction. Therefore, additional functions such as information exchanges, platforms, and supporting tools are required to be developed further. It is also necessary to verify the reliability of the waste calculation by the system and to improve the flexibility of the proposed framework in adopting the organization code related to waste management. Moreover, the level of work breakdown structure needs to be evaluated to integrate the 4D and 5D BIM models and also to develop an appropriate BIM-based sorting system. The scope of the proposed waste management system can also be extended by considering the design and construction alternatives in order to minimize wastes. Furthermore, it is recommended that the proposed system be tested with a case research after it has been fully developed.

#### DISCLAIMER

The authors declare no conflict of interest.

#### AVAILABILITY OF DATA AND MATERIALS

All data are available from the author

#### AUTHOR CONTRIBUTION STATEMENTS

Tantri N. H conceived the idea and designed the analysis. Kartika N. R. P analyzed the literature regarding BIM, Nurul A. I. improving the topic on waste management, and Veerasak L. contributed on circular economy concept. All authors took a substantial contribution in developing the framework, discussing the result, and drafting the manuscript

#### ACKNOWLEDGMENTS

The author appreciates the Civil and Environmental Engineering Department, Universitas Gadjah Mada for funding this research.

#### REFERENCES

- Adams, K.T., Osmani, M., Thorpe, T. and Thornback, J., 2017. Circular economy in construction: current awareness, challenges and enablers. *Proceedings of Institution of Civil Engineers: Waste and Resource Management*, 170(WR1), pp.15–24.
- Ajayi, S.O., Oyedele, L.O., Bilal, M., Akinade, O.O., Alaka, H.A., Owolabi, H.A. and Kadiri, K.O., 2015. Waste effectiveness of the construction industry: Understanding the impediments and requisites for improvements. *Resources, Conservation and Recycling*, 102, pp.101–112.
- Akanbi, L.A., Oyedele, L.O., Omoteso, K., Bilal, M., Akinade, O.O., Ajayi, A.O., Davila Delgado, J.M. and Owolabi, H.A., 2019. Disassembly and deconstruction analytics system (D-DAS) for construction in a circular economy. *Journal of Cleaner Production*, 223, pp.386–396.
- Akbarieh, A., Jayasinghe, L.B., Waldmann, D. and Teferle, F.N., 2020. BIM-based end-of-lifecycle decision making and digital deconstruction: Literature review. *Sustainability (Switzerland)*, 12(7).
- Akinade, O.O., Oyedele, L.O., Ajayi, S.O., Bilal, M., Alaka, H.A., Owolabi, H.A. and Arawomo, O.O., 2018. Designing out construction waste using BIM technology: Stakeholders' expectations for industry deployment. *Journal of*

*Cleaner Production*, 180, pp.375-385.

Akinade, O.O., Oyedele, L.O., Bilal, M., Ajayi, S.O., Owolabi, H.A., Alaka, H.A. and Bello, S.A., 2015. Waste minimisation through deconstruction: A BIM based Deconstructability Assessment Score (BIM-DAS). *Resources, Conservation and Recycling*, 105, pp.167–176.

Akinade, O.O., Oyedele, L.O., Omoteso, K., Ajayi, S.O., Bilal, M., Owolabi, H.A., Alaka, H.A., Ayris, L. and Henry Looney, J., 2017. BIM-based deconstruction tool: Towards essential functionalities. *International Journal of Sustainable Built Environment*, 6(1), pp.260–271.

Anastasiades, K., Blom, J., Buyle, M. and Audenaert, A., 2020. Translating the circular economy to bridge construction: Lessons learnt from a critical literature review. *Renewable and Sustainable Energy Reviews*, 117, pp.1-11.

Arif, M., Bendi, D., Toma-Sabbagh, T. and Sutrisna, M., 2012. Construction waste management in India: An exploratory research. *Construction Innovation*, 12(2), pp.133–155.

Bao, Z., Lu, W., Chi, B., Yuan, H. and Hao, J., 2019. Procurement innovation for a circular economy of construction and demolition waste: Lessons learnt from Suzhou, China. *Waste Management*, 99, pp.12–21.

BRE, 2021. *SmartWaste -Environmental site monitoring and reporting software*. [Online] Available at: <https://www.bresmartsite.com/products/smartwaste/> [Accessed 26 July 2021]

Cheng, J.C.P. and Ma, L.Y.H., 2013. A BIM-based system for demolition and renovation waste estimation and planning. *Waste Management*, 33(6), pp.1539–1551.

DEFRA, 2021. *UK Statistics on Waste*. [Online] Available at: <https://www.gov.uk/government/statistics/uk-waste-data>. [Accessed 22 July 2021]

EPA, 2020. *Advancing Sustainable Materials Management*. Washington, DC. [online] Available

at: <https://www.epa.gov/facts-and-figures-about-materials-waste-and-recycling/advancing-sustainable-materials-management>. [Accessed 22 July 2021]

Forť, J. and Černý, R., 2020. Transition to circular economy in the construction industry: Environmental aspects of waste brick recycling scenarios. *Waste Management*, 118, pp.510–520.

Ge, X.J., Livesey, P., Wang, J., Huang, S., He, X. and Zhang, C., 2017. Deconstruction waste management through 3D reconstruction and BIM: a case research. *Visualization in Engineering*, 5(1).

Geissdoerfer, M., Savaget, P., Bocken, N.M.P. and Hultink, E.J., 2017. The Circular Economy – A new sustainability paradigm? *Journal of Cleaner Production*, 143, pp.757–768.

Ghaffar, S.H., Burman, M. and Braimah, N., 2020. Pathways to circular construction: An integrated management of construction and demolition waste for resource recovery. *Journal of Cleaner Production*, [online] 244, p.118710.

Ginga, C.P., Ongpeng, J.M.C. and Daly, M.K.M., 2020. Circular economy on construction and demolition waste: A literature review on material recovery and production. *Materials*, 13(13), pp.1–18.

Guerra, B.C., Bakchan, A., Leite, F. and Faust, K.M., 2019. BIM-based automated construction waste estimation algorithms: *Waste Management*, 87, pp.825-832.

Hamidi, B., Tanyel, B., Annie, P. and Walid, T., 2014. Potential Application of BIM in Cost-benefit Analysis of Demolition Waste Management. In: *Construction Research Congress 2014*. pp.279–288.

Handayani, T.N., Likhitrungsilp, V. and Yabuki, N., 2019. A building information modeling (BIM)-integrated system for evaluating the impact of change orders. *Engineering Journal*, 23(4), pp.67–90.

Hang, T.T.L., Likhitrungsilp, V. and Yabuki, N.,

2020. A BIM-integrated relational database management system for evaluating building life-cycle costs. *Engineering Journal*, 24(2), pp.75-86.

Hossain, M.U., Ng, S.T., Antwi-Afari, P. and Amor, B., 2020. Circular economy and the construction industry: Existing trends, challenges and prospective framework for sustainable construction. *Renewable and Sustainable Energy Reviews*, 130, p.109948.

Hossain, M.U., Wu, Z. and Poon, C.S., 2017. Comparative environmental evaluation of construction waste management through different waste sorting systems in Hong Kong. *Waste Management*, 69, pp.325-335.

Hwang, B.G. and Yeo, Z.B., 2011. Perception on benefits of construction waste management in the Singapore construction industry. *Engineering, Construction and Architectural Management*, 18(4), pp.394-406.

Iacovidou, E. and Purnell, P., 2016. Mining the physical infrastructure: Opportunities, barriers and interventions in promoting structural components reuse. *Science of the Total Environment*, 557-558, pp.791-807.

Jayasinghe, L.B. and Waldmann, D., 2020. Development of a BIM-based web tool as a material and component bank for a sustainable construction industry. *Sustainability (Switzerland)*, 12(5), pp.1-15.

Jones, P. and Comfort, D., 2018. The Construction Industry and the Economy. *International Journal of Management Cases*, 20(1), pp.4-15.

Kang, L.S., Moon, H.S., Park, S.Y., Kim, C.H. and Lee, T.S., 2010. Improved link system between schedule data and 3D object in 4D CAD system by using WBS code. *KSCE Journal of Civil Engineering*, 14(6), pp.803-814.

Kim, Y.C., Hong, W.H., Park, J.W. and Cha, G.W., 2017. An estimation framework for Building Information Modeling (BIM)-based demolition waste by type. *Waste Management and Research*, 35(12), pp.1285-1295.

Kirchherr, J., Reike, D. and Hekkert, M., 2017. Conceptualizing the circular economy: An analysis of 114 definitions. *Resources, Conservation and Recycling*, 127, pp.221-232.

López Ruiz, L.A., Roca Ramón, X. and Gassó Domingo, S., 2020. The circular economy in the construction and demolition waste sector – A review and an integrative model approach. *Journal of Cleaner Production*, 248.

Likhitrungsilp, V., Le, H.T.T., and Yabuki, N., 2019. Integrating Building Information Modeling and Visual Programming for Building Life-Cycle Cost Analysis. *Proc. of the Tenth International Structural Engineering and Construction Conference (ISEC 2019)*, Chicago, Illinois, US, May 20-25, 2019.

Lu, W., Chen, X., Peng, Y. and Shen, L., 2015. Benchmarking construction waste management performance using big data. *Resources, Conservation and Recycling*, 105, pp.49-58.

Lu, W. and Tam, V.W.Y., 2013. Construction waste management policies and their effectiveness in Hong Kong: A longitudinal review. *Renewable and Sustainable Energy Reviews*, 23, pp.214-223.

Lu, W., Webster, C., Chen, K., Zhang, X. and Chen, X., 2017. Computational Building Information Modelling for construction waste management: Moving from rhetoric to reality. *Renewable and Sustainable Energy Reviews*, 68, pp.587-595.

Mahpour, A., 2018. Prioritizing barriers to adopt circular economy in construction and demolition waste management. *Resources, Conservation and Recycling*, 134, pp.216-227.

Nagapan, S., Rahman, I.A., Asmi, A., Memon, A.H. and Latif, I., 2012. Issues on construction waste: The need for sustainable waste management. *CHUSER 2012 - 2012 IEEE Colloquium on Humanities, Science and Engineering Research*, pp.325-330.

Nasi, M., Genovese, A., Acquaye, A.A., Koh, S.C.L. and Yamoah, F., 2017. A comparison

between linear and circular supply chains: a case research from the construction industry. *International Journal of Production Economics*, 183, Part B: 443-457.

Núñez-Cacho, P., Górecki, J., Molina, V. and Corpas-Iglesias, F.A., 2018. New Measures of Circular Economy Thinking In Construction Companies. *Journal of EU Research in Business*, 2018, pp.1-16.

Osmani, M., Glass, J. and Price, A.D.F., 2008. Architects' perspectives on construction waste reduction by design. *Waste Management*, 28(7), pp.1147-1158.

Osmani, M. and Villoria-Sáez, P., 2019. Current and Emerging Construction Waste Management Status, Trends and Approaches. *Waste*, pp.365-380.

Osobajo, O.A., Oke, A., Omotayo, T. and Obi, L.I., 2020. A systematic review of circular economy research in the construction industry. *Smart and Sustainable Built Environment*, 260, p.121046.

Papargyropoulou, E., 2011. *Sustainable construction waste management in Malaysia: a constructor's perspective*. Proceeding of Management and Innovation for a Sustainable Built Environment.

Poon, C.S., Yu, A.T.W., Wong, A. and Yip, R., 2013. Quantifying the Impact of Construction Waste Charging Scheme on Construction Waste Management in Hong Kong. *Journal of Construction Engineering and Management*, 139(5), pp.466-479.

Saez, P.V., Del Río Merino, M., San-Antonio González, A. and Porrás-Amores, C., 2013. Best practice measures assessment for construction and demolition waste management in building constructions. *Resources, Conservation and*

*Recycling*, 75, pp.52-62.

Sanchez, B. and Haas, C., 2018. Capital project planning for a circular economy. *Construction Management and Economics*, 36(6), pp.303-312.

Smol, M., Kulczycka, J., Henclik, A., Gorazda, K. and Wzorek, Z., 2015a. The possible use of sewage sludge ash (SSA) in the construction industry as a way towards a circular economy. *Journal of Cleaner Production*, 95, pp.45-54.

Solís-Guzmán, J., Marrero, M., Montes-Delgado, M.V. and Ramírez-de-Arellano, A., 2009. A Spanish model for quantification and management of construction waste. *Waste Management*, 29(9), pp.2542-2548.

Won, J. and Cheng, J.C.P., 2017. Identifying potential opportunities of building information modeling for construction and demolition waste management and minimization. *Automation in Construction*, 79, pp.3-18.

Won, J., Cheng, J.C.P. and Lee, G., 2016. *Quantification of construction waste prevented by BIM-based design validation: Case researches in South Korea*. *Waste Management*, 49, pp. 170-180.

WRAP, 2010. *Designing out Waste Tool for Buildings*. [online] *Designing out Waste Tool for Buildings, Quick Start Guide, Version 1.0*, Available at: <<http://dowtb.wrap.org.uk/>>. [Accessed 22 July 2021]

Yuan, H., 2012. A model for evaluating the social performance of construction waste management. *Waste Management*, 32(6), pp.1218-1228.

Yuan, H., 2013. A SWOT analysis of successful construction waste management. *Journal of Cleaner Production*, 39, pp.1-8.

[This page is intentionally left blank]

# Seismic Ground Response Analysis of Input Earthquake Motion and Site Amplification Factor at KUET

Sonia Akter\*

Department of Civil Engineering, Ahsanullah University of Science and Technology, Bangladesh  
141 Love Rd, Dhaka 1208, Bangladesh

\*Corresponding authors: [sonia.akter0907@ygmail.com](mailto:sonia.akter0907@ygmail.com)

SUBMITTED 10 February 2020 REVISED 19 September 2021 ACCEPTED 21 September 2021

**ABSTRACT** Ground motion is the movement of the earth's surface due to explosions or the propagation of seismic waves. In the seismic design process, ground response analysis evaluates the impact of local soil conditions during earthquake shaking. However, it is difficult to determine the dynamic site response of soil deposits in earthquake hazard-prone areas. Structural damage has a great influence on the selection of input ground motion, and in this study, the importance of bedrock motion upon the response of soil is highlighted. The specific site response analysis is assessed through "DEEPSOIL" software with an equivalent linear analysis method. Furthermore, four input motions including Kobe, LomaGilroy, Northridge, and Chi-Chi were selected to obtain normalized response spectra. This study aims to obtain the site amplification of ground motion, peak spectral acceleration (PSA), and maximum peak ground acceleration (PGA) based on shear wave velocity from the detailed site-specific analysis of Bangabandhu Sheikh Mujibur Rahman hall at Khulna University of Engineering & Technology. The maximum shear wave velocity obtained was 205 m/s while the amplification factor varied from 4.01 (Kobe) to 1.8 (Northridge) for rigid bedrock properties. Furthermore, the Kobe earthquake produced the highest (4.3g) PSA and the Northridge earthquake produced the lowest (1.08g) PSA for bedrock, with  $V_s=205$  m/s. The surface PGA values were acquired in the range of 0.254g (Northridge) to 0.722g (Kobe), and the maximum strain values for Kobe earthquakes were in the range of 0.016 to .303. Therefore, the surface acceleration values were very high ( $>0.12g$ ) for the Kobe earthquake motion.

**KEYWORDS** Amplification Factor; PSA; PGA; DEEPSOIL; Shear Wave Velocity.

© The Author(s) 2022. This article is distributed under a Creative Commons Attribution-ShareAlike 4.0 International license.

## 1 INTRODUCTION

Earthquakes are common phenomena that represent nature's most catastrophic and frightening event. However, an induced earthquake can be produced by an extended range of activities like mining, cave-ins, liquid injection, withdrawal, fracturing projects (Rubinstein & Mahani, 2015), and geothermal reservoir implementation (Majer *et al.*, 2007). They are directly generated due to the sudden release of stress and strain in the Earth's crust to produce a jerky movement. These events are characterized by small magnitudes concerning non-structural seismic damage (Filiatrault, Christopoulos, & Stearns, 2002) to buildings and infrastructure.

The geology of Bangladesh indicates a tectonically active country in the world for earthquakes. This is shaped by the movement of

the Indian, Eurasian, and Burmese tectonic plates. There are many active faults along this boundary, which can also produce massive earthquakes. A significant earthquake can devastate the country at any time, for example, the epicentral distance in Dhaka was 230 km, and 1542 people died. This caused extensive damages to masonry buildings in many parts of Bangladesh (Ansary, Noor & Yasin, 2005; Govindaraju & Bhattacharya, 2012).

In the case of an earthquake event, the seismic design provides a dynamic response on a structure, which causes great losses in humans. With advanced technologies, a wide range of latest methodologies are demonstrated for earthquake-resistant structural design. In seismic design, the influence of local soil conditions, site topography, and rock properties on the expected

seismic movements play a critical aspect. The effects of soil conditions are then estimated through seismic site response analysis (Govindaraju & Bhattacharya 2012).

This study focused on the seismic site response analysis in Bangabandhu Sheikh Mujibor Rahman hall at Khulna University of Engineering & Technology (KUET). Hashash, *et al.* (2011) conducted the analyses using DEEPSOIL software by an equivalent linear method. Furthermore, soil properties like the thickness of the layer, unit weight, shear wave velocity, and damping ratio were used as input to the study. The depth of the clay layer ranges from 3.0 to 30.0 meters, and the thickness of the sand layer ranges from 1.5 m to 3.0 m. The Shear Wave Velocity profile was first generated using some empirical formula of Ohta and Goto (1978) from SPT N value. Four input earthquake motions including Kobe, LomaGilroy, Northridge, and Chi-Chi were selected to estimate ground motion amplification, design response spectra. In addition, the motions determine the forces produced due to an earthquake which causes the instability of bedding planes' slopes (Boore & Atkinson, 2008).

**2 METHODS**

**2.1 Site Information**

The investigated area is “Bangabandhu Sheikh Mujibor Rahman hall” at Khulna University of Engineering & Technology of latitude 22°53'N and a longitude of 89°30'E (Figure 1). The area contained medium sand to clay type soil, and the depth of the clay layer ranges from 3.0 to 30.0 m. Furthermore, the cohesive nature of the soil with high organic, liquid, and plastic contents showed medium to high sensitivity to moisture, and cannot support heavily loaded infrastructure. Therefore, seismic ground response analysis is important to comprehend the impact of typical site conditions.

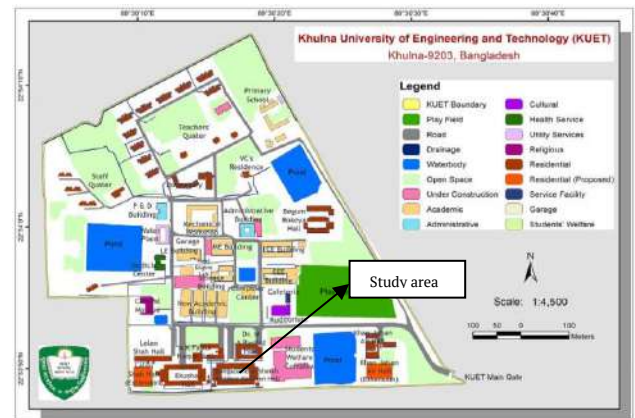
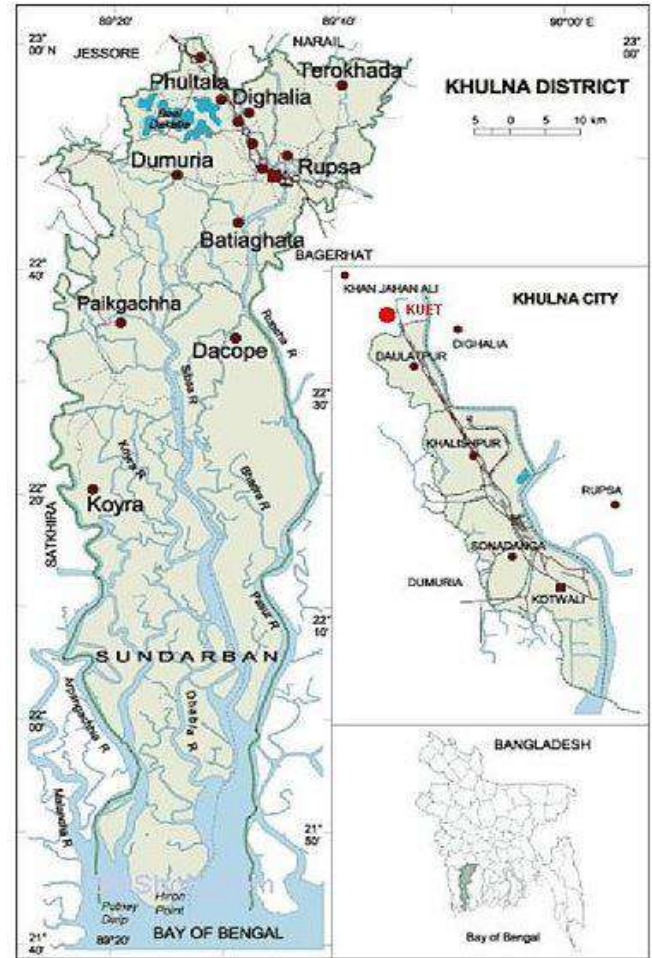


Figure 1. Site location

**2.2 Sub Soil Investigation**

The field investigation was conducted for “Bangabandhu Sheikh Mujibor Rahman hall” at

the KUET campus through Standard Penetration Test. The execution of seven borings was up to the maximum depth of 30 m from the level of the ground surface. Meanwhile, the topsoil was clayey silt, bur grey at the depth of 1.5 m, and the medium sand was found from depth 1.5m to 3.0 m. The level of the groundwater table was 2’-3’’ from the top of the subsurface, and the angle of internal friction for sandy soil was 30.9°. In addition, the maximum average of SPT value was 11 and using empirical relationship (Hossain, 2018) the collected borehole data was converted and the SPT- N value is commonly used to draw the soil profile in the subsurface.

The shear wave velocity is the most important property of soil due to its great effect in site response analysis (Boore & Joyner, 1997). The site amplification is assumed to change linearly with the change of  $V_{S30}$  (Boore & Atkinson, 2008; Chiou & Youngs, 2008; Choi & Stewart, 2005; Sandikkaya, Akkar, & Bard, 2013; Walling, Silva,

into shear wave velocity for the seismic site response study (Farrokhzad & Choobbasti, 2016).

### 2.3 The Velocity Profile

The main input parameter for the DEEPSOIL analysis is shear wave velocity and using an empirical equation of Ohta and Goto’s (1978), the profile was generated ( Figure 2) for “Bangabandhu Sheikh Mujibor Rahman hall”. This empirical equation converts the standard penetration test-N value into shear wave velocity,

& Abrahamson, 2008; Seyhan & Stewart, 2014; and Kamai, Abrahamson, & Silva, 2014). The velocity profile was conducted by assuming the fixed reference of bedrock elevation at 30 meters below the existing ground surface, and can be time-dependent or independent (Salic et al., 2017). Furthermore, the linear site scaling does not control period independent and dependent values (Martin & Dobry, 1994).

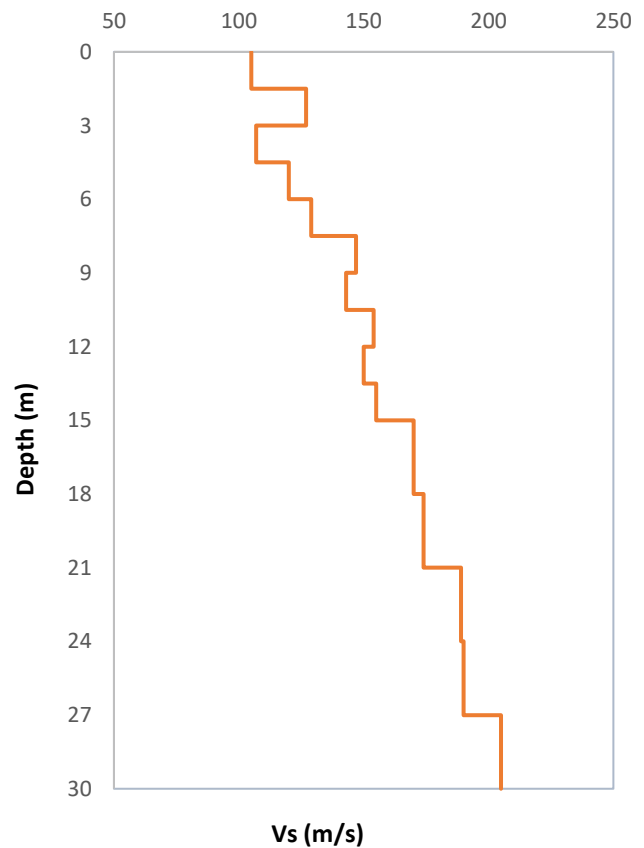
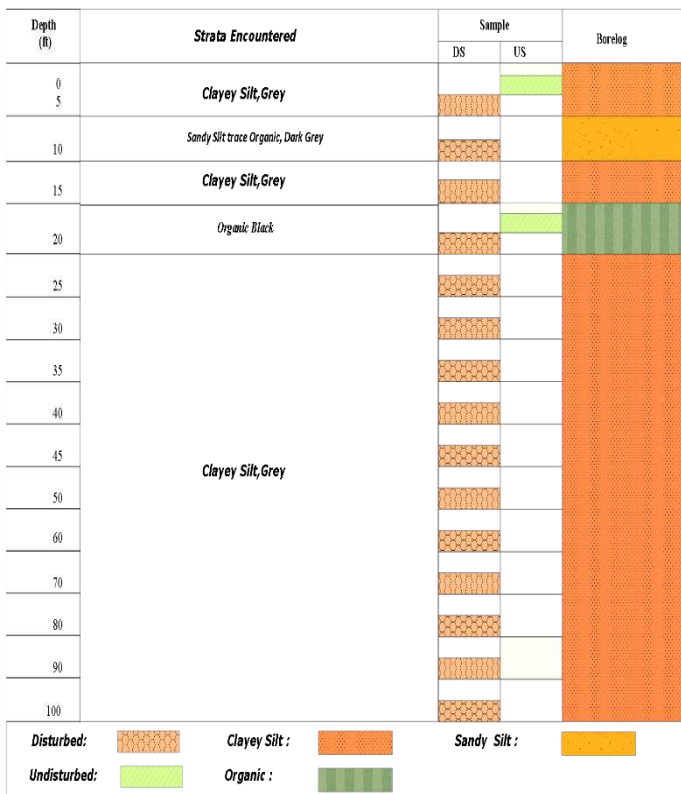


Figure 2. Site characterization.

### 2.4 Ground Response Analysis

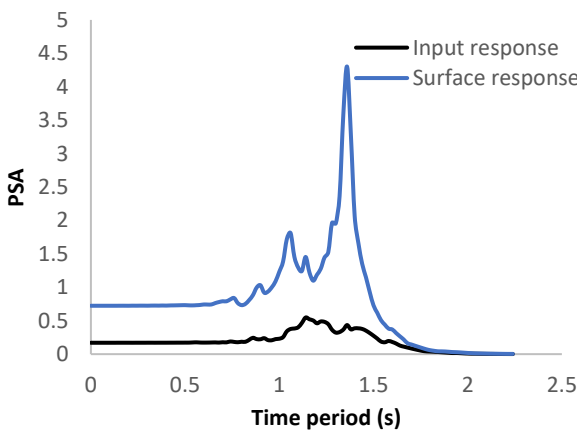
Ground response analysis contains the determination of soil amplification, potentiality of liquefaction, periods and soil stability analysis, etc. The relationship between stress and strain can be represented using three different methods. At low strain, the behavior of the soil is linear while at high strain it prevails nonlinearly. For seismic ground response analysis of the site consideration, the equivalent linear method was performed using the DEEPSOIL (Kwok, Stewart, & Hashash, 2008). It is accurate for computing PGA up to 3 seconds for general projects (Martin & Dobry, 1994; Dickenson & Seed, 1996; Dobry *et al.*, 2000). In this analysis, the bedrock properties are considered as rigid halfspace, and the solution type in equivalent linear analysis in the DEEPSOIL is frequency domain. Meanwhile, the

input acceleration-time histories have an influential effect on the computed ground response analysis. The Kobe earthquake, LomaGilroy, Northridge earthquake, and Chi-Chi earthquake are chosen as the input ground motion, and the input rock motion is scaled to 0.12g value.

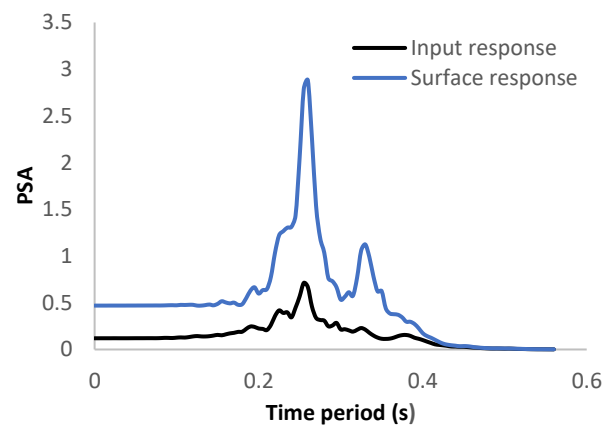
## 3 RESULTS AND DISCUSSION

### 3.1 Response Spectra

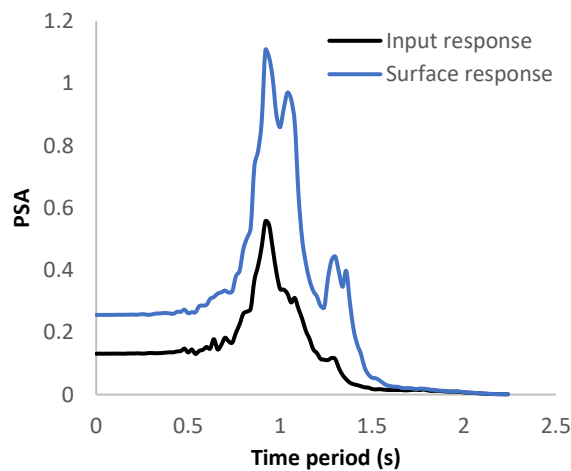
For rigid halfspace bedrock, the response spectra of four input earthquake motions are shown in Figure 3. Kobe earthquake generates the largest (4.30g) peak spectral acceleration (PSA) for this site while the Northridge earthquake generates the lowest (1.08g) peak spectral acceleration (PSA).



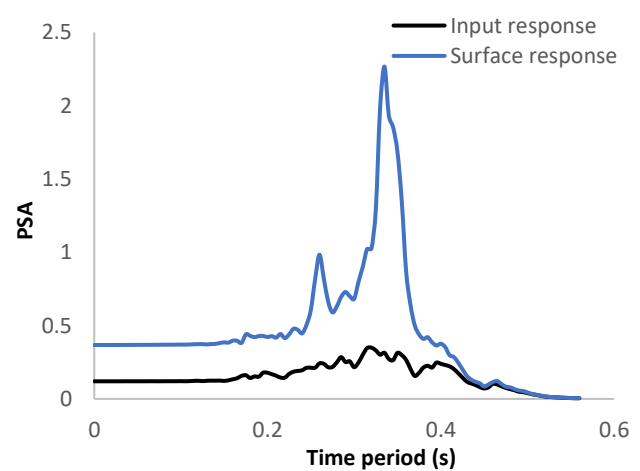
a) Kobe Earthquake



b) LomaGilroy Earthquake



c) Northridge Earthquake



d) Chi - Chi Earthquake

Figure 3. Response spectra

### 3.2 Time Histories

For rigid half-space bedrock, the design soil profile was excited with input motion of four earthquakes to measure the dynamic response of local soil, and an equivalent linear ground response analysis method was used for site response analysis. Figure 4 showed the acceleration of soil at the ground surface, and the ordinates of the value fluctuate with time.

### 3.3 Maximum Peak Ground Acceleration (PGA)

The maximum Peak Ground Acceleration (PGA) variation from the ground surface to 30 meters depth for this site is shown in Figure 5. Furthermore, the value of PGA at the surface and bedrock is attained from the analysis. The peak

ground acceleration values at the surface are found to be in the range of 0.251g (Northridge) to 0.722g (Kobe) and that of the bedrock was found to vary from 0.118g (Chi-chi) to 0.180g (Kobe). Meanwhile, the level of damage to the building and infrastructure depends on the maximum PGA.

Site amplification factors are often used as one of the significant parameters to characterize the intensity of ground motion. The amplification factor is defined as the ratio of peak ground acceleration at surface and reference rock. Therefore, the amplification factors have also been computed and shown in Figure 6, and the variation is within 1.80 (Northridge) to 4.01 (Kobe).

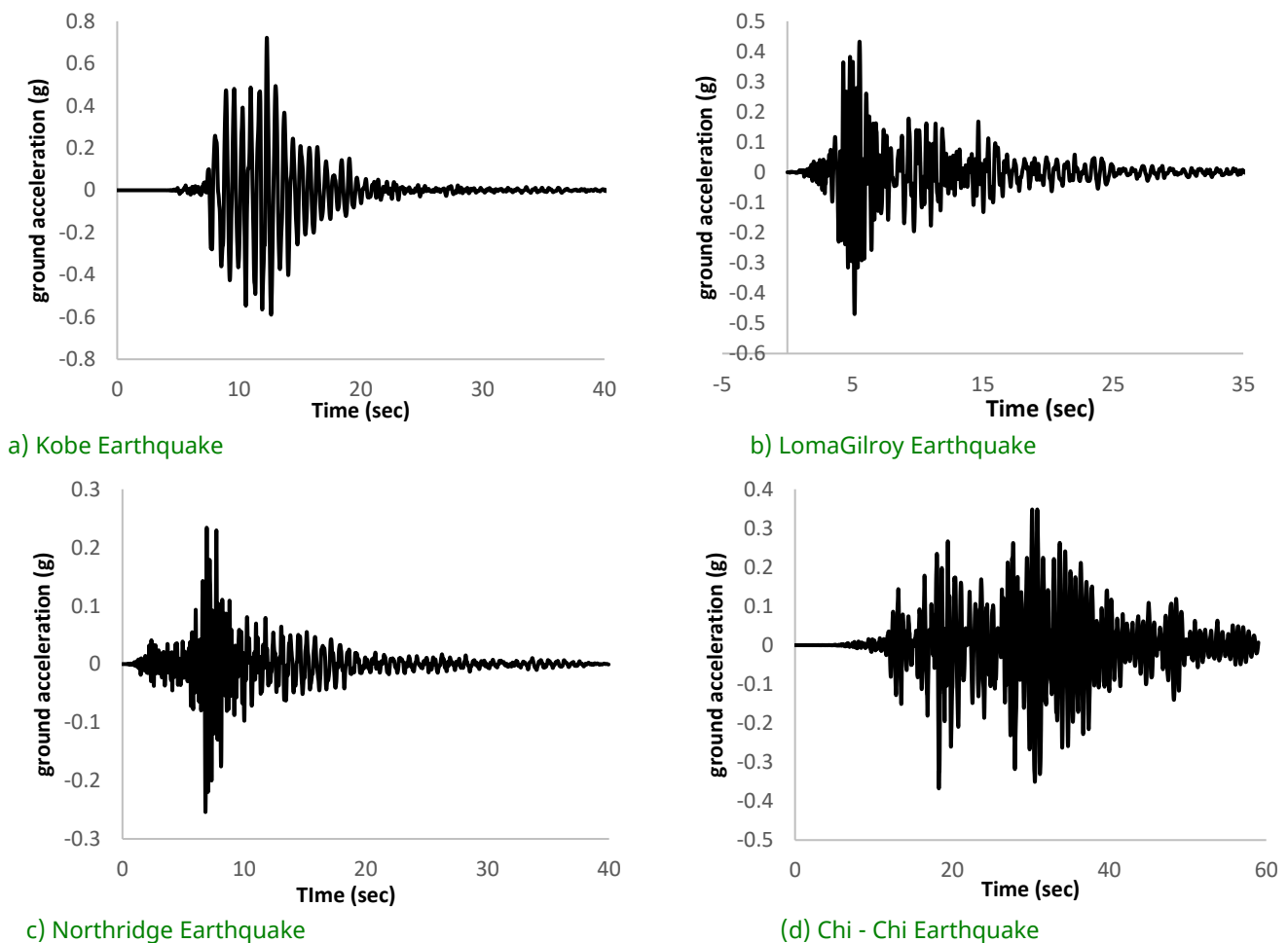


Figure 4. Time histories for local site effect

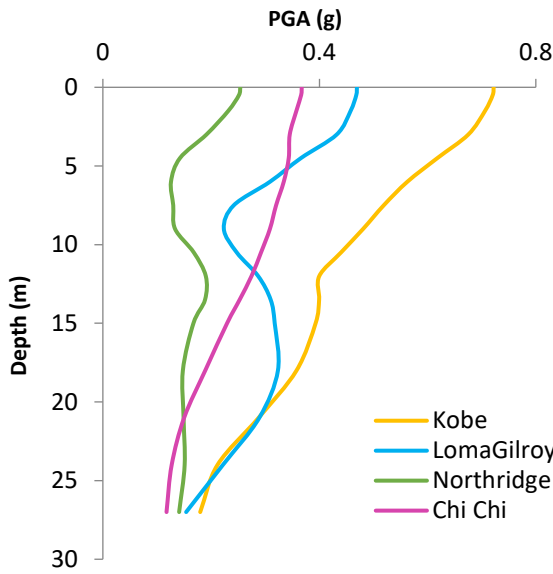


Figure 5. Maximum Peak Ground Acceleration

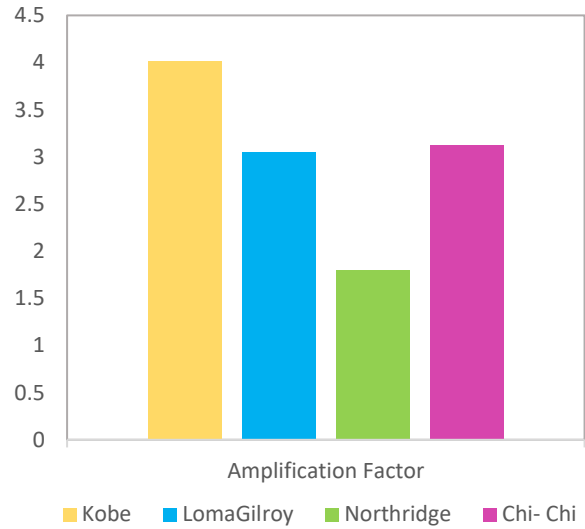


Figure 6. Site Amplification Factor

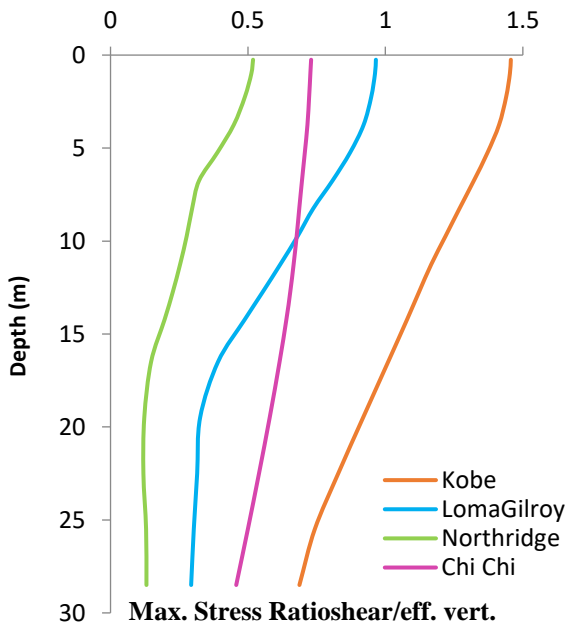


Figure 7. Maximum stress ratio for local site effect

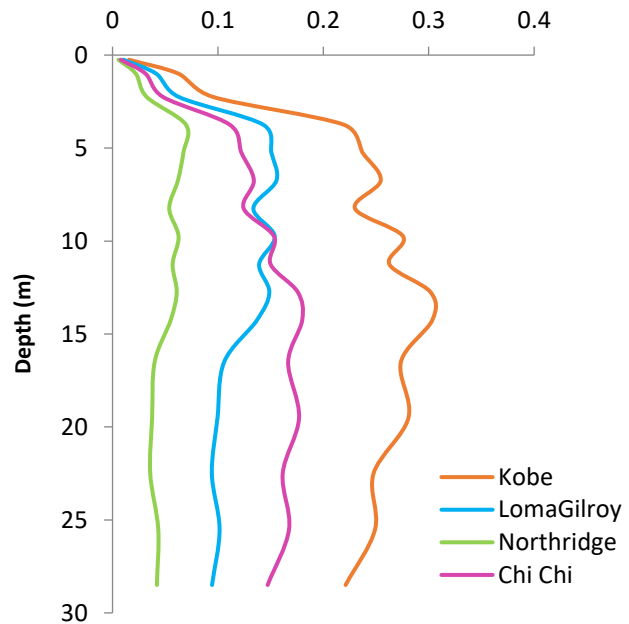


Figure 8. Maximum strain for local site effects

### 3.4 Maximum Stress Ratio

For rigid halfspace bedrock, the Maximum Stress Ratio of four input motions for this site is shown in Figure 7. Meanwhile, the Maximum stress ratio values for Kobe and Northridge earthquakes are in the range of 0.687 to 1.45, and 0.12 to 0.519 respectively.

### 3.5 Maximum Strain

A high range of strain values subjected to the input motions represents higher energy content. Meanwhile, the SPT-N value and the stiffer soils

which released higher maximum strain are directly proportional. Due to cyclic loading, more energy is dissipated, and it represents a higher strain range. For rigid halfspace bedrock, the Maximum Strain for this typical site is shown in Figure 8, and the values for this site are obtained from the analysis. The Maximum strain values for Kobe and LomaGilroy earthquakes are in the range of 0.016 to .303, and 0.0104 to .155 respectively. In addition, the Maximum strain values for Northridge and Chi-Chi earthquakes are in the range of 0.006 to .0697, and 0.0079 to 0.18 respectively.

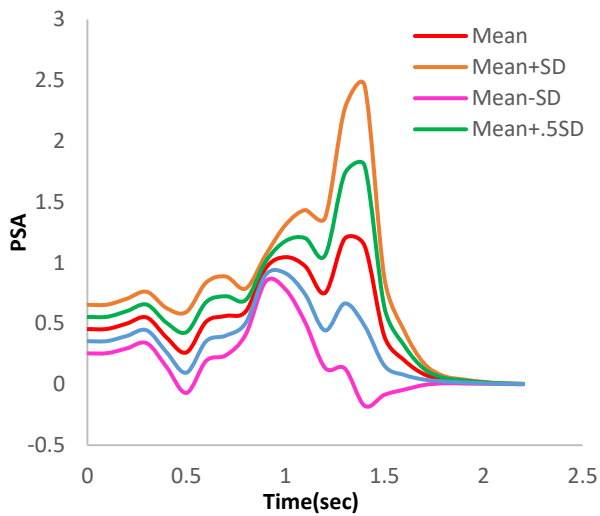


Figure 9 Comparison of Mean and Standard Deviation for Surface PSA

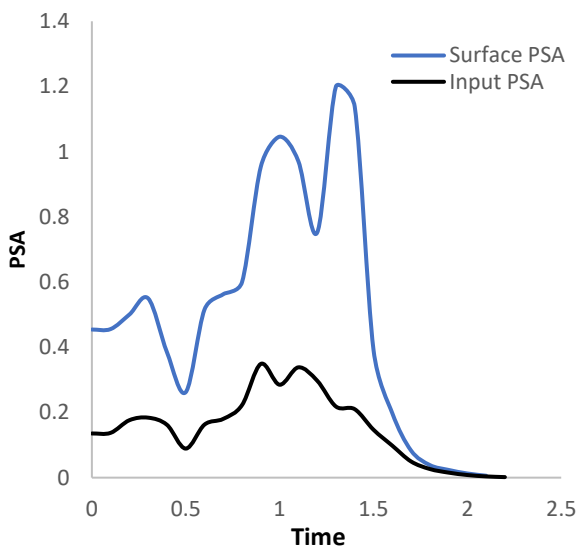


Figure 10 Comparison of Mean Input PSA and Mean Surface PSA

Figure 9 showed the comparison between Mean and Standard Deviation for surface PSA and Figure 10 showed the comparison between Mean Input PSA and Mean Surface PSA produced for different input motions.

#### 4 CONCLUSION

As the behavior of the soil is dynamic during seismic loading, the site response analysis is very important in hazard analysis and checking the effect of the local site. The two important factors that affect the level of ground shaking are surface

rock properties and local soil conditions. For a typical site, the ground response analysis method is considered equivalent linear. Furthermore, Kobe, LomaGilroy, Northridge, and Chi-Chi earthquake motions were chosen to comprehend the ground motion criteria representing the nearby and distant sources of earthquake hazard for the site under consideration. The depth of the clay layer varies from 3 m to 30 m. The analysis results showed that the soil subjected to input motions has a large amplification factor while considering the bedrock properties as rigid. The rate of amplification factor was maximum for Kobe earthquake motion (4.01) and minimum for Northridge Earthquake motion (1.8). More input motions can be attained to obtain the design response spectrum, and the peak ground acceleration value ranges from 0.722g (Kobe) to 0.118g (Chi-Chi). Furthermore, this study provides a guideline for generating the normalized response spectra under certain earthquake phenomena and it suggests suitable ground improvement techniques for such areas. It also found that the strong wave propagation of input motion affects the subsurface of the soil's response and its characteristics. Meanwhile, weaker soils that are prone to strong motions have high residual strain after seismic events.

#### DISCLAIMER

The authors declare no conflict of interest.

#### AVAILABILITY OF DATA AND MATERIALS

All data are available from the author.

#### AUTHOR CONTRIBUTION STATEMENTS

Sonia A. performed the analytical analysis and took a substantial contribution in discussing the result and drafting the manuscript.

#### ACKNOWLEDGEMENT

The author is grateful to the Geotechnical Lab, Department of Civil Engineering, Khulna University of Engineering & Technology (KUET) for providing data and information regarding the study.

## REFERENCES

- Ansary, M.A., Noor, M.A. and Yasin, M., 2005. Seismic Hazard Analysis of Bangladesh. *Proceedings of First Bangladesh Earthquake Symposium*. Dhaka, 14-15 December 2005.
- Boore, D.M. and Atkinson, G.M., 2008. Ground-motion prediction equations for the average horizontal component of PGA, PGV, and 5%-damped PSA at spectral periods between 0.01 s and 10.0 s. *Earthquake Spectra*, 24(1), pp.99–138.
- Boore, D.M. and Joyner, W.B., 1997. Site amplifications for generic rock sites. *Bulletin of the seismological society of America*, 87(2), pp.327–341.
- Chiou, B. J. and Youngs, R.R., 2008. An NGA model for the average horizontal component of peak ground motion and response spectra. *Earthquake spectra*, 24(1), pp.173–215.
- Choi, Y. and Stewart, J.P., 2005. Nonlinear site amplification as function of 30 m shear wave velocity. *Earthquake spectra*, 21(1), pp.1–30.
- Dickenson, S.E. and Seed, R.B., 1996. Nonlinear dynamic response of soft and deep cohesive soil deposits. In: *Proceedings of the international workshop on site response subjected to strong earthquake motions*. pp.67–81.
- Dobry, R., Borcherdt, R.D., Crouse, C.B., Idriss, I.M., Joyner, W.B., Martin, G.R., Power, M.S., Rinne, E.E. and Seed, R.B., 2000. New site coefficients and site classification system used in recent building seismic code provisions. *Earthquake spectra*, 16(1), pp.41–67.
- Farrokhzad, F. and Choobbasti, A.J., 2016. Empirical correlations of shear wave velocity ( $V_s$ ) and standard penetration resistance based on soil type in Babol city. *Indian Journal of Geo Marine Sciences*, 45(11), pp. 1566–1577.
- Filiatrault, A., Christopoulos, C. and Stearns, C., 2002. *Guidelines, specifications, and seismic performance characterization of nonstructural building components and equipment*. Pacific Earthquake Engineering Research Center.
- Govindaraju, L. and Bhattacharya, S., 2012. Site-specific earthquake response study for hazard assessment in Kolkata city, India. *Natural hazards*, 61(3), pp.943–965.
- Hossain, A.S.M.F., 2018. GROUND INVESTIGATION AND RESPONSE OF JHILMIL RESIDENTIAL TOWN GROUND INVESTIGATION AND RESPONSE OF JHILMIL. (July 2019).
- Kamai, R., Abrahamson, N.A. and Silva, W.J., 2014. Nonlinear horizontal site amplification for constraining the NGA-West2 GMPEs. *Earthquake Spectra*, 30(3), pp.1223–1240.
- Kwok, A.O.L., Stewart, J.P. and Hashash, Y.M.A., 2008. Nonlinear ground-response analysis of Turkey Flat shallow stiff-soil site to strong ground motion. *Bulletin of the Seismological Society of America*, 98(1), pp.331–343.
- Majer, E.L., Baria, R., Stark, M., Oates, S., Bommer, J., Smith, B. and Asanuma, H., 2007. Induced seismicity associated with enhanced geothermal systems. *Geothermics*, 36(3), pp.185–222.
- Martin, G.R. and Dobry, R., 1994. Earthquake site response and seismic code provisions. *NCEER Bulletin*, 8(4), pp.1–6.
- Rubinstein, J.L. and Mahani, A.B., 2015. Myths and facts on wastewater injection, hydraulic fracturing, enhanced oil recovery, and induced seismicity. *Seismological Research Letters*, 86(4), pp.1060–1067.
- Salic, R., Sandikkaya, M.A., Milutinovic, Z., Gulerce, Z., Duni, L., Kovacevic, V., Markusic, S., Mihaljevic, J., Kuka, N. and Kaludjerovic, N., 2017. Reply to “Comment to BSHAP project strong ground motion database and selection of suitable ground motion models for the Western Balkan Region” by Carlo Cauzzi and Ezio Faccioli. *Bulletin of Earthquake Engineering*, 15(4), pp.1349–1353.
- Sandikkaya, M.A., Akkar, S. and Bard, P., 2013. A nonlinear site-amplification model for the next pan-European ground-motion prediction equations. *Bulletin of the Seismological Society of*

*America*, 103(1), pp.19–32.

Seyhan, E. and Stewart, J.P., 2014. Semi-empirical nonlinear site amplification from NGA-West2 data and simulations. *Earthquake Spectra*, 30(3), pp.1241–1256.

Walling, M., Silva, W. and Abrahamson, N., 2008. Nonlinear site amplification factors for constraining the NGA models. *Earthquake spectra*, 24(1), pp.243–255.

(This page is intentionally left blank)

# The Use of Drop-Structures to Increase the Dissolved Oxygen Level along the Cibarani Channel

Jonathan Wijaya, Doddi Yudianto, Finna Fitriana\*

Department of Civil Engineering, Parahyangan Catholic University, Bandung, INDONESIA  
Jalan Ciumbuleuit No. 94, Hegarmanah, Cidadap, Bandung City, West Java

\*Corresponding authors: [finnafitriana@unpar.ac.id](mailto:finnafitriana@unpar.ac.id)

SUBMITTED 18 Maret 2021 REVISED 13 September 2021 ACCEPTED 10 October 2021

**ABSTRACT** The Cikapundung river basin community uses the Cibarani channel as a drainage system and water source for fishing. However, the test result released on 9<sup>th</sup> November 2020 revealed that the channel's water quality failed to reach the class II raw water standards due to various domestic waste discharges. This led to the performance of various studies to identify pollution control techniques by limiting the wastewater discharge and quality, controlling the intake discharge, and using baffles. The Cibarani channel has a drop-structure that can improve the water quality, though the effect has not been previously detailed. Therefore, this study was intended to comprehensively examine the effect of the drop-structure along the Cibarani channel to improve water quality conditions, specifically the Dissolved Oxygen (DO) parameter. This study employed the one-dimensional HEC-RAS software to simulate the hydrodynamic and water quality conditions along the Cibarani channel, and the drop-structure was modelled using two alternatives consisting of a vertical wall and a steep riverbed. Subsequently, the drop-structure fitted with a vertical wall gave a more plausible reaeration rate of 125 day<sup>-1</sup> and Root Mean Square Error (RMSE) value of 0.50. The placement of a similar configuration before the first housing of the channel increased the DO concentrations by an average of 4.37 mg/L. This was followed by the modelling of another drop-structure after the first housing to increase the DO levels at the downstream part. Eventually, the combination of the two new drop-structures succeeded in increasing the DO concentrations along the Cibarani channel to 3.3 - 6.9 mg/L.

**KEYWORDS** Dissolved Oxygen; Drop-Structure; HEC-RAS; Reaeration Rate; Water Quality Modelling.

© The Author(s) 2022. This article is distributed under a Creative Commons Attribution-ShareAlike 4.0 International license.

## 1 INTRODUCTION

Cikapundung is one of the rivers located strategically in Bandung City, used by the community and government for several purposes, including recreational sports and as a clean water source. Meanwhile, the developments in Bandung City have led to some changes in the Cikapundung river basin (Bachrein, 2012), such as population growth, which resulted environmental problems such as water pollution (Rahayu *et al.*, 2018).

Cibarani is one of the Cikapundung river basin channels which water is exploited for irrigational purposes. However, its function has changed into a drainage system for the wastewater of the community. This has led to a decrease in the water quality of the Cibarani channel. Currently, the water is turbid and produces a foul odour, which inconveniences the surrounding community.

The Cibarani channel is classified to be consistent with class II of the raw water standards in article 55 of Government Regulation No. 82 of 2001. Subsequently, two studies have been performed on improving the Cibarani water quality. They involved raising the discharge, limiting the wastewater discharge and quality, and using baffles (Trisnojoyo, 2017; Hayhera, 2019). Generally, the Cibarani irrigation has several water structures, such as a culvert, gutter, weirs, and a drop-structure. The downstream part of this drop-structure experienced a change from supercritical to subcritical flow, resulting in a hydraulic jump, which may increase air entrainment that could affect the water quality (Arief, 2014). However, these two studies did not simulate the drop-structure in the Cibarani channel, though previous investigations suggested that drop-structures can increase the

water quality (Damarany *et al.*, 2009; Triane and Suharyanto, 2015).

Therefore, this study aimed at evaluating the effect of a drop-structure on the water quality parameters along the Cibarani channel based on another sampling. The second aim was to model and simulate the drop-structure configuration for improving the dissolved oxygen, using HEC-RAS software to simulate hydraulic and water quality analyses.

This study comprised three scopes, first, the investigated area spanned 1.3 km, from the Cilimus weir intake to its downstream parts, as seen in Figure 1. Second, HEC-RAS 4.1 was used to conduct the hydraulic and water quality analyses. Third, various nutrient parameters, such as Biochemical Oxygen Demand (BOD), Total Nitrogen (TN), and Total Phosphorous (TP) were tested, though the model focused on the Dissolved Oxygen parameter.

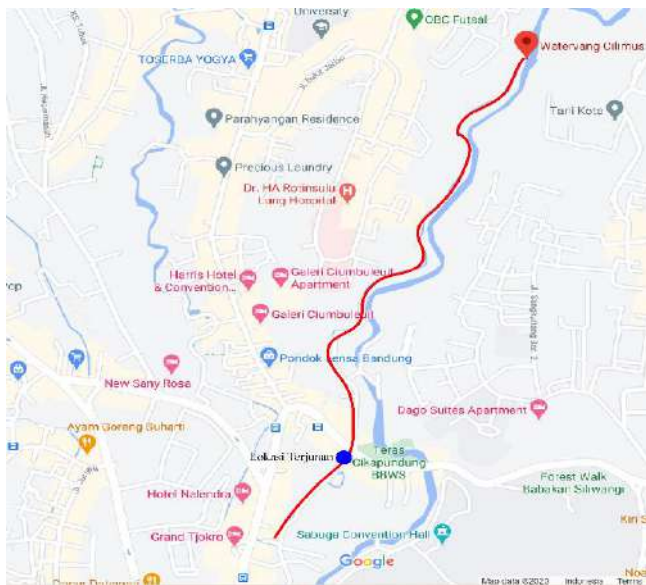


Figure 1. Study location.

## 2 METHOD

HEC-RAS is utilized by the U.S. Army Corps of Engineers and can be used freely. It can evaluate four analysis components, namely steady flow water surface profile, unsteady flow simulation, sediment transport boundary computations, and water quality (Brunner and CEIWR-HEC, 2010). Generally, the hydrodynamic condition in the Cibarani channel is simulated only in steady-state

conditions as the flow can be adjusted from the Cilimus weir intake. This HEC-RAS steady-state condition uses the energy equation and iterative method of the standard step to calculate the water surface profiles. Meanwhile, the water quality analysis performed by the program is based on the conservation of mass. For this modelling, HEC-RAS evaluates nine nutrient parameters, namely Algae, Dissolved Oxygen, Carbonaceous BOD, Organic Nitrogen, Ammonium Nitrogen, Nitrite Nitrogen, Nitrate Nitrogen, Organic Phosphorus, and Orthophosphate.

The basis of the water quality analysis is the conservation of mass, which uses the depletion of oxygen for its estimation. The equation assumes that BOD has a first-order degradation reaction and deoxygenation rate ( $k_d$ ) of the Ohio river (Streeter and Phelps, 1925).

Streeter-Phelps equation

$$\bar{u} \frac{dC}{dx} = -k_d L + k_a (C_s - C) \quad (1)$$

The mass balance equation in the Streeter-Phelps calculation can be modified to describe the ultimate BOD and DO deficits reactions.

Mass balance equation from Streeter-Phelps formula:

$$\frac{dC}{dt} = -\bar{u} \frac{dC}{dx} - k_d L + k_a (C_s - C) \quad (2)$$

Mass balance equation for ultimate BOD and DO deficit:

$$\frac{dL}{dt} = -\bar{u} \frac{dL}{dx} - k_d L \quad (3)$$

$$\frac{dD}{dt} = -\bar{u} \frac{dD}{dx} - k_d L + k_a D \quad (4)$$

Where  $\bar{u}$  is the average flow velocity in cross-section,  $C$  is the DO concentration,  $L$  is the ultimate BOD concentration,  $C_s$  is the saturated dissolved oxygen concentration,  $D$  is the DO deficit concentration,  $k_d$  is the first order deoxygenation rate constant, and  $k_a$  is the first order reaeration rate constant.

The formula above can be modified with mass balance equations for advective and dispersive systems. This is because dispersion is essential for

distributing oxygen, as well as for various morphological changes, slopes, pools, riffles, drop-structure, and large turbulent eddies (Yudianto and Xie, 2008).

The mass balance equations for the advective and dispersive systems:

$$\frac{dC}{dt} = -\bar{u} \frac{dC}{dx} + E_x \frac{d^2C}{dx^2} - k_d L + k_a (C_s - C) \quad (5)$$

$$\frac{dC}{dt} = -\bar{u} \frac{dC}{dx} + E_x \frac{d^2C}{dx^2} - k_d L + k_a (C_s - C) \quad (6)$$

$$\frac{dD}{dt} = -\bar{u} \frac{dD}{dx} + E_x \frac{d^2D}{dx^2} - k_d L + k_a D \quad (7)$$

where  $E_x$  is longitudinal dispersion coefficient.

The reaeration rate used the empirical equation developed by Jha *et al.* (2001) for the upper and lower channel streams, alongside the trial-and-error method and the drop-structure. Tables 1 and 2 show the range of reaeration rate values in the physical drop-structure models.

Reaeration rate equation from Jha *et al.* (2001)

$$k_{a(20)} = 5.792 \frac{\sqrt{\bar{u}}}{H^{0.25}} \quad (8)$$

where  $k_{a(20)}$  is the reaeration rate at temperature 20°C, and  $H$  is the average water depth in cross-section.

The deoxygenation rate depends on the type of waste disposed to the water and was used as a calibration variable since it is not measured in the laboratory (Ji, 2008).

Table 1. Reaeration rate values from Ughbebor *et al.* (2012)

Types of water bodies	Value of $k_a$ (day <sup>-1</sup> )
Small pond	0.05 – 1.0
Sluggish streams/lakes	1.0 – 1.5
Large streams with low velocity	1.5 – 2.0
Large streams with moderate velocity	2.0 – 3.0
Swift Streams	3.0 – 5.0
Rapids	> 5.0

Table 2. Reaeration rate values from Peavy, Rowe, and Tchobanoglous (1985)

Stream type	$k_a$ at 20°C (day <sup>-1</sup> )
Sluggish river	0.23 – 0.35
Large river of low velocity	0.35 – 0.46
Large stream of normal velocity	0.46 – 0.69
Swift streams	0.69 – 1.15
Rapids and waterfalls	> 1.15

The longitudinal dispersion coefficient applied in this study was delivered by one-dimensional simulation. Consequently, Fischer's (1975) equation gave the best result of DO curves (Kashefipour and Falconer, 2002).

Dispersion coefficient from Fischer's (1975) equation

$$E_x = 0.011 \frac{\bar{u}^2 B^2}{H U_*} \quad (9)$$

Where  $B$  is channel width, and  $U_*$  is shear velocity. The water quality rates are influenced by temperature, usually specified at 20°C. Therefore, a correction with the Arrhenius rate law is required by using the relationship between the water quality rates and temperature.

$$k_T = k_{20} \theta^{(T-20)} \quad (10)$$

Where  $k_T$  is the rate constant at temperature  $T$ ,  $k_{20}$  is the rate constant at temperature 20°C, and  $\theta$  is the temperature correction coefficient.

In this study, the evaluations of the observed data with the modelled data were calculated using Root Mean Square Error (RMSE). The value of RMSE close to zero indicates that the modelled data can deliver more accurate results.

RMSE equation

$$RMSE = \sqrt{\frac{1}{N} \sum_{i=1}^N (x_i - \hat{x}_i)^2} \quad (11)$$

Where  $RMSE$  is Root Mean Square Error,  $N$  is some observational data,  $x_i$  is observational value,  $\hat{x}_i$  is modelled value.

The sampling points indicated in this study comprised six water stations along the channel and five wastewater inlets. Figures 2 and 3 show the channel scheme and locations of the sampling, respectively. The water was collected from the sampling points and measured during the dry season on the 9<sup>th</sup> November 2020, while the wastewater was collected and evaluated on the 17<sup>th</sup> and 24<sup>th</sup> November 2020. Figure 4 presents the sampling conditions.

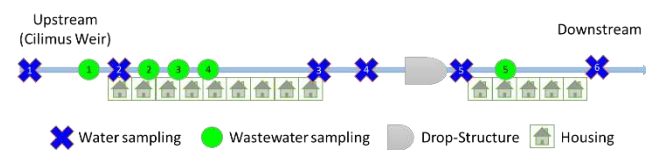


Figure 2. Cibarani channel scheme.

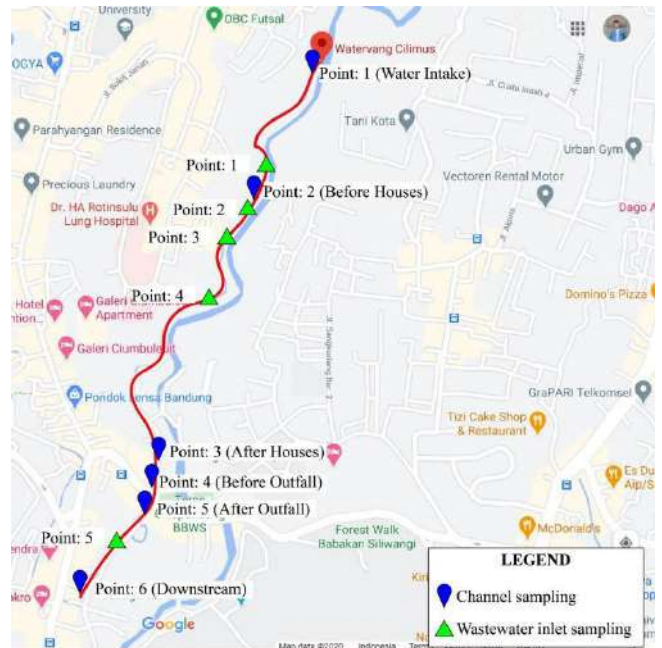


Figure 3. Sampling locations.



(a)



(b)

Figure 4. The condition of sampling points (a) along the channel (b) in the wastewater inlet.

Also, the hydraulic data along the channel, consisting of velocity, water depth, and cross-section, were collected and measured. The velocity and water depth were determined using the current meter and a ruler, respectively, while the cross-sectional data of the channel was collected from a previous study of the Cibarani channel. The hydraulic data used in this study are presented in Table 3. Since the channel's flow is constant, a steady flow simulation was employed, while the water quality, which was the only changing variable, was represented by the Dissolved Oxygen (DO) parameter. It was measured directly on-site using a dissolved oxygen probe to generate a more accurate result. The Dissolved Oxygen (DO) parameter data for each sampling point are shown in Table 4.

Table 3. Hydraulic data (a) along the channel (b) in the wastewater inlet

(a)

Cibarani channel				
Date	Points	$\bar{U}$ [m/s]	H [m]	Q [m <sup>3</sup> /s]
09/11/2020	1	0.470	0.100	0.02000
	2	0.060	0.130	0.02023
	3	0.200	0.115	0.02046
	4	0.100	0.175	0.02059
	5	0.090	0.133	0.02060
	6	0.165	0.070	0.02560

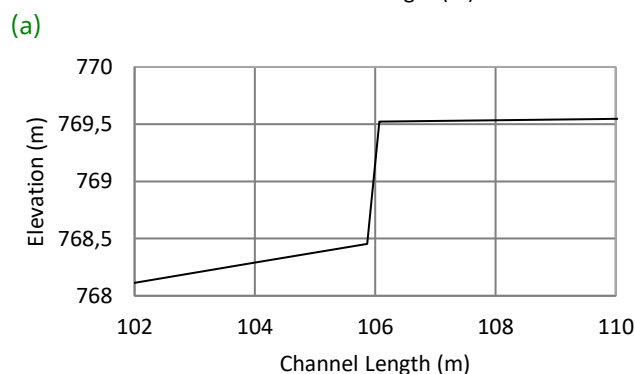
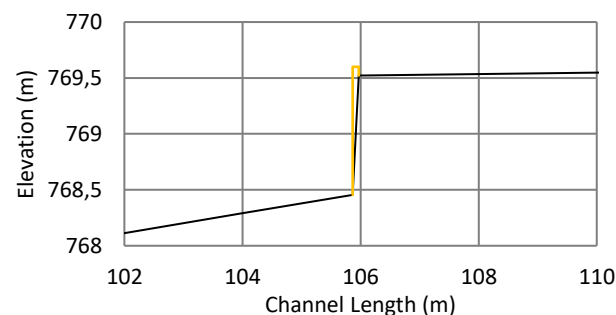
(b)

Wastewater inlet		
Date	Points	Q [m <sup>3</sup> /s]
17/11/2020	1	0.000304
	2	0.000171
	3	0.000213
	4	0.000008
	5	0.005000
24/11/ 2020	1	0.000157
	2	0.000290
	3	0.000048
	4	0.000007
	5	0.005000

Table 4. Wastewater quality data (a) along the channel, (b) in the wastewater inlet

(a) Cibarani channel			(b) Wastewater inlet		
Date	Points	C [mg/L]	Date	Points	C [mg/L]
09/11 2020	1	6.0	17/11 2020	1	1.9
	2	4.0		2	0.3
	3	0.8		3	2.3
	4	0.9		4	5.9
	5	2.8		5	2.0
	6	1.3		24/11 2020	1
			2	3.9	
			3	1.5	
			4	6.4	
			5	2.0	

The drop-structure in the HEC-RAS program can be modelled with inline weir or cross-sections. Meanwhile, two types of drop-structures were simulated in this study to give plausible results of the hydrodynamic and water quality aspects. However, the two types were a vertical wall and a steep riverbed, also their longitudinal sections are shown in Figure 5.



(a) (b) Figure 5. Longitudinal section of the (a) vertical wall (b) steep riverbed as the drop-structures.

### 3 RESULTS AND DISCUSSION

#### 3.1 Hydrodynamic Calibration

Manning’s roughness coefficient for the Cibarani channel was set to 0.023, according to the “Open Channel Hydraulics” by Chow (1959). Conversely, some parts of the channel filled with garbage were set at 0.05 due to the increase in the coefficient value. The HEC-RAS hydrodynamic modelling results were presented with the water surface (WS) and velocity profile along the channel from the different drop-structure models, as presented in Figures 6 and 7, respectively. According to the tests, the water depths from both drop-structure configurations ranged from 0.05 to 0.98 m, while the velocities ranged from 0.009 to 4.3 m/s. Hence, the hydrodynamic modelling in this study can represent the actual condition as the water

depth and velocity RMSE value for both drop-structure configurations gave the exact value of 0.06 and 0.24, respectively. This signified that the water quality analysis could be conducted to determine the drop-structure configuration. The RMSE values of both drop-structures are shown in Table 5

Table 5. Water surface and velocity RMSE

Points	Vertical wall and steep riverbed	
	WS	Velocity
1	0.03	0.13
2	0.05	0.11
3	0.09	0.56
4	0.01	0.02
5	0.11	0.02
6	0.00	0.03
RMSE	0.06	0.24

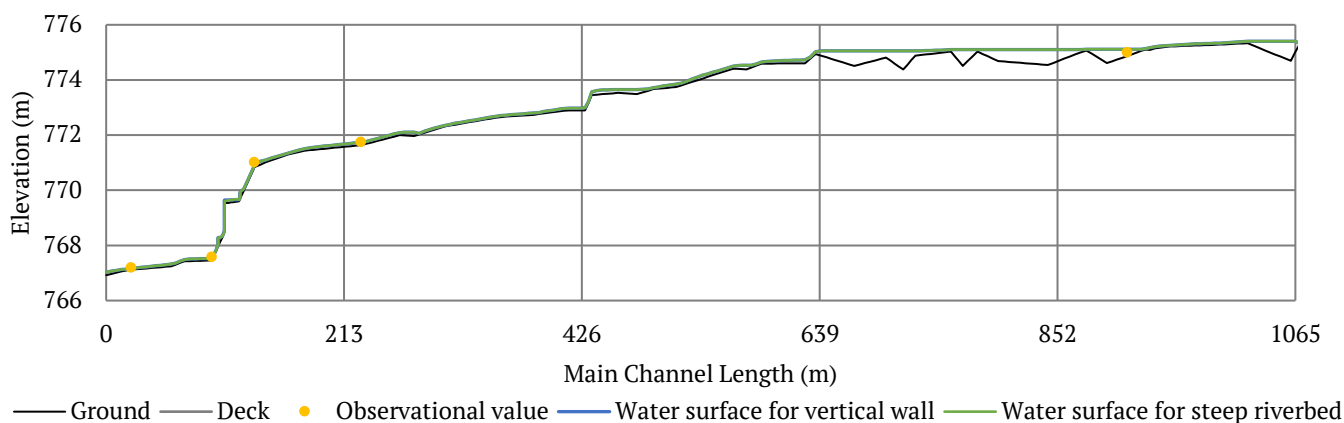


Figure 6. Water surface profiles.

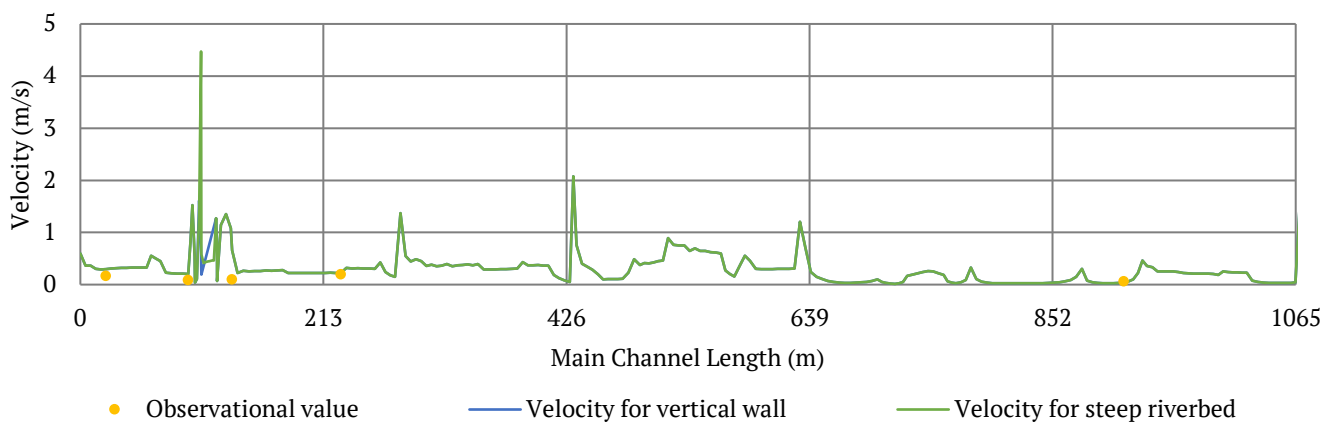


Figure 7. Velocity profiles.

### 3.2 Existing Water Quality Conditions

The values of the reaeration rate and dispersion coefficient, which are a function of velocity and water depth, were divided into three sections, namely first housing, drop-structure, and the second housing. Table 6 presents the dispersion coefficient values for each section and the type of drop-structure.

Table 6. Dispersion coefficient values of calibration process

Section	Vertical wall [m <sup>2</sup> /s]	Steep riverbed [m <sup>2</sup> /s]
First housing	0.082	0.082
Drop-structure	0.160	0.485
Second housing	0.216	0.216

Subsequently, the dispersion coefficients for each model and section, other parameters, as well as the initial and boundary conditions were needed for the water quality analysis. The initial conditions were acquired from the water quality data at the Cilimus weir intake, while the boundary conditions were obtained from the measurements at the wastewater inlets. In this study, the samples were collected at 08:00 a.m. to represent the time of wastewater discharge, as the normal discharge time is between 06:00 a.m. to 10:00 a.m., based on the residents' interviews. The reaeration rate values in the housing sections were estimated using the empirical equation from Jha *et al.* (2001), as it gives the best DO curve results. However, it could not be used for the

drop-structure section, leading to the application of the trial-and-error method. The reaeration rates were different in both types of drop-structures, as the values were generated mainly based on velocity and water depth, though these parameters remained constant in the observational points. Hence, the reaeration rate values of the mathematic model using HEC-RAS and the physical model differed from Tables 1 and 2. The values for each section and type of the drop-structure are shown in Table 7.

Table 7. Reaeration rate values of the calibration process

Section	Vertical wall [day <sup>-1</sup> ]	Steep riverbed [day <sup>-1</sup> ]
First housing	3.044	3.044
Drop-structure	125.0	135.0
Second housing	4.267	4.267

The drop-structure sections employed the same method in obtaining the reaeration rate and deoxygenation, which had no laboratory measurement. At 3.15 day<sup>-1</sup>, the deoxygenation rate could give the best DO curve results ranging from the HEC-RAS suggestion limit of 0.02 to 3.40 day<sup>-1</sup>.

Figure 8 shows the DO simulation curves of three drop-structure types from the calibration process. Their average water quality measurements were obtained by running the model for seven days. Table 8 presents the RMSE of the modelled values with the observed data.

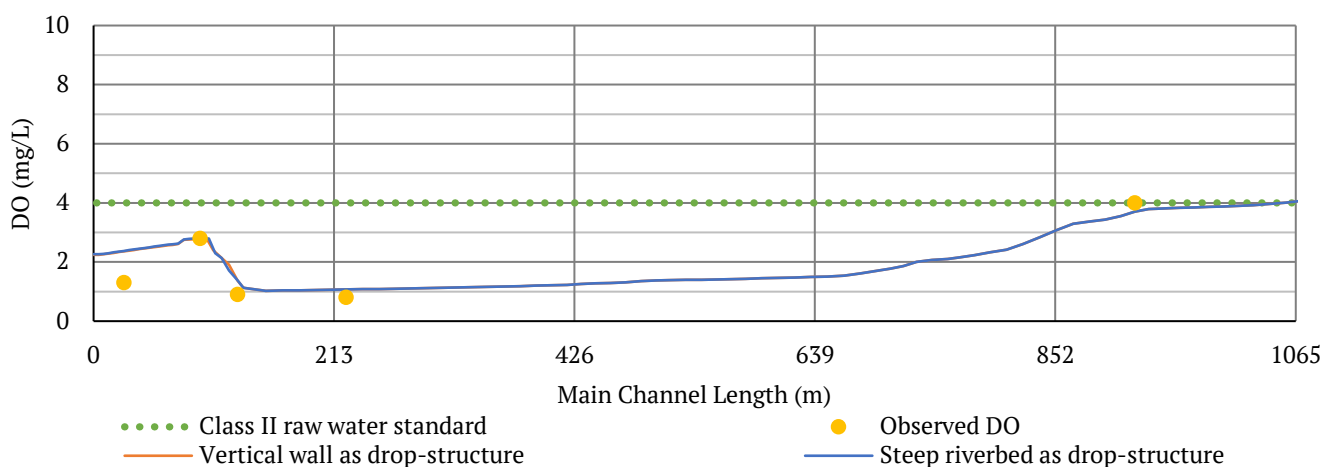


Figure 8. DO curve with the different types of drop-structure.

Table 8. The RMSE values of the calibration process

Points	Vertical wall	Steep riverbed
1	0.00	0.00
2	0.30	0.30
3	0.27	0.27
4	0.47	0.48
5	0.02	0.00
6	1.06	1.08
RMSE	0.50	0.51

The range of RMSE values from 0.50 to 0.51 for each type of drop-structure displayed in Table 8 indicates that the HEC-RAS water quality model can simulate the DO curves. Meanwhile, the vertical wall drop-structure generated a better RMSE value of 0.50. Although the reaeration rate was above the recommended value from the HEC-RAS program, this type of drop-structure can represent the actual conditions. This led to the use of the vertical wall in this study. According to Figure 8, the DO value showed a 210% increase from 0.9 mg/L to 2.8 mg/L after the water flowed through an existing drop-structure located 100 m from the downstream part. However, the structure could not increase the value of DO to 4.0 mg/L. This necessitates an improvement through the use of an additional drop-structure to elevate the DO values along the channel.

### 3.3 An Additional Drop-Structure at the First Housing

The simulation result in Figure 8 shows that the DO values failed to reach the class II of raw water

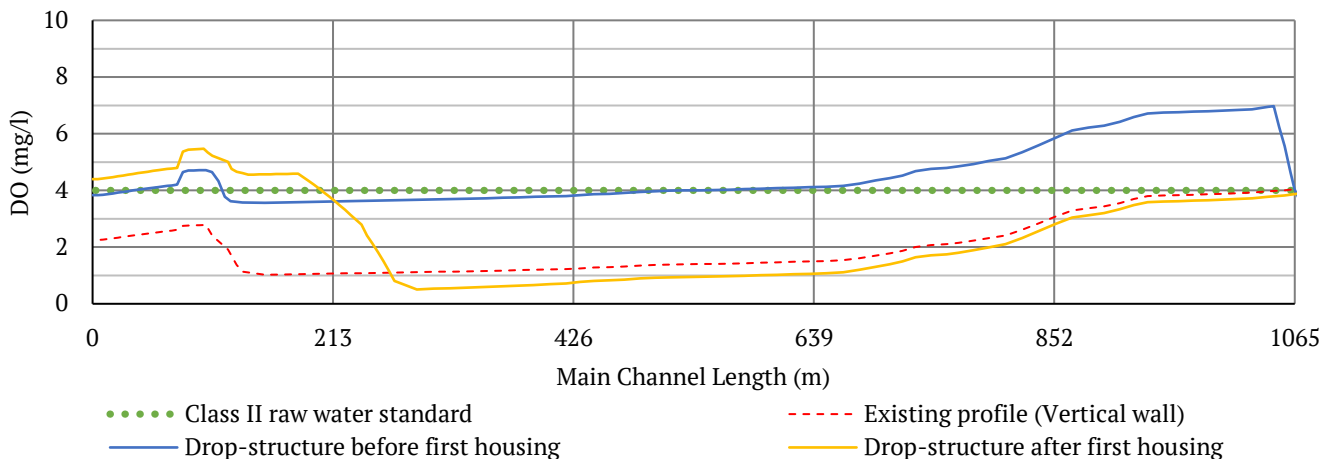


Figure 10. DO curve of the new drop-structure

standards. Therefore, this study tried to improve the DO values by adding a drop-structure in two possible places. First, a new drop-structure was placed before the first housing, around 200 m to the downstream part from the Cilimus weir intake. Then, the second, new drop-structure was placed after the first housing, around 1000 m downstream from the Cilimus weir intake. Both schemes can be seen in Figure 9.

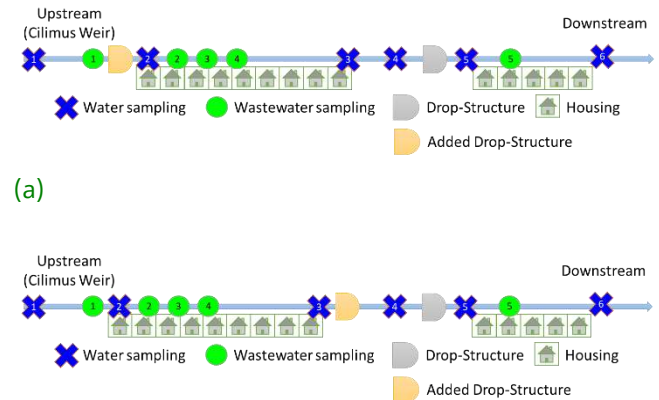


Figure 9. Scheme of additional drop-structure (a) before the first housing (b) after the first housing.

Changes in the reaeration rate and dispersion coefficient were recorded after modelling the new drop-structure. These parameters were obtained using the same procedure as the calibration process, while the deoxygenation rate was estimated exactly at 3.15 day<sup>-1</sup>. The dispersion coefficient and reaeration rate for each place are listed in Tables 9 and 10.

Table 9. Dispersion coefficient and reaeration rate of the new drop-structure before the first housing

Section	$E_x$ [m <sup>2</sup> /s]	$k_a$ [day <sup>-1</sup> ]
Before housing	0.00067	0.887
New drop-structure	0.00163	125
First housing	0.096	3.371
Existing drop-structure	0.108	125
Second housing	0.216	4.267

Table 10. Dispersion coefficient and reaeration rate of the new drop-structure after the first housing

Section	$E_x$ [m <sup>2</sup> /s]	$k_a$ [day <sup>-1</sup> ]
First housing	0.056	2.629
New drop-structure	0.073	125
After first housing	0.211	5.237
Existing drop-structure	0.124	125
Second housing	0.213	4.267

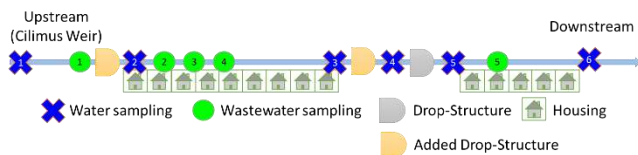


Figure 11. Scheme of the additional drop-structures before and after the first housing.

Table 11. Dispersion coefficient and reaeration rate of the new drop-structures before and after the first housing

Section	$E_x$ [m <sup>2</sup> /s]	$k_a$ [day <sup>-1</sup> ]
Before housing	0.00067	0.886
New drop-structure	0.00148	125
First housing	0.063	2.867
New drop-structure	0.073	125
After first housing	0.224	5.273
Existing drop-structure	0.124	125
Second housing	0.216	4.267

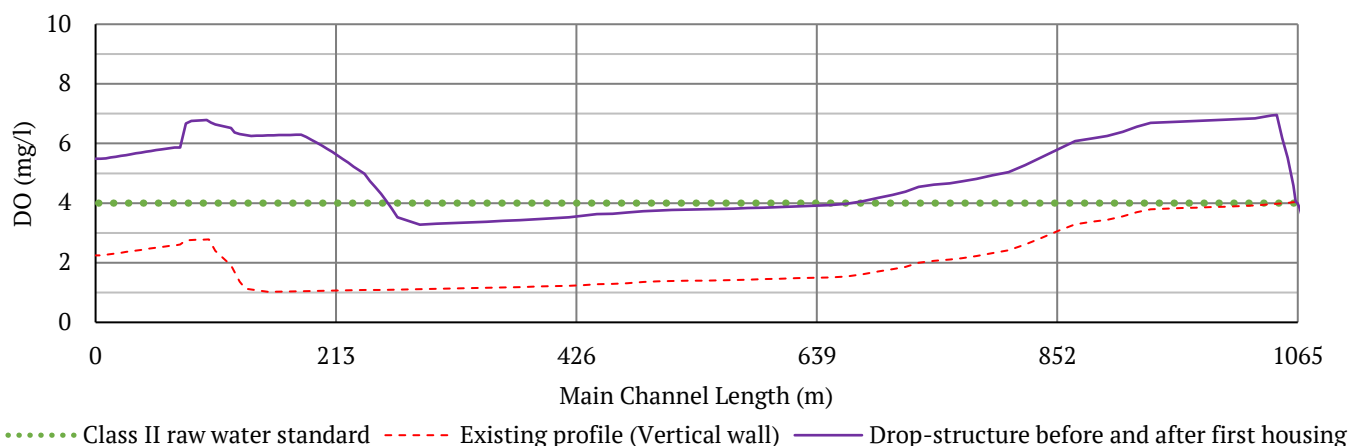


Figure 12. DO curve of the two new drop-structures.

The DO curves in Figure 10 indicate that the additional drop-structure after first housing could affect the DO value at the upstream part because of the limited cross-sections. A difference in DO value of around 10% signified that an additional drop-structure before the first housing is enough to improve the DO profile along the channel. Also, an additional drop-structure after the housing could improve the DO value for the second housing section. This led to the completion of the study analysis through the placement of two drop-structures along the channel.

### 3.4 Additional Drop-Structure Before and After the First Housing

As shown in Figure 11, this section involved an additional drop-structure before and after the first housing to observe the improvement of the DO value along the channel and around the downstream part. Table 11 presents the dispersion coefficient and reaeration rate for each section.

The DO curve results for the two additional drop-structures are shown in Figure 12. According to the illustration, the average DO value increased by 88% from 2.6 mg/L to 4.9 mg/L. The values at the downstream part of the channel also elevated by 135% from 2.3 mg/L to 5.4 mg/L. Therefore, the best combination to improve the DO value along the channel is placing two drop-structures before and after the first housing.

## 4 CONCLUSION

According to the water test results, the Cibarani channel fell short of class II of raw water standards with an average DO value of 2.6 mg/L. The DO concentrations increased from 0.9 to 2.8 mg/L after the water flowed through a drop-structure near Siliwangi Street. Subsequently, this study conducted a water quality simulation using the vertical wall type of drop-structure. This technique produced a smaller RMSE value and a more suitable reaeration rate of  $125 \text{ day}^{-1}$  than the other configuration, despite a significant difference in the reaeration rate value between the mathematicians' estimation and the physical

model. Although an additional drop-structure at the channel's upper stream was enough to improve the averaged DO values, the downstream part of the channel still needed improvement. This led to the combination of a drop-structure before and after the first housing to significantly increase the DO concentrations between the ranges of 3.3 to 6.9 mg/L along the channel to reach the class II raw water standards. Meanwhile, further observation and data collection are needed to improve and obtain better study results.

### DISCLAIMER

The authors declared no conflict of interests.

### AVAILABILITY OF DATA AND MATERIALS

All data are available from the author

### AUTHOR CONTRIBUTION STATEMENTS

All authors conceived and designed the study. Jonathan W performed data collection, hydraulic modelling, and prepared original writing; Finna F developed the research methodology and model validation; Finna F and Jonathan W carried out the water quality test; Finna F and Doddi Y developed the concept, review and editing, and visualization. All authors contributed to manuscript revisions. All authors approved the final version of the manuscript and agree to be held accountable for the content therein.

### ACKNOWLEDGMENTS

The author is grateful to the personnel at the Centre of Water Resources Engineering, Parahyangan Catholic University, who provided support, guidance, suggestions, and recommendations during this study. The author is also grateful to other persons that cannot be mentioned individually.

### REFERENCES

- Arief, A., 2014. Pengaruh Keberadaan Bendung dan Terjunan pada Konsentrasi Oksigen dalam Air. *Jurnal Rekayasa Sipil*, 2(2), pp. 154-166.
- Bachrein, S., 2012. Pengembangan Daerah Aliran Sungai Cikapundung: Diagnostik Wilayah. *Jurnal*

- Bina Praja: Journal of Home Affairs Governance*, 4(4), pp. 227-236.
- Brunner, G. W. & CEIWR-HEC., 2010. *HEC-RAS River Analysis System User's Manual*. Davis, CA: Hydrologic Engineering Center.
- Damarany, P., Fachrul, M. F. & Astono, W., 2009. Kajian Kualitas Air Sungai Cipinang Bagian Hilir Ditinjau dari Parameter BOD dan DO menggunakan Model Qual2E. *Jurnal Teknologi Lingkungan*, 5(2), pp. 62-74.
- Government of Indonesia., 2001. Peraturan Pemerintah Republik Indonesia Nomor 82 Tahun 2001 tentang Pengelolaan Kualitas Air dan Pengendalian Pencemaran Air.
- Hayhera, F. O. & Yudianto, D., 2019. *Studi Pengaruh Perubahan Kecepatan Aliran Air terhadap Peningkatan Kualitas Air pada Saluran irigasi Cibarani*. Bandung, Seminar Nasional Teknik Sumber Daya Air.
- Jha, R., Ojha, C. S. P. & Bhatia, K. K. S., 2001. Refinement of Predictive Reaeration Equations for a Typical Indian River. *Hydrological Process*, 15, pp. 1047-1060.
- Ji, Z. G., 2008. *Hydrodynamics and water quality. Modeling River, Lakes, and Estuaries*. Hoboken, NJ: Wiley-Interscience.
- Kashefipour, S. M. & Falconer, R. A., 2002. Longitudinal Dispersion Coefficient in Natural Channels. *Water Research*, 36(6), pp. 1596-1608.
- Peavy, H. S., Rowe, D. R. & Tchobanoglous, G., 1985. *Environmental Engineering*. New York: McGraw-Hill.
- Rahayu, Y., Juwana, I. & Marganingrum, D., 2018. Kajian Perhitungan Beban Pencemaran Air Sungai di Daerah Aliran Sungai (DAS) Cikapundung dari Sektor Domestik. *Jurnal Rekayasa Hijau*, 2(1), pp. 61-71.
- Triane, D. & Suharyanto., 2015. Pemodelan Kualitas Air menggunakan Model QUAL2K (Studi Kasus: DAS Ciliwung). *Jurnal Teknik Lingkungan*, 21(2), pp. 190-200.
- Trisnojoyo, R. R., Yudianto, D. & Wijaya, O. T., 2017. *Studi Estimasi Beban Limbah Cair pada Saluran Irigasi menggunakan HEC-RAS*. Bandung, Seminar Nasional Teknik Sumber Daya Air.
- Ughbebor, J. N., Agunwamba, J. C. & Amah, V. E., 2012. Determination of Reaeration Coefficient K<sub>2</sub> for Polluted Stream as a Function of Depth, Hydraulic Radius, Temperature and Velocity. *Nigerian Journal of Technology*, 31(2), pp. 174-180.
- Yudianto, D. & Xie, Y., 2008. The Development of Simple Dissolved Oxygen Sag Curve in Lowland Non-Tidal River by using Matlab. *Journal of Applied sciences in Environmental Sanitation*, 3(3), pp. 137-

[This page is intentionally left blank]

# Optimizing The Functional Performance of Road Network using Vulnerability Assessment to Cope with Unforeseen Road Incidents

Mukhammad Rizka Fahmi Amrozi<sup>1,\*</sup>, Raihan Pasha Isheka<sup>2</sup>

<sup>1</sup>Department of Civil and Environmental Engineering, Universitas Gadjah Mada, Yogyakarta, INDONESIA  
Jalan Grafika No 2 Yogyakarta

<sup>2</sup> Department of Civil Engineering, Vocational College, Universitas Gadjah Mada, Yogyakarta, INDONESIA  
Jalan Yacandra Unit IV Yogyakarta

\*Corresponding authors: [fahmi.amrozi@ugm.ac.id](mailto:fahmi.amrozi@ugm.ac.id)

**SUBMITTED** 09 August 2021 **REVISED** 09 September 2021 **ACCEPTED** 02 October 2021

**ABSTRACT** An Urban Road network is often used for multipurpose trips, due to their transportation functions, such as attractiveness and orientation, as well as social, ecological, and economic features. In Indonesia, road incidents have reportedly increased during the last decade because of a higher frequency of natural hazards, accidents, and on-street mass demonstrations. These incidents are found to degrade or terminate road access, forcing users to utilize alternative routes and decreasing the service performance in adjacent directions. Due to the unexpected occurrences at any location and time, there is a need to investigate the impact of random incidents on road performances. Several accessibility indexes have also been used to evaluate the vulnerability of road networks. However, this is less practical in Indonesia, with the road authority using functional performances as the indicator. This indicates the need for an index to be developed based on road performance parameters. Therefore, this study aims to develop a road performance-based vulnerability index known as the RCI (Road Criticality Index). Combined with a traffic simulation tool, this system is used as an alternative index to assess vulnerabilities, by identifying the road(s) providing worse consequences due to unforeseen incidents. This simulation was conducted by using the PTV Visum, assuming a road section is closed due to the worst incident scenarios. The result showed that the RCI offered a more comprehensive assessment than the existing indicator (volume capacity ratio). The RCI included travel speed and mobility components for evaluating both local and global road performances. With the knowledge of the most vulnerable locations and their consequences, road authorities can prioritize maintenance and development strategies based on the criticality index. Also, preventive measures should be conducted to mitigate risk under a constrained budget. This methodology can be applied to sustainably enhance the resilience of urban road networks.

**KEYWORDS** Urban Road; Vulnerability Index; Road Performance; PTV Visum; Road Network Resilience.

© The Author(s) 2022. This article is distributed under a Creative Commons Attribution-ShareAlike 4.0 International license.

## 1 INTRODUCTION

### 1.1 Background

Most Indonesian areas located on the Pacific Ring of Fire and at the meeting point of three continental plates are prone to natural disasters, such as earthquakes and volcanic activities (Stanton-Geddes and Vun, 2019). According to The World Bank (2019), Yogyakarta as one of the most prone metropolitan cities in Indonesia, was categorized vulnerable to unforeseen road incidents and major natural disasters, such as strong winds, landslides, earthquakes, tsunami, and volcanic activity. As an educational city where several prestigious public and private universities are established, the road sections/junctions in Yogyakarta are often

disrupted due to mass demonstration activities, which are essentially legal to convey aspirations based on human rights and law protection. These are often carried out by marching through several streets and staying at a specific location like Malioboro road and KM-0 intersection (Mahpudin *et al.*, 2020). According to BPS statistics (2021), road disruptions increased by 1-3% due to a higher frequency of natural hazards, traffic accidents, and on-street mass demonstrations during previous decades. This raised public awareness regarding the consequences of these incidents on the road networks' performance reliability.

Transport networks should be managed to achieve a reliable and optimum level of performance to all locations in need of commutation service (Amrozi and Evdorides, 2019). Depending on the type of threat, road incidents are found to degrade or terminate transport access, as well as worsen service performance on the adjacent networks. Since these incidents are bound to unexpectedly occur at any location and time, the need to investigate the impact of any random road occurrences on network performance is very essential, through vulnerability assessment. This is important due to the massive impact of the disturbance on the critical road(s), which triggers a systemic chain effect on the overall network performances, including socio-economic activity losses. Several accessibility indexes have reportedly been used to assess the vulnerability of road networks (Sugishita and Asakura, 2021). However, this is less practical in Indonesia, as the road authority used functional performance as the standard indicator. Also, most of them are found to only use a single indicator, such as travel time, cost, distance, and link volume. Therefore, a new performance-based vulnerability index should be developed based on some road performance parameters, to measure the impact and identify the most susceptible network section(s). Road managers should also prioritize performances based on the criticality index value, and adopt preventive measures to mitigate exposure risks under a constrained budget.

### 1.2 Vulnerability Assessment

Vulnerability is defined as the susceptibility to any incidents capable of reducing road network performances (Berdica, 2002). This concept emphasizes the consequences of several incomplete components (links or nodes), regardless of the possibility of the failure (Taylor and Susilawati, 2012), indicating that network susceptibility focuses on the weaknesses and shortcomings for connectivity. Furthermore, this provides a more sensitive analysis of road network impact performance when there is a disruption at a specific link. The high vulnerability index states that the occurrence of

disruptions at any component(s) leads to a massive negative impact on all road networks. At the planning stage, vulnerability analysis is used as guidance for generating a new road alignment and standard, utilized as an alternative route. Meanwhile, this evaluation is used to identify the most vulnerable road during the operation stage. Depending on the threat, different actions were adopted to swiftly minimize impact and restore road performances.

Vulnerability is generally assessed using several methods, including inventory-based risk assessment, as well as topological, serviceability, and accessibility methods (Taylor, 2017). According to Jenelius and Mattsson (2015), the concept and measurement of vulnerability focused on the potential degradation of road networks and their impacts on society. Although serviceability and accessibility methods are often used for the measurement of network vulnerabilities, they still offered better clarity as performance standards. The incident types reducing serviceability often include vehicle crashes, roadworks, traffic congestions, on-street and weather events, as well as natural hazards, which are known to cause partial or complete blockages (Taylor, 2017).

Vulnerability methods are known to consider the exposure level of negative impacts, based on the performance measurement changes for a different road network state, such as with and without degraded scenarios. According to the study of Oliveira *et al.* (2016), the identification of critical links was an outcome of vulnerability assessment. A ranking system for these links is often carried out based on the degree of a negative network impact. Moreover, the traditional practices of road infrastructure management still use volume capacity ratio (VCR) to measure vulnerability, due to being simple and easy to carry out (El-Rashidy and Grant-Muller, 2014). As alternatives, several methods used to measure vulnerability includes (i) Link Importance Index (Rupi *et al.*, 2015), (ii) Network Robustness Index (Scott *et al.*, 2006), (iii) Network Trip Robustness Index (Sullivan *et al.*, 2010), (iv) NQ Index (Nagurney and Qiang, 2008), and (v)

Network Vulnerability Index (Balijepalli and Oppong, 2014). However, these indices are previously developed to serve a specific purpose and consideration. For example, NTRI emphasizes travel demand variable while LII focuses on link volume and travel cost. Although these models function when appropriately used, they are still likely to lead to bias interpretation when the usage constraint/limitation is violated. Therefore, the selection of these models to assess vulnerability should consider the definition, purpose, scope, and limitation of the index.

### 1.3 Functional Performance of Road Network

Road networks are a fundamental asset to support socio-economic activities, due to being expected to offer convenient, safe, and efficient transportation services to communities (Karlaftis and Kepaptsoglou, 2012). Also, the performance measurement is theoretically a systematic process to ensure the road achieves predetermined goals. According to the OECD (2001), the indicator performance varied depending on the perspectives of the stakeholders. For instance, road users demand top-level performances to minimize cost (RUC). However, road administration aims to optimize total benefit by balancing RUC and RAC (road agency cost) in achieving optimum rewards. Each country is found to probably have different standards and policies in measuring road performance, although most of them still rely on the level of service (LOS) measure developed by The American Association of State Highway and Transportation Officials (AASHTO). This is primarily based on volume capacity ratio (VCR) (Scott *et al.*, 2006), which is argued to likely be insufficient towards assessing the overall traffic condition and performance. In addition, some variables are considered and added to the VCR, towards measuring road performances, e.g. travel time, speed, delay, congestion index, VKT (vehicle-kilometre of travel), PKT (person-kilometre of travel), system reliability, and GTC (generalized travel cost) (Taylor, 2017).

## 2 METHODS

Road incidents and natural disasters are events that often occur unexpectedly. The impact of these events is mostly tough to estimate, as the type, exposure, time, and location of their occurrences are still unknown (Auerbach *et al.*, 2016). These conditions are then assessed using a worst-case scenario, assuming that access on a specific road is terminated due to the occurrence of an incident (Susilawati and Taylor, 2008). Therefore, the worst impact of an incident(s) at a road section is modeled as a link closure. Using the PTV Visum software, the impact of this closure within the road network was simulated and compared to normal conditions. This indicated that worse changes led to more critical links in the overall road network performance.

The aim of this study is based on the development of a performance-based vulnerability index, which is to be used as an indicator with the analysis of a traffic simulation tool. This is to compare and assess the degree of road closure impact on the overall network performance, due to the occurrence of incidents. The index value was also compared to normal conditions (without incident) and all possible link scenarios. Subsequently, the overall procedures are shown in Figure 1.

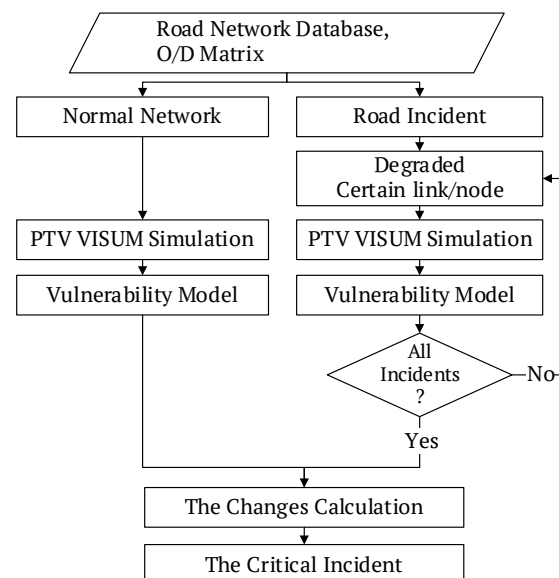
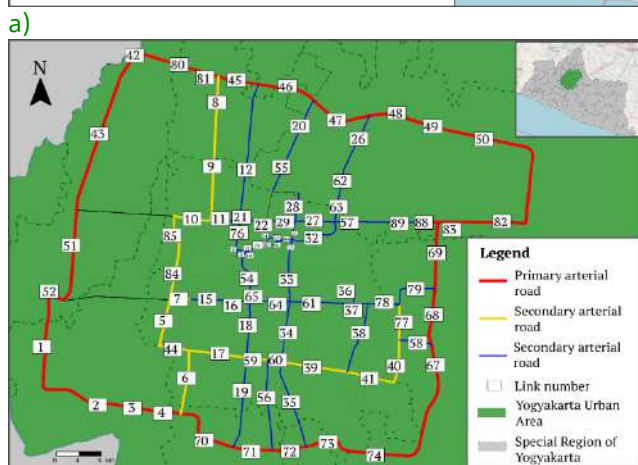
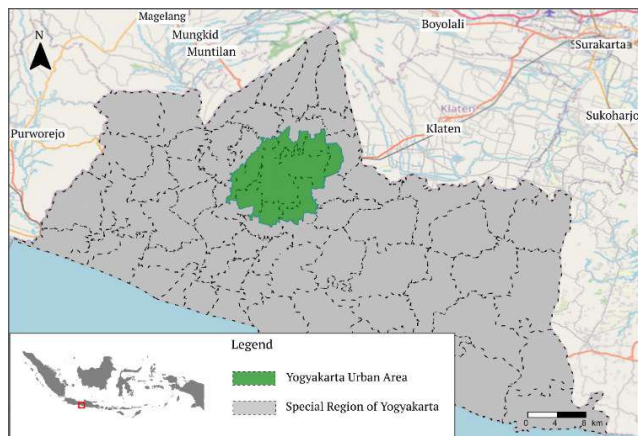


Figure 1. Research methodology flowchart.

### 2.1 Development of Road Network Model

The location of this study is the urban area of Yogyakarta, an agglomeration region covering the regency of Sleman, Bantul, and Yogyakarta City. This area was selected due to being one of the most vulnerable metropolitan cities in Indonesia (Chapter 1.1.). Also, the selection was based on the identification of the urban road network boundaries, such as the area within the ring road. According to Fitrada *et al.* (2019), the Yogyakarta road models were developed based on the PTV Visum design of the Special Region of Yogyakarta network. Based on the administrative boundaries of 17 sub-district zones in the urban region of Yogyakarta, the locations for the O/D matrix were formed. To represent the location of a road incident, 89 sections (165 links) were modeled in the PTV Visum, including three types of network function, including primary arterial, as well as secondary artery and collector roads, as shown in Figure 2.



b) Figure 2. Road network modeled in PTV Visum: a) Location of case study, b) Road sections modeled as links.

### 2.2 Traffic Simulation using PTV Visum

The traffic modeling in this study was simulated using the PTV Visu, based on travel demand (O/D matrix) and networks during a peak hour period in 2019. In the traffic assignment process, the equilibrium method was applied to represent the urban network characteristics. This assignment assumed that travelers were familiar with the Yogyakarta road network or use a guidance tool, such as google maps, to locate the best route with minimum travel time (PTV, 2021). Moreover, the validation value (R-squared) between the realistic traffic flow base model and average speed was 0.91 each, respectively. This indicated that the base model represented the actual condition. For the incident scenario, a road link was sequentially deleted in each simulation process, with the running procedure being carried out 89 times. Also, the outputs from this modeling procedure were the volume capacity ratio, travel speed, *VKT*, and *VHT* (vehicle hours travel).

### 2.3 Development of Vulnerability Index

The vulnerability index in this study was developed based on multi-parameters, where the selected components were aggregated into a single composite model, through the referral of a theoretical framework. Also, the development procedure of this index adopted the methodology from Nardo *et al.* (2008), as shown in Figure 3.

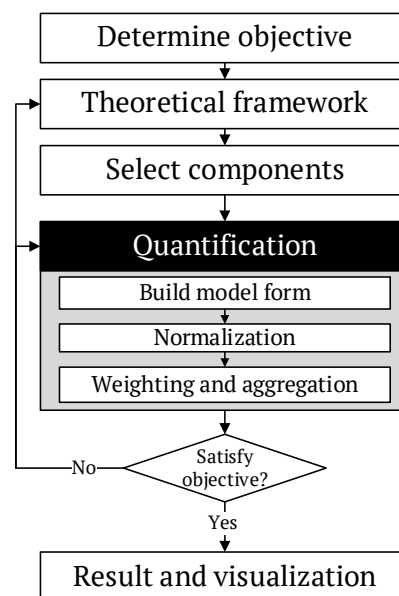


Figure 3. Development of vulnerability model.

### 2.3.1 Components of the vulnerability index

The functional performances of Indonesian roads are often measured based on the volume capacity ratio and travel speed, known as the level of service (LoS) (Tamin, 2000). This LoS value represents the DOF (degree of freedom) of vehicle movement, which ranges from level A-F as the best to worst services, respectively. However, there was no quantitative threshold stated in the latest standard (PM 96/2015) for assessing volume capacity ratio, due to being in KM 14/2006. This indicated that the ratio referred to other associated standards, such as the IHCM (1997), where a road section was categorized as having good performance when  $VCR \leq 0.75$  (Table 1).

Based on speed parameters, the Ministry of Transport (2015) proposed a very high threshold that was hard to achieve. For example, a 70 km/h regulation of an average velocity as the minimum performance standard on primary arterial roads. However, setting up 50 and 60 km/h for local and secondary arterial/collector roads was impractical for urban networks, due to violating the limit standard. This was in line with Sudibyo *et al.* (2017), which demonstrated that meeting the PM 96/2015 standards (minimum LoS B or C) was very hard in Indonesia, as most roads were rated LoS E or worse. Despite the argument, an alternative threshold was still developed based on the expected operational speed from the study of BSN (2004), regarding the provision of a more reasonable value (Table 1). Meanwhile, the threshold for a secondary urban road should be

adjusted to 75%, due to often having a lower speed limit and higher disruption, such as on-street parking and other obstacles.

According to the road section parameters, mobility (network parameter output from PTV Visum) was added to assess the overall impact on the network as a system (global parameter). This is defined as the movement of people or goods, often measured by trips, distance, and speed (Litman, 2016). There is often an assumption that a travel mileage increase benefits society, due to improving the choice and number of destinations attained by people. However, the travel demand in this study was predetermined using a fixed O/D matrix. Furthermore, the number and pattern of trips should be similar for the scenario, with and without the occurrence of incidents. This indicated that an increase in travel mileage signified a delay in reaching a destination worsening road performances. However, there was recently no minimum standard on the existence of mobility in Indonesia. Based on the most critical incidents, the identification process focused on the mobility value changes with and without incidents, to assess the degree of impact. Therefore, the overall vulnerability measurement in this study used four parameters, namely volume capacity ratio, travel speed,  $VHT$ , and  $VKT$ , which represented the local and global indicators of road performance. Since these parameters are also available as PTV Visum simulation outputs, their utilization was theoretically approved and practically.

Table 1. Performance standard in Indonesia based on road function

Road function		Expected operational speed (km/h)*	Good road performance service standard **					Preferred bad threshold***	
			Maximum $VCR$		Minimum operational speed (km/h)			Volume Capacity Ratio	Speed (km/h)
			IHCM/ 1997	KM 14/2006	KM 14/2006	PM 96/2015	BSN/ 2004		
Arterial	Primary	50 - 100	0.75	0.45 (LoS B)	80 (LoS B)	70 (LoS B)	50	> 0.75	< 50
	Secondary	50 - 80	0.75	0.80 (LoS C)	30 (LoS C)	60 (LoS C)	50	> 0.75	< 40
Collector	Primary	40 - 80	0.75	0.50 (LoS B)	90 (LoS B)	70 (LoS B)	40	> 0.75	< 30
	Secondary	30 - 50	0.75	0.80 (LoS C)	30 (LoS C)	60 (LoS C)	30	> 0.75	< 25
Local	Secondary	30 - 50	0.75	0.85 (LoS D)	15 (LoS D)	50 (LoS D)	30	> 0.75	< 15

\* based on BSN (2004);  $VCR$ =volume capacity ratio; LoS= Level of Service;

\*\* Based on IHCM (1997), BSN (2004), Ministry of Transport (2006), and Ministry of Transport (2015).

\*\*\* threshold for bad road performance used to measure vulnerability index.

### 2.3.2 Quantification of the vulnerability index

Based on this study, the vulnerability parameters were measured based on the results obtained from the PTV Visum simulation. This indicated that the unit of analysis for the indexes was in line with the analytical features of the simulation software, i.e., road section by direction. For instance, a one and two-way network count as one and two analytical units. The general equations to quantify the vulnerability indexes are described in Equation (1) and (2).

$$RCI = f(VCR, v, VHT, VKT) \quad (1)$$

$$RCI = VCR + v + VHT + VKT \quad (2)$$

Where  $RCI$  is the road criticality index,  $VCR$  is the volume capacity ratio,  $v$  is the travel speed (km/h),  $VHT$  is the vehicle hour travel (vehicle hour), and  $VKT$  is the vehicle kilometre travel (vehicle km). To investigate the practical use of the vulnerability measurement, the index was developed and tested using four different quantification techniques, i.e., M1, M2, M3, and M4.

- a) Model 1 (M1) was measured based on the percentage changes in each parameter, due to the scenario of incidents. Afterwards, the change values were sorted. For each parameter, the top five worst changes were provided with 1 point. This was due to the model having four parameters, with scores ranging from 0-4.
- b) Model 2 (M2) applied thresholds to count the number of bad performance links, due to the road incidents (Table 1). With a value exceeding the threshold, the direction of the link was counted and categorized as having a bad performance. Afterwards, the increased number of bad links were orderly sorted, as the top five worst changes for each incident were provided with 1 point. Similar to M1, the vulnerability score ranged from 0 to 4.
- c) Model 3 (M3) calculated the percentage changes of each parameter as observed in M1.

However, the results were normalized and not sorted as top five, i.e., divided by its maximum value for each term. Similar to M1 and M2, the score ranged from 0-1 and 0-4 for each component and total marks. However, M3 provided a decimal value to offer more detail and sensitive measurements.

- d) Model 4 (M4) is a hybrid approach between M2 and M3, which applied a threshold for each unit of analysis.

## 3 RESULTS

### 3.1 Changes in Road Performance

More than half of the roads (51.5%) in the Yogyakarta urban area were in severe congestion ( $VCR > 0.75$ ) during peak hours, based on the normal conditions without incident. With the incident scenarios, the simulation showed that the road performance was worsened at approximately 58.2%, as shown in Figure 4. This indicated that the impact of incidents on vulnerability parameters was in line with the model assumption, except for mobility values (Table 2). Moreover, the results consistently provided a higher VCR and lower travel speed when a particular road was disrupted. However, the  $VKT$  and  $VHT$  (Vehicle Kilometre Travel and Vehicle Hour Travel) values were inconsistent due to having a positive or negative outcome, depending on the road closure scenario. For example, road users that often use the northern ring network (Purworejo-Surakarta route) were forced to use alternative routes through the city centre, because of the closure scenario shown in Figure 4. Although this route offered a shorter distance, the travel time was still longer. Meanwhile, the southern ring distance was farther than the inner-city route and relatively delivered a faster trip. Each area also had a different configuration, indicating the variation of an incident impact based on the density and geometric patterns of the network. This was found to provide a reliable alternative route option.

Table 2. The impact of road incidents on the road network performance in Yogyakarta (the Year 2019)

Incident location (link number)	Road Function	Changes in road section parameter (local)								Changes in network parameter (global)			
		By raw value (M1 & M3)				By threshold (M2 & M4)				Mobility (M1, M2, M3, M4)			
		VCR		Travel speed		VCR		Travel speed		VHT		VKT	
(VCR)	(%)	(km/h)	(%)	(VCR)	(%)	(km/h)	(%)	(Veh hour)	(%)	(Veh km)	(%)		
1	AP	47.2	36.5	-1,018	-18.8	39.0	49.4	28	30.8	3,141.3	12.8	-12,209.8	-2.0
2	AP	37.7	29.1	-1,005	-18.6	32.0	40.0	23	25.3	240.7	1.0	-22,538.2	-3.7
⋮	⋮	⋮	⋮	⋮	⋮	⋮	⋮	⋮	⋮	⋮	⋮	⋮	⋮
47	AP	51.6	40.1	-1,269	-23.4	46.0	58.2	38	42.2	5,323.1	21.6	28,104.7	4.7
48	AP	43.8	33.8	-1,120	-20.7	40.0	50.0	33	36.3	3,161.2	12.8	8,504.2	1.4
⋮	⋮	⋮	⋮	⋮	⋮	⋮	⋮	⋮	⋮	⋮	⋮	⋮	⋮
87(1way)	KS	35.0	27.0	-1,024	-18.6	33.0	41.8	25	27.8	164.0	0.7	1,134.1	0.2
88	AP	36.8	28.5	-1,056	-19.4	33.0	42.3	31	34.8	1,261	5.1	13,243.5	2.2
89	KS	37.4	29.0	-1,063	-19.5	33.0	42.3	28	31.5	1,070.6	4.3	7,856.1	1.3
Min		33.3	25.6	-1,269	-23.4*	27.0	33.8	19	21.1	-113.2	-0.5	-30,289.9	-3.7
max		51.6	40.1*	-937	-17.4	46.0	58.2*	38	42.2*	5,430.3	22.0*	28,104.7	4.7*

\* Max value (used for normalization procedure in M2 and M4); AP= primary artery, AS= secondary artery, KS= secondary collector.

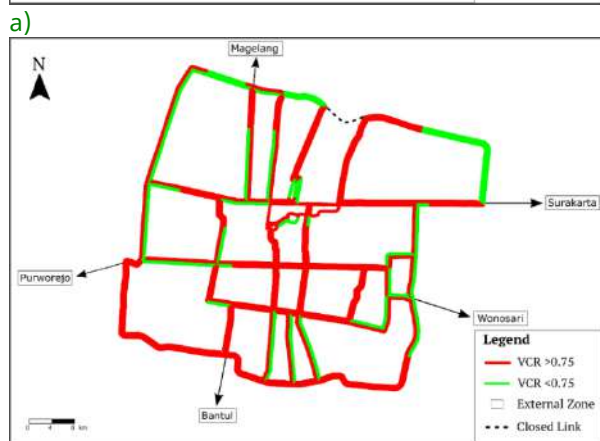
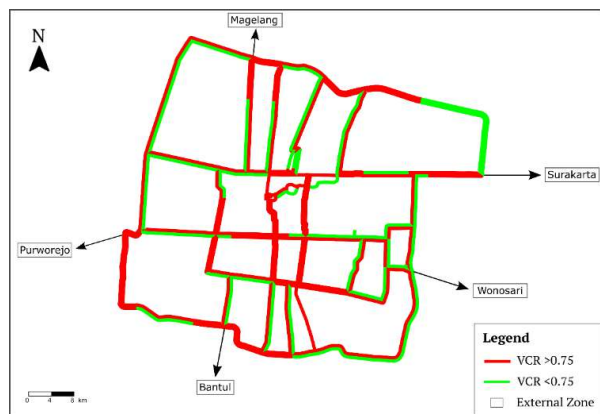


Figure 4. Simulation result of road condition between with and without incident during peak hour: a) The Volume Capacity Ratio without road closure/incident, b) The Volume Capacity Ratio with road closure/incident

### 3.2 Quantification of Vulnerability Index

The vulnerability models in this study were developed based on four different quantification mechanisms, which had similar scoring variations

(1 to 4). The higher the vulnerability score, the worse the road performance impact. Therefore, the most critical road incident was identified by the highest vulnerability score. Based on Table 3, the four vulnerability models (M1, M2, M3, M4) showed that the worst impact occurred at a closure link of 47, i.e., Jalan Ring Road Utara Kentungan-Gejayan (Figure 4b). However, the subsequent order for the top 5 most vulnerable roads was different. The M3 and M4 models also provided a clear priority order from the best to the worst, although M1 and M2 produced indefinite orders, e.g., some roads with similar scores. Despite the simple quantification procedures on M1 and M2, the M3 and M4 models still offered more sensitive and accurate results through decimal scores. In addition, M1 and M2 did not show the priority order outside the top 5, compared to the M3 and M4 models.

Based on Table 3, all vulnerability components had a positive value except the vehicle kilometre travel. This indicated that the road disturbance provided an opposite impact from the presumption. Although the incident worsened the other performance indicators ( $VCR$ ,  $v$ ,  $VHT$ ), it still offered certain benefits such as increased mobility performance (reduced  $VKT$ ), due to shorter travel distance. Meanwhile, an argument stated that the benefit should be ignored due to the vulnerability focusing on negative impact or

exposure. Furthermore, a shorter travel distance was found to be meaningless with a drastic increase in time, indicating that the total road user cost (RUC) is continuously integrated due to delays (longer travel times). Therefore, the negative scores were ignored and set as zero. In this case, there was no significant difference for the top 5 worst impacts. Also, the changing priority order was only identified at the lowest two impacts, such as 88 and 89. This indicated that the choice to set the negative value at zero was optional in measuring the RCI, based on the insignificance of the impact.

**Table 3. The most critical incidents based on vulnerability model alternatives**

<b>M1</b>							
Location		Component				RCI score	Priority
Link	F*	VCR	Speed	VHT	VKT		
47	AP	1	1	1	1	4	1
52	AP	1	1	1	0	3	2
69	AP	1	1	1	0	3	2
83	AP	0	1	0	1	2	3
70	AP	1	0	1	0	2	3
<b>M2</b>							
Location		Component				RCI score	Priority
Link	F*	VCR	Speed	VHT	VKT		
47	AP	1	1	1	1	4	1
49	AP	0	0	1	1	2	2
48	AP	0	0	1	1	2	2
83	AP	0	1	0	1	2	2
82	AP	0	0	1	1	2	2
<b>M3</b>							
Location		Component				RCI score	Priority
Link	F*	VCR	Speed	VHT	VKT		
47	AP	1.00	1.00	0.98	1.00	3.98	1
52	AP	0.96	0.94	1.00	0.55	3.45	2
83	AP	0.82	0.90	0.74	0.92	3.38	3
69	AP	0.94	0.91	0.99	0.27	3.11	4
49	AP	0.84	0.89	0.59	0.61	2.94	5
⋮	⋮	⋮	⋮	⋮	⋮	⋮	⋮
42	AP	0.68	0.74	0.11	-0.94	0.59	88
43	AP	0.69	0.76	0.12	-1.07	0.50	89
<b>M4</b>							
Location		Component				RCI score	Priority
Link	F*	VCR	Speed	VHT	VKT		
47	AP	1.00	1.00	0.98	1.00	3.98	1
83	AP	0.76	0.89	0.74	0.92	3.32	2
52	AP	0.79	0.67	1.00	0.55	3.00	3
49	AP	0.87	0.89	0.59	0.61	2.97	4
69	AP	0.78	0.68	0.99	0.27	2.73	5
⋮	⋮	⋮	⋮	⋮	⋮	⋮	⋮
42	AP	0.72	0.52	0.11	-0.94	0.40	88
43	AP	0.76	0.52	0.12	-1.07	0.33	89

\* F=function; AP=primary artery

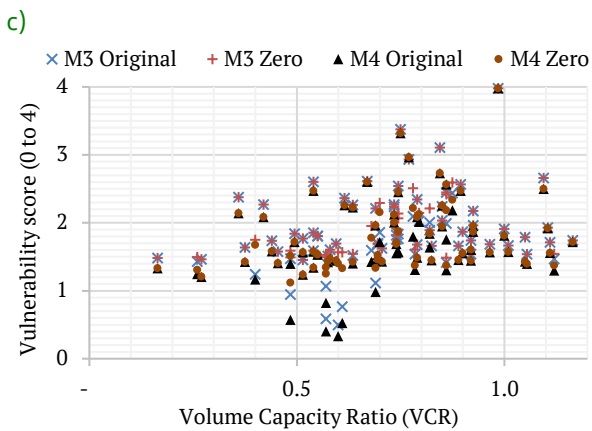
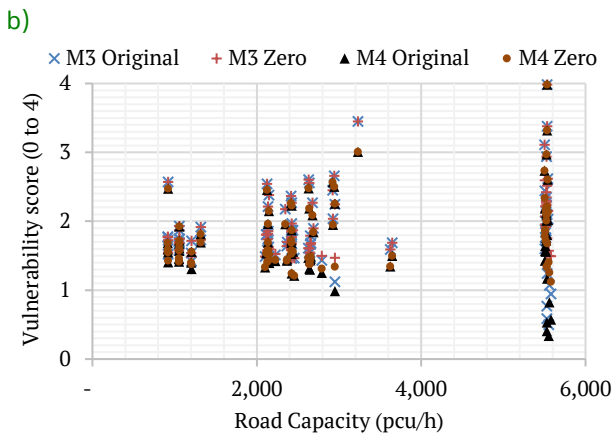
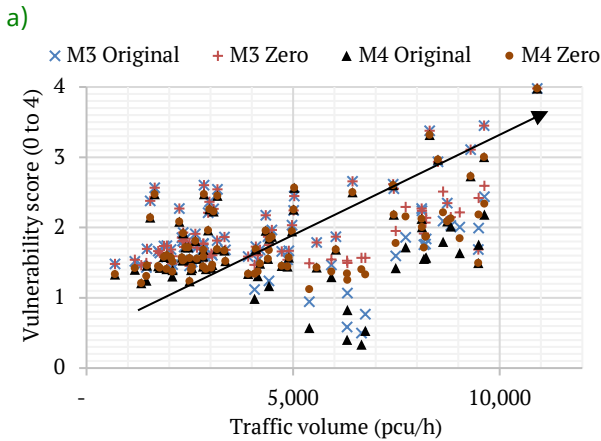
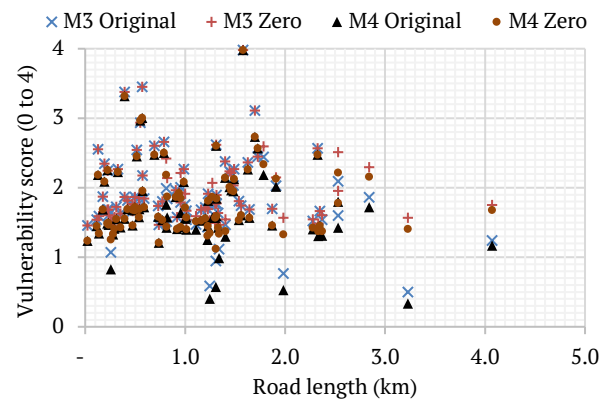
## 4 DISCUSSION

### 4.1 Vulnerability Index

The vulnerability model in this study combined a local (road section) and global (network) parameter into a single index. As a local parameter, VCR and travel speed described the service performance of a road section, while VHT and VKT defined the mobility efficiency of a systematic network. For behavioural knowledge, a relationship between vulnerability score and basic road features such as capacity and volume were explored (Figure 5).

Based on Figure 5, most of the data were scattered, as there was no strong relationship pattern between the road characteristics and vulnerability score. However, the most delicate pattern was identified on traffic volume, which had a positive relationship, therefore, representing the most significant parameter to briefly identify the critical location. This indicated that higher traffic volume led to more road network vulnerability with the occurrence of disruption. When a linear regression was applied, the highest relationship between traffic volume and vulnerability score was observed in the M3 and M4 models, at the determination coefficient (R-squared) values of 0.34 and 0.28, respectively. Although M3 was the best model to show this relationship, the R-squared value indicated that traffic volume only contributed 34% to the overall vulnerability score. This showed that the remaining contribution (66%) was influenced by other parameters, including non-traffic-related factors such as road density and infrastructure conditions. Therefore, the RCI measurement using the M3 model was suitable for the general conditions, due to being the most sensitive parameter. Meanwhile, the M4 was considered when an official minimum standard/threshold for road service performance was available.

The RCI calculation indicated the similarities of the two most critical roads (link 47 and 52), compared to the existing performance indicator in Indonesia (VCR or VCR+speed). However, the remaining ranking orders were found to be different (Table 4). For instance, the result



d) Figure 5. Relationship between basic road characteristics with the vulnerability score (RCI): a) Road length, b) Traffic volume, c) Road capacity, d) Volume capacity ratio (VCR).

indicated that link 69 had a worse impact on local road performance than 83. Meanwhile, when the network performance was considered, the RCI model indicated that link 83 was more significant than 69. Based on this study, the vulnerability assessment generally encouraged road managers to spend maintenance/development budgets on the most critical network(s). Since the budget is limited, the prioritization mechanism for allocation was crucial. According to these considerations, the RCI application offered a more comprehensive approach than the existing (*VCR* or *VCR+Speed*) indicator, to measure the criticality level of road(s) in an urban network. This RCI is specially developed based on urban road characteristics, as well as providing a more sensitive score result and combining both local and global network parameters. Therefore, this model offered a better approach that satisfied both the theoretical and practical aspects of this study.

Table 4. Top 10 most critical road

Indicator	Priority order									
	1	2	3	4	5	6	7	8	9	10
<i>VCR</i>	47	52	69	70	1	4	51	71	3	48
Speed ( <i>v</i> )	47	52	69	83	49	48	70	11	82	68
<i>VCR + v</i>	47	52	69	70	4	49	48	51	71	1
RCI-M3	47	52	83	69	49	57	48	11	56	23

#### 4.2 Application of Vulnerability index

The concept of vulnerability focuses on weakness and failure consequences of network degradation (Taylor *et al.*, 2006). Based on this study, a sequential link(s) removal procedure to investigate the most vulnerable road section(s) has successfully been confirmed. According to the study of Balijepalli and Oppong (2014), NVI was applied as a vulnerability assessment to the road network due to flooding. Furthermore, El-Rashidy and Grant-Muller (2014) demonstrated the use of six assessment variables, such as *VCR*, volume, travel time, road capacity and length, as well as the shortest route, for measuring vulnerability in the urban network. The study of Taylor (2017) also used *VHT* for calculating the network trip robustness index (NTRI), a vulnerability parameter used in regional road structures. These previous studies indicated that vulnerability

should be measured using various indicators. However, the selection of vulnerability index should consider the measurement objectives and theoretical frameworks. For example, accessibility indicators such as the NTRI or Hansen index should be more effective when being applied for regional road networks (Susilawati and Taylor, 2008). The implementation of these indexes in an urban network is likely to be biased, based on sharing different characteristics (Sugishita and Asakura, 2021).

According to the theoretical concept, vulnerability analysis is the first stage to maintain road network connectivity and performance. Based on the knowledge of the most vulnerable road locations and their consequences, authorities should prioritize maintenance and development strategies to protect and improve alternative routes for mitigating the traffic detour impacts. Also, road managers can practically use the vulnerability assessment to raise public awareness, and support the feasibility of network development. Furthermore, several management strategies should be proposed, including an infrastructure-based approach such as road density increase. This is because a higher road density is known to offer a more resilient network as alternative routes options when a particular link is disrupted. However, the strategy to build a new road(s) should not always be the best solution, because of the expensive cost and limited land for development. Using suitable traffic management systems, the optimization of the existing road asset is found to be more favoured.

In terms of transportation management, the information system played a crucial role in mitigating the impact of road disruption or closure. Although access is disrupted, road users still need to reach their destination as fast as possible. When these users are well-informed on the occurrence of incidents, immediate reactions are actively carried out by identifying and selecting the best alternative route option. This was in line with the equilibrium traffic assignment procedure applied in the PTV Visum

model. However, the impact dramatically worsens when the information is not accurately delivered. In this case, the implementation of intelligent transport systems in urban road networks, such as vehicle message signs (VMS) and route guidance systems, should be prioritized to assist the police/traffic officers in normalizing and diverting vehicle flow from the disruptions.

The concept of road maintenance is generally responsive in developing countries, where waiting until a section is damaged near the tolerance threshold is often observed. In this condition, roadwork is immediately carried out without considering the sustainability of investment value from road assets. This is because a road network is always technically wanted in a prime condition. However, a road manager only realistically optimizes a limited budget far from the required cost. Therefore, these managers should make efforts to handle investments, and focus on more significant impact roads. To solve this problem, the concept of vulnerability should be used to examine potential impacts, and also identify the most critical road(s) with the worst consequences on the overall network performance. By analyzing this vulnerability, the road manager should prioritize roadworks based on the criticality index, and also conduct preventive measures to mitigate risk under a constrained budget.

## 5 CONCLUSION

This study developed an alternative vulnerability model (RCI) and indicated the identification of the most critical location of road incidents in an urban area. Due to unforeseen incidents, the vulnerability of road network performance varied based on traffic volume and pattern, as well as road density and configuration. This assessment encouraged road managers to spend maintenance/development budgets on the most critical network(s). The vulnerability assessment was also important due to the massive impact of disturbance on the critical road(s), which triggered a systemic chain effect on the overall network performances, including substantial losses on social-economic activity. Since the management budget was always limited, the

prioritization mechanism for allocating the budget was often crucial. By analyzing this vulnerability, the road manager should prioritize roadworks based on the criticality index, and conduct preventive measures to mitigate risk under a constrained budget. Based on this study, the results emphasized that vulnerability mitigation in urban road networks was an issue of prevention and preparedness for quick restoration, compared to providing expensive infrastructure investment such as building new road(s). A link closure is not likely to be crucial in vulnerability analysis when it has an alternative route to mitigate the impact. Although the best response to optimize road network performance was through vulnerability analysis, the risk and road asset investment value through socio-economic analysis should also be considered. Despite the test of the overall approaches in this study, the developed vulnerability model can be adopted and applied to other areas or countries. For further studies, the transport mode, destination choice, budget allocation, and socio-economic impact can be considered in assessing vulnerability levels, as well as developing road management standards and strategies.

#### DISCLAIMER

The authors declare no conflict of interest.

#### AVAILABILITY OF DATA AND MATERIALS

All data are available from the author.

#### AUTHOR CONTRIBUTION STATEMENTS

Mukhammad R. F. A. developed the concept, methodology and performed the analytical results. Raihan P. I. carried out the PTV Visum simulation. Both authors took a substantial contribution in discussing the result and writing the manuscript.

#### ACKNOWLEDGMENTS

The authors are grateful to the Civil and Environmental Engineering Department, as well as the Computation Laboratory of Master Program in Transport System and Engineering, Faculty of Engineering, Universitas Gadjah Mada

(DTSL FT UGM), for financially supporting this study and facilitating the PTV Visum software, respectively.

#### REFERENCES

- Amrozi, M.R.F. and Evdorides, H.T. 2019. Economic Optimisation of Road Network Accessibility. *Bituminous Mixtures and Pavements VII*. CRC Press. pp. 499-506.
- Auerbach, M., Hammoum, F., Huber, F., Hunyadi, D., Krieger, B., Marchese, A., Maruntu, C., Murphy, H. and Reeves, S. 2016. *Transport Strategies for Climate Change Mitigation and Adaptation*. France: The World Road Association (PIARC).
- Balijepalli, C. and Oppong, O. 2014. Measuring vulnerability of road network considering the extent of serviceability of critical road links in urban areas. *Journal of Transport Geography* 39 145-155.
- Berdica, K., 2002. An Introduction to Road Vulnerability: What Has Been Done, is Done and Should be Done. *Transport Policy* ,9(2), pp. 117-127.
- BPS-statistics, 2021. *Yogyakarta Municipality in Figures 2021*. Yogyakarta: BPS-Statistic of Yogyakarta Municipality.
- BSN, 2004. RSNI T-14-2004: *Urban Road Geometry*. Jakarta: National Standardization Agency (BSN).
- El-Rashidy, R.A. and Grant-Muller, S.M., 2014. An Assessment Method for Highway Network Vulnerability. *Journal of Transport Geography*, 34, pp. 34-43.
- Fitrada, A.G., Munawar, A., and Dewanti, 2019. Investigating the Impact of Airport Relocation on the Transport Network in Special Region of Yogyakarta, Indonesia. *Journal of The Civil Engineering Forum*, 5 (2), pp. 93-104.
- IHCM 1997. *Indonesia Highway Capacity Manual (MKJI)*. Jakarta: Ministry of Public Work Republic Indonesia.

- Jenelius, E. and Mattsson, L.-G., 2015. Road Network Vulnerability Analysis: Conceptualization, Implementation and Application. *Computers, Environment and Urban Systems*, 49, pp. 136-147.
- Karlaftis, M. and Kepaptsoglou, K., 2012. *Performance Measurement in The Road Sector: A Cross-Country Review of Experience*, International Transport Forum Discussion Paper.
- Litman, T. 2016. *Accessibility for Transportation Planning: Measuring People's Ability to Reach Desired Goods and Activities*. Victoria Transport Policy Institute.
- Mahpudin, M., Kelihu, A., and Sarmiasih, M. 2020. The Rise of Student Social Movement: Case Study of #GejayanCalling Movement in Yogyakarta. *International Journal of Demos*, 2(1), pp.21-42.
- Ministry of Transport, 2006. *Kepmenhub KM 14/2006 concerning Road Traffic Management and Engineering*. Jakarta : Ministry of Transport.
- Ministry of Transport, 2015. *Permenhub PM 96/2015 concerning Guidelines for the Implementation of Traffic Management and Engineering Activities*. Jakarta: Ministry of Transport.
- Nagurney, A. and Qiang, Q. 2008. A Network Efficiency Measure with Application to Critical Infrastructure Networks. *Journal of Global Optimization*, 40(1-3), pp. 261-275.
- Nardo, M., Saisana, M., Saltelli, A., Tarantola, S., Hoffmann, A., and Giovannini, E., 2008. *Handbook on Constructing Composite Indicators: Methodology and User Guide*. Ispra: OECD publishing.
- OECD 2001. *Performance Indicators for the Road Sector*. Paris: Organisation for Economic Co-Operation and Development (OECD).
- Oliveira, E.L.D., Portugal, L.D.S., and Junior, W.P., 2016. Indicators of Reliability and Vulnerability: Similarities and Differences in Ranking Links of a Complex Road System. *Transportation Research Part A: Policy and Practice*, 88, pp. 195-208.
- PTV, A. 2021. *PTV Visum 2021 Manual*. Karlsruhe: PTV Group.
- Rupi, F., Bernardi, S., Rossi, G., and Danesi, A., 2015. The Evaluation of Road Network Vulnerability in Mountainous Areas: A Case Study. *Networks and Spatial Economics*, 15(2), pp. 397-411.
- Scott, D.M., Novak, D.C., Aultman-Hall, L., and Guo, F., 2006. Network Robustness Index: A new method for identifying critical links and evaluating the performance of transportation networks. *Journal of Transport Geography* 14(3) 215-227.
- Stanton-Geddes, Z. and Vun, Y.J., 2019. *Strengthening the Disaster Resilience of Indonesian Cities*, Washington DC.: World Bank.
- Sudibyoy, T., Mahardi, P., and Prasetyo, T., 2017. Comparison of Road Service Level Assessment based on PM 96/2015 and KM 14/2006. *Prosiding Konferensi Nasional Teknik Sipil*, 11, pp. 183-188.
- Sugishita, K. and Asakura, Y., 2021. Vulnerability Studies in the Fields of Transportation and Complex Networks: A Citation Network Analysis. *Public Transport*, 13(1), pp. 1-34.
- Sullivan, J.L., Novak, D.C., Aultman-Hall, L., and Scott, D.M., 2010. Identifying Critical Road Segments and Measuring System-Wide Robustness in transportation Networks with isolating links: A Link-Based Capacity-Reduction Approach. *Transportation Research Part A: Policy and Practice*, 44(5), pp. 323-336.
- Susilawati and Taylor, M., 2008. *An Accessibility Approach in Assessing Regional Road Network Vulnerability*. Gold Coast: 31st Australasian Transport Research Forum.
- Tamin, O.Z., 2000. *Transportation Planning and Modeling*: Bandung: ITB Publisher.
- Taylor, M., 2017. *Vulnerability Analysis for Transportation Networks*, Amsterdam: Elsevier.

Taylor, M.A.P., Sekhar, S.V.C., and D'Este, G.M., 2006. Application of Accessibility Based Methods for Vulnerability Analysis of Strategic Road Networks. *Networks and Spatial Economics*, 6(3-4), pp. 267-291.

Taylor, M.A.P. and Susilawati 2012. Remoteness and Accessibility in the Vulnerability Analysis of Regional Road Networks. *Transportation Research Part A: Policy and Practice*, 46(5), pp. 761-771.

[This page is intentionally left blank]

# Analysis of Spatial Distribution of the Drought Hazard Index (DHI) by Integration AHP-GIS-Remote Sensing in Gorontalo Regency

Muhammad Ramdhan Oliy<sup>1,\*</sup>, Aleks Oliy<sup>1</sup>, Ririn Pakaya<sup>2</sup>

<sup>1</sup>Department of Civil Engineering, Universitas Gorontalo, Gorontalo, INDONESIA  
Jalan A.A. Wahab No. 247, Limboto, Gorontalo

<sup>2</sup>Department of Public Health, Universitas Gorontalo, Gorontalo, INDONESIA  
Jalan A.A. Wahab No. 247, Limboto, Gorontalo

\*Corresponding authors: [kakaramdhanolii@gmail.com](mailto:kakaramdhanolii@gmail.com)

SUBMITTED 24 August 2021 REVISED 22 September 2021 ACCEPTED 25 October 2021

**ABSTRACT** Several regions across the world are presently experiencing a continuous increase in water scarcity due to the rise in water consumption resulting from population development, agricultural and industrial expansion, climate change, and pollution. Droughts are increasing in recurrence, severity, duration, and spatial extent as a result of climate change. Drought will be one of the most serious threats posed by climate change, often in conjunction with other effects such as rising temperatures and shifting ecosystems. Therefore, this study analyzes the spatial distribution of the Drought Hazard Index (DHI) by integrating AHP-GIS-Remote Sensing in Gorontalo Regency. AHP was used to determine the significance of each map as an input parameter for the DHI, while GIS-Remote Sensing was utilized to supply and analyze all input maps and the study outcome. The DHI assessment consists of four criteria, namely with Normalized Difference Vegetation Index accounting for the highest proportion at 42.9%, followed by Land Surface Temperature (33.6%), Normalized Difference Moisture Index (16.8%), and Topographic Wetness Index (6.7%), with the consistency of the underlying expert opinion measured by the consistency ratio of 0.048. The results indicated that the general hazard of drought in the Gorontalo Regency area was low (43.53%), with 17.87% of the whole area experiencing high hazard. The high class of drought was discovered to be centered in the central region of Gorontalo Regency, which was mostly used for agricultural and economic purposes, thereby enabling policymakers to have evidence to develop management policies suitable for local conditions. Therefore, despite the limits of climatology data, this study established the value of satellite-derived data needed to support policymakers in guiding operational actions to drought hazards reduction.

**KEYWORDS** Analytic Hierarchy Process; Geographic Information System; Remote Sensing; Drought Hazard Index; Gorontalo Regency.

© The Author(s) 2022. This article is distributed under a Creative Commons Attribution-ShareAlike 4.0 International license.

## 1 INTRODUCTION

Hydrometeorological disasters are influenced by significant meteorological and weather factors, such as drought. According to (Sheffield & Eric, 2011). Drought is a condition in an area that experiences water shortages compared to normal conditions in various hydrological cycle components. This disaster occurs in almost all parts of the world, including tropical countries such as Indonesia. Generally, drought occurs due to extreme human activities, such as land degradation, overexploitation of water, and desertification (Wijitkosum & Sriburi, 2019). Human activities increase the risk of drought, thereby making it difficult to accurately predict its occurrence and level of hazards (Loon *et al.*, 2016).

Drought is classified as a hydrometeorological disaster with serious environmental, social, agricultural, and economic consequences (Ekrami *et al.*, 2016). It causes issues such as a lack of groundwater, an imbalance of water for crops, and a reduction in agricultural yields (Wu *et al.*, 2017). Drought is influenced by natural and anthropogenic factors and seriously impacts global water and food security. Therefore, developing a thorough drought risk assessment is imperative, particularly in underdeveloped countries (Wijitkosum, 2018). In addition, conducting an assessment of the level of drought hazard in areas at risk of this disaster is very important for planning future land development,

preventing its occurrence, and minimizing the negative impacts (Loon *et al.*, 2016).

Drought is an inherently complex multidimensional process with unknown quantitative and qualitative factors (Wijitkosum, 2018). Real-time drought monitoring systems can analyze a large area as Remote Sensing technology, and geographic information systems (GIS) advances. These systems are increasingly being considered drought detection techniques, as evidenced by their use in many parts of the world. (Belal *et al.*, 2012). For example, Remote Sensing data is used to calculate the Normalized Difference Vegetation Index (NDVI), Normalized Difference Wetness Index (NDWI), Land Surface Temperature (LST), Normalized Difference Built-up Index (NDBI), and Normalized Difference Moisture Index (NDMI). They are employed in the monitoring and controlling agricultural drought and crop growth (Chang, 1996; Karnieli *et al.*, 2010; Prasetya *et al.*, 2020; Malik *et al.*, 2019; Sholihah *et al.*, 2016).

Several studies developed numerous models to analyze the level of hazard, vulnerability, or risk of hydrometeorological disasters with fairly good results, such as floods, flash floods, landslides, and drought. The most widely used analysis is AHP due to its ability to determine the complexity of the factors that cause disasters. AHP-GIS is a modern graphic visualization tool used by decision-makers to disseminate and interpret spatial information on the level of hazards, vulnerabilities, and disaster risks (Patel & Prashant, 2013; Haq *et al.*, 2012; Chen *et al.*, 2003; Prasad *et al.*, 2016; Chakraborty & Joshi, 2016; Ollie *et al.*, 2021). The Standardized Precipitation Index (SPI) is widely used for describing meteorological droughts over a wide range of timescales (McKee *et al.*, 1993). This is in contrast to a fairly broad scale of spatial variability displayed on maps, which often contains limited information concerning local-scale differences in drought severity across the area. Conversely, climate-based drought index maps are limited because they provide a generalized spatial perspective value of drought conditions and fluctuations across wide areas. However, improved and more effective drought

monitoring approaches are needed to aid early warning systems. Several studies recently used AHP to analyze the level of hazard, vulnerability, and danger of drought, which yielded positive results despite the complexity of the influencing factors. (Moghari *et al.*, 2017; Cheng & Tao, 2010; Ekrami *et al.*, 2016; Wijitkosum, 2018; Wijitkosum and Sriburi, 2019). In this study, GIS and Remote Sensing are integrated with mathematical models such as AHP and expected to contribute to region-based drought analysis significantly.

This study was carried out in Gorontalo, which is one of the regencies in Gorontalo Province prone to drought. According to the Disaster Management Agency's 2019 Indonesian Disaster Risk Index, Gorontalo received a score of 104.14, therefore it is in the moderate category (13-144). The Recommendation Priority 2 (Integrated Risk Assessment and Planning) used by regencies in the moderate category is the Preparation of Risk, Hazard and Vulnerability Maps. However, the map's limitation in containing information on the distribution of the level of hazard, vulnerability, and risk of drought is one factor that hinders its ability to resolve the drought problem. It is important to determine the hazard areas of drought in order to prevent a wider impact of the disaster. Therefore, this study aims to integrate AHP, GIS, and Remote Sensing to predict the spatial distribution of drought hazard levels in Gorontalo Regency using a variety of indices, such as Land Surface Temperature (LST), Normalized Difference Vegetation Index (NDVI), Normalized Difference Moisture Index (NDMI), and Topographic Wetness Index (TWI) as references for planning, and management of drought.

## 2 METHODS

### 2.1 Study Area

Gorontalo Regency is geographically located between 0°28'23.22"-0°55'45.08" North Latitude and 122°14'43.69"-123°4'48.27" East Longitude with a landmass of 2159 km<sup>2</sup>. The altitude ranges from 0 to 2,062 m, with an average elevation of 50 m above sea level. According to a 2020 survey, the administrative area of this regency consists of 19 districts and 205 villages, with Limboto as its

capital city. The largest and smallest districts are Asparaga and Tilango, with an area of 430.51 km<sup>2</sup> or 20.25% and 5.79 km<sup>2</sup> or 0.27% of the overall land area in Gorontalo Regency. This regency's northern, eastern, southern, and western parts are bordered by Gorontalo Utara, Bone Bolango Regency & Gorontalo City, Tomini Bay, and Boalemo Regency. The highest temperature of 35.2°C in 2020 occurred in October, while the lowest was in September, at 18.8°C. The highest humidity in March and June reaches 97%, while the lowest is obtained in January, which reaches 65% in October. The highest and lowest duration of exposure was in September at 79.90% and 45.10%. The highest rainfall occurs in December, with 27 rainy days.

## 2.2. Data

In this study, all maps were displayed in the GIS environment as raster models with the Digital

elevation model (DEM), consisting of a grid size of 30 x 30 m<sup>2</sup> used to analyze the Topographic Wetness Index (TWI). Landsat TM 8 OLI (path 113; row 59; date acquired = 2019-12-02; path 113; row 60; date acquired = 2019-12-02) accessed from USGS with a grid size of 30 x 30 m<sup>2</sup> was used to analyze Land Surface Temperature (LST), Normalized Difference Vegetation Index (NDVI), and Normalized Different Wetness Index (NDWI). Cloud cover of Landsat TM 8 OLI was removed by Fmask 3.2 version Windows package. Additionally, the Gorontalo Regency administrative boundaries were-downloaded from GADM.

## 2.3 Methodology

Remote Sensing is the science and art of obtaining information on an object, area, or phenomenon through the analysis of data acquired by a device that is not in contact with the object, area, or phenomenon under investigation. In this study,

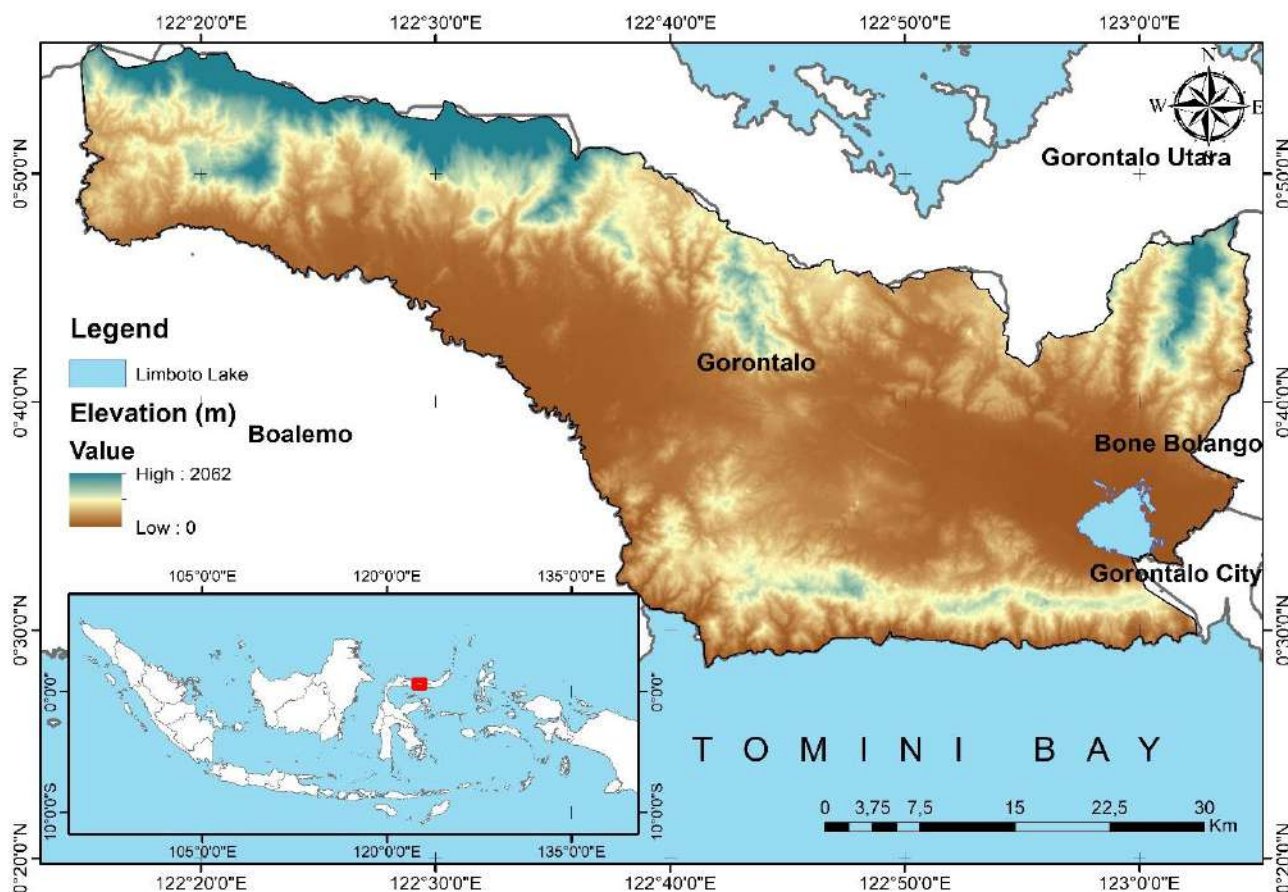


Figure 1. Location of the study area

the factors that influence a Drought Hazard Index (DHI) such as Land Surface Temperature (LST), Normalized Difference Vegetation Index (NDVI), and Normalized Different Wetness Index (NDWI) were demarcated from Landsat TM 8 OLI image using the standard methods of visual interpretation of Remote Sensing data. Digital Terrain Analysis (DTA) calculated the Topographic Wetness Index (TWI) was calculated by Digital Terrain Analysis (DTA) using the GIS package. The overlay operation is used by most GIS, which provides information through the combination and use of several maps. During the overlay operation, new special elements are created based on multiple maps and performed using the raster, a data structure well suited for this type of operation. All of the maps used in the analysis have the same georeference and a similar number of grids organized in the same row and column. They also have the same grid size and coordinate with a program used to examine each grid when several maps are combined, thereby allowing the same figures to be checked from different maps during image combination. In a raster overlay, grid numbers are combined in a specific way, and the figures obtained are assigned to the corresponding grids in the output layer of the image. A raster overlay is applied to data that contains explicit or ordinal numbers, with each grid consisting of a string of characters. The figures in each grid correspond to the items of raster variables. Further explanation for each DHI factor is shown below.

1. Normalized Difference Vegetation Index (NDVI). This method is frequently used to measure and assess the vegetation index value of a given area. According to the NDVI analysis, green plants develop successfully by absorbing radiation in the visible light spectrum (PAR or Photosynthetically Active Radiation) and reflecting it at the near-infrared area. The spectral pattern definition is also based on this theory in addition to the use of RED band images, Karnieli *et al.* (2010) discovered a clear negative relationship between NDI and LST, indicating that healthy

green vegetation lowers the surface temperature. NDVI is used as a response variable to identify and quantify drought disturbance in semiarid and arid lands, with low values indicating stressed vegetation (Table 1 and Figure 2) (Tucker & Choudhury, 1987). NDVI is calculated using Equation (1) (Tucker, 1979):

$$NDVI = \frac{NIR-RED}{NIR+RED} = \frac{band\ 5-band\ 4}{band\ 5+band\ 4} \quad (1)$$

where *NIR* and *RED* are the reflection in the near-infrared (*band 5*) and red range (*band 4*) spectrums.

2. Land Surface Temperature (LST). LST is the land's radiative skin temperature as determined by infrared radiation. It is a critical parameter in all physical processes consisting of surface energy and water balance at both local and global scales (Malik, *et al.*, 2019; Karnieli *et al.*, 2010). LST is necessary to land surface processes for climatic reasons and regulates sensible and latent heat flux exchange (Sun & Pinker, 2003). It can be used in various fields, including evapotranspiration, climate change, the hydrological cycle, plant monitoring, urban climate, and environmental studies (Weng, 2009; Voogt & Oke, 2003; Arnfield, 2003). LST classes are shown in Table 2 and Figure 3 use LANDSAT-8 with the following steps:

Conversion to Top of Atmosphere (TOA) radiance in Equation (2) (USGS, 2019).

$$L_{\lambda} = M_L \times Q_{cal} + A_L - O_i \quad (2)$$

Table 1. NDVI ranges that are appropriate for the land cover classes (Akbar *et al.*, 2019)

No.	Land Cover Class	NDVI Range	Score
1.	Built-Up	0.015-0.14	6
2.	Barren Land	0.14-0.18	5
3.	Shrub and Grassland	0.18-0.27	4
4.	Sparse Vegetation	0.27-0.36	3
5.	Dense Vegetation	>0.36	2
6.	Water	<0.015	1

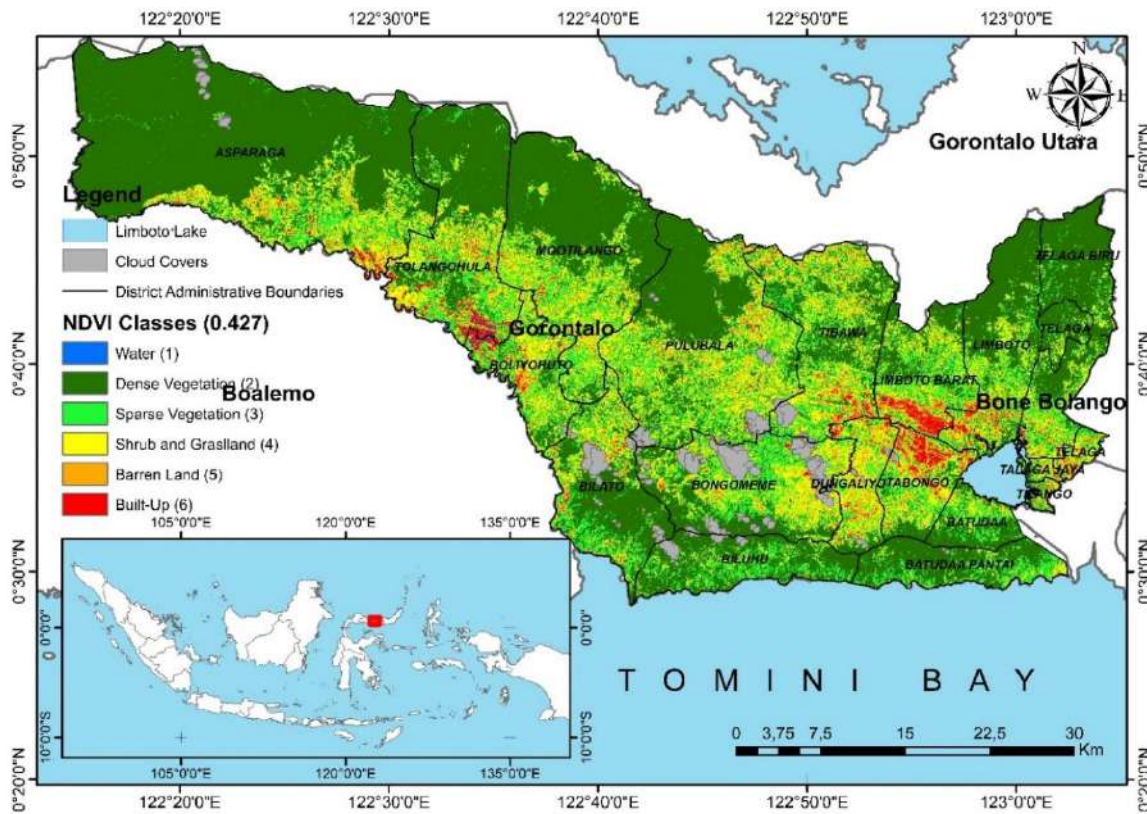


Figure 2. Normalized Difference Vegetation Index (NDVI) classes

Table 2. LST range in degree celcius (Alavipannah *et al.* 2017)

No.	LST Class	LST Range	LST Range	Score
1.	Very Low	$LST < LST_{mean} - 1.5 \text{ Stdv}$	$< 20.6 \text{ }^\circ\text{C}$	1
2.	Low	$LST_{mean} - 1.5 \text{ Stdv} < LST < LST_{mean} - \text{Stdv}$	$20.6 \text{ }^\circ\text{C} - 22.6 \text{ }^\circ\text{C}$	2
3.	Moderate	$LST_{mean} - \text{Stdv} < LST < LST_{mean} + \text{Stdv}$	$22.6 \text{ }^\circ\text{C} - 30.6 \text{ }^\circ\text{C}$	3
4.	High	$LST_{mean} + 1.5 \text{ Stdv} < LST < LST_{mean} + 1.5 \text{ Stdv}$	$30.6 \text{ }^\circ\text{C} - 32.7 \text{ }^\circ\text{C}$	4
5.	Very High	$> LST_{mean} + 1.5 \text{ Stdv}$	$> 32.7 \text{ }^\circ\text{C}$	5

Note: LST Mean = 26.61 °C; Stdv (Standart Deviation) = 4.03

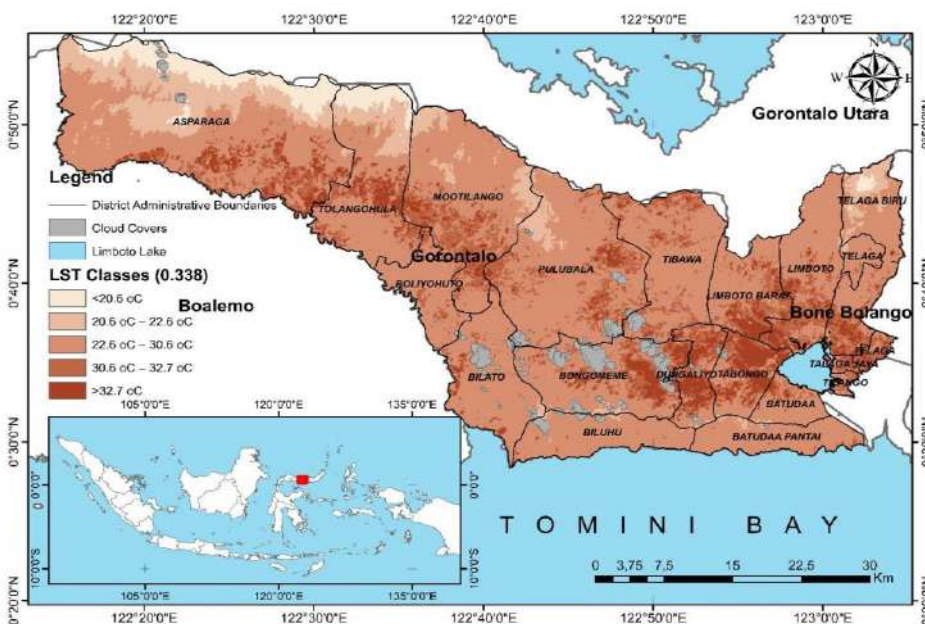


Figure 3. Land Surface Temperature (LST) classes

where  $L_\lambda$  is TOA spectral radiance (Watts/m<sup>2</sup> sr  $\mu$ m),  $M_L$  is radiance multiplicative bands,  $A_L$  is radiance add band,  $Q_{cal}$  is quantized and calibrated standard product pixel values (DN),  $O_i$  is correction value for band 10 is 0.29.

Conversion to Top of Atmosphere (TOA) Brightness Temperature (BT) in Equation (3) (USGS, 2019).

$$B_T = \frac{K_2}{\ln\left(\frac{K_1}{L_\lambda+1}\right)} - 273.15 \quad (3)$$

where  $B_T$  denotes TOA brightness temperature (oC),  $L_\lambda$  is TOA spectral radiance (Watts/m<sup>2</sup> sr  $\mu$ m),  $K_1$  is  $K_1$  constant band, and  $K_2$  is  $K_2$  constant band.

Proportion of Vegetation in Equation (4) (Wang *et al.*, 2015).

$$P_V = \left(\frac{NDVI-NDVI_{min}}{NDVI_{max}-NDVI_{min}}\right)^2 \quad (4)$$

where  $P_V$  denotes the proportion of vegetation,  $NDVI$  is DN values of its image,  $NDVI_{max}$  and,  $NDVI_{min}$  are the maximum and minimum DN values from  $NDVI$  image. Land Surface Emissivity in Equation (5) (Barsi *et al.*, 2014)

$$E = 0.004P_V + 0.986 \quad (5)$$

where  $E$  island surface emissivity, and  $P_V$  is proportion of vegetation. Land Surface Temperature (LST) in Equation (6) (Jin *et al.*, 2015).

$$LST = \frac{B_T}{\left(1 + \left(\frac{\lambda B_T}{h \times c}\right) \ln(E)\right)} \quad (6)$$

where  $B_T$  denotes TOA brightness temperature (oC),  $\lambda$  is the wavelength of emitted radiance (for band 10 is 10.8 and band 11 is 12.0),  $E$  denotes land surface emissivity,  $h$  is Planck's constant (6.626 x 10<sup>-34</sup> J s),  $s$  is Boltzmann

constant (1.38 x 10<sup>-23</sup> J K),  $c$  is the velocity of light (2.998 x 10<sup>8</sup> m/s).

3. Normalized Different Moisture Index (NDMI). NDMI is calculated as the ratio of the difference and number of refracted radiations in the NIR and SWIR regions, and it is used to identify the crop's level of water stress. NDMI's absolute value allows for the interpretation of immediate identification of farm or field areas experiencing water stress. It is extremely sensitive to drought events (Hais *et al.*, 2019) and its values range from -1 to 1. Furthermore, each value corresponds to a different agronomic situation, irrespective of crop type, as shown in Table 3 and Figure 4. The following is the Equation (7) used to calculate NDMI (Gao, 1996).

$$NDMI = \frac{NIR-SWIR1}{NIR+SWIR1} = \frac{band\ 5-band\ 6}{band\ 5+band\ 6} \quad (7)$$

where  $NIR$  is a reflection in the near-infrared spectrum (*band 5*), and  $SWIR$  is a reflection in the short-wave infrared of the spectrum (*band 6*).

Table 3. NDMI ranges are land cover classes appropriate for moisture content (Gulácsi & Kovács 2015; Amalo *et al.* 2018)

No.	Land Cover Class	NDMI Range	Score
1.	Very High Moisture Content	>0.7	1
2.	High Moisture Content	0.6-0.7	2
3.	Moderate Moisture Content	0.5-0.6	3
4.	Low Moisture Content	0.4-0.5	4
5.	Weak Drought	0.3-0.4	5
6.	Moderate Drought	0.2-0.3	6
7.	Strong Drought	0-0.2	7
8.	Very Strong Drought	<0.0	8

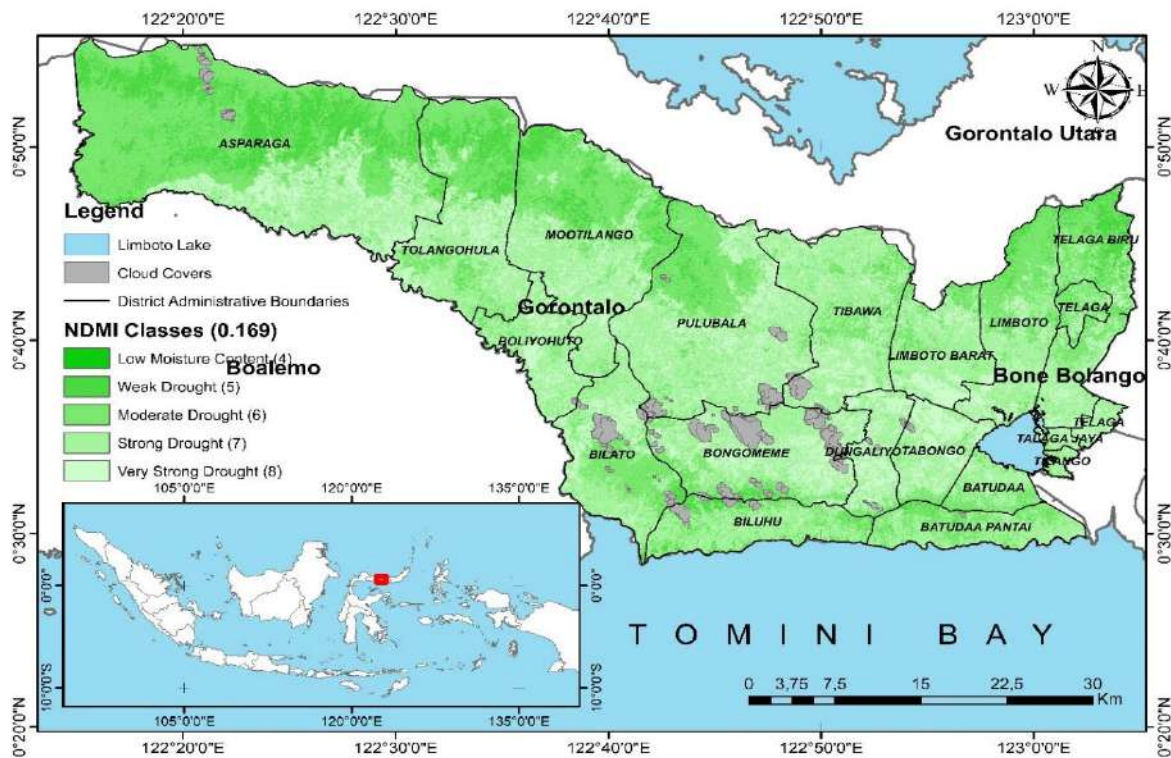


Figure 4. Normalized Different Moisture Index (NDMI) classes

4. Topographic Wetness Index (TWI). TWI predicts that a significant part of hillslope flow occurs as slope-parallel lateral, implying that flow accumulation increases with local contributing and decreases in local slopes (Beven and Kirkby, 1979). TWI is derived by integrating the upper and local slopes area, which both represent the location's wetness. It is structurally appropriate for delineating the soil wetness pattern, as shown in Table 4 and Figure 5. According to (Yang *et al.*, 2015). TWI correlates positively with soil moisture at the soil surface of 0–1 m. It is calculated using the following Equation (8) (Beven & Kirkby, 1979):

$$TWI = \ln\left(\frac{\alpha}{\tan \beta}\right) \quad (8)$$

where  $\alpha$  is the local upslope area draining through a unit contour length, which in this study equals grid cell width, and  $\beta$  is the gradient of the local slope.

Table 4. TWI ranges based on DEM (Rahmati *et al.*, 2019)

No.	TWI Class	TWI Range	Score
1.	Very Low Accumulate Water	<5	5
2.	Low Accumulate Water	5 - 10	4
3.	Moderate Accumulate Water	10 - 15	3
4.	High Accumulate Water	15 - 20	2
5.	Very High Accumulate Water	>20	1

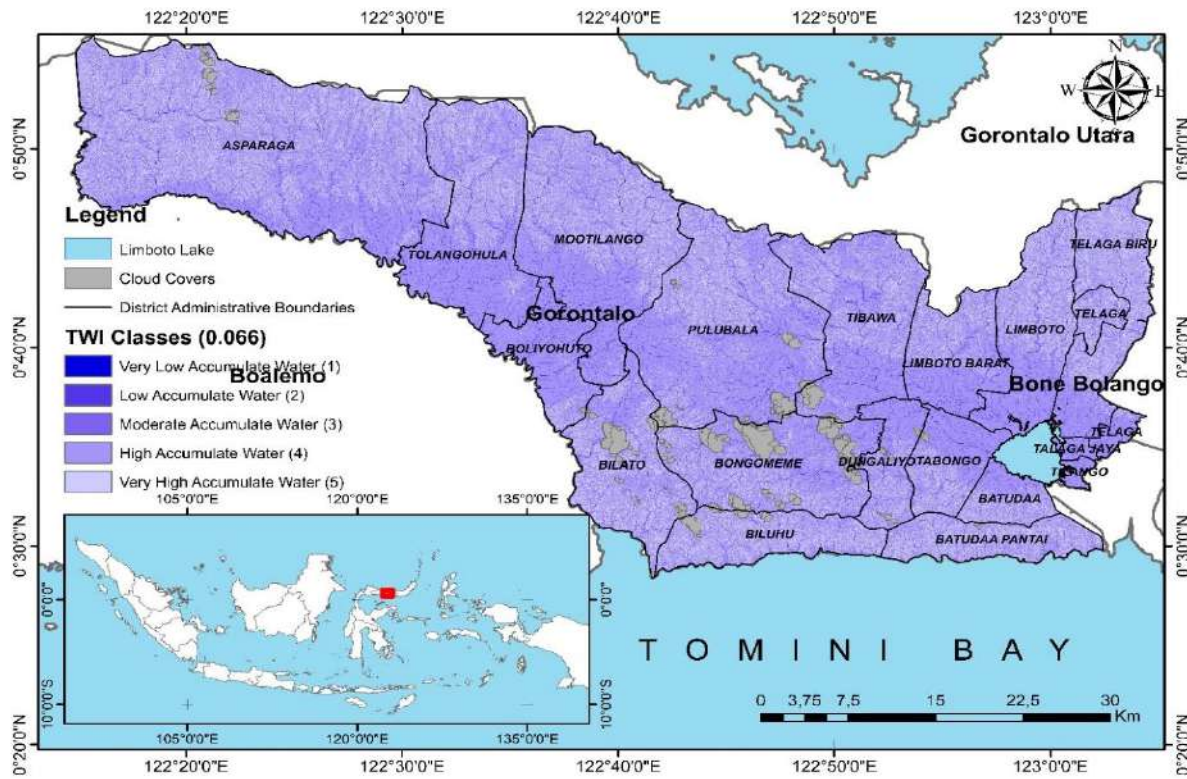


Figure 5. Topographic Wetness Index (TWI) classes

### 3 ANALYTICAL HIERARCHY PROCESS (AHP) METHOD

The Analytical Hierarchy Process (AHP) is a multicriteria decision-making technique that establishes a systematic framework for examining and integrating the effects of many factors by utilising different levels of dependent or independent qualitative and quantitative data (Saaty, 1980, 2008). This process is carried out by structurally comparing all possible paired combinations of criteria using a table-matrix with relevant values. The tool used to determine the weight of each factor is the AHP Excel Template compiled by Goepel (2013). The principle of AHP is shown in the following matrix (Saaty, 1980, 2008):

1. Determine the eigenvectors ( $V_p$ ) of each criterion for each item, As given in Equation (9).

$$V_p = \sqrt{W_1 \times W_2 \times W_3 \times \dots \times W_n} \tag{9}$$

where  $n$  denotes the number of criteria and compared  $W_n$  rating main parameters.

2. Determine the weighting coefficients ( $C_p$ ) using the formula in Equation (10).

$$C_p = \frac{V_p}{V_{p_1} \times V_{p_3} \times V_{p_3} \times \dots \times V_{p_n}} \tag{10}$$

where  $n$  is several criteria and  $V_p$  is the eigenvectors.

3. Normalize the matrix by dividing each element by the column total
4. Calculate the priority vector by averaging each line
5. To determine the overall priority, multiply each column of the matrix by the appropriate priority vector;
6. Divide each global priority by the appropriate priority vector to obtain the rational priority;
7. Calculate the consistency index ( $CI$ ) expressed by Equation (11).

$$CI = \frac{\lambda_{max} - n}{n - 1} \tag{11}$$

where  $n$  is number of criteria and  $\lambda_{max}$  is the maximum eigenvalue of the comparison matrix.

8. Calculate the consistency ratio ( $CR$ ) using Equation (12).

$$CR = \frac{CI}{RI} \quad (12)$$

where  $RI$  is a random index that represents the consistency of a pairwise comparison matrix generated at random. Table 5 shows the average random consistency index from a sample of 500 matrixes (Saaty, 1980) When the  $CR$  value is less than 10%, the judgment is consistent, and the assessment requires correction when it is greater than 10%.

#### 4 RESULTS

AHP provides a strategy for calibrating a numerical scale by employing a pairwise methodology, which is particularly beneficial in new areas where measurements and quantitative comparisons are unavailable. All criteria's pairwise comparison matrices, as well as their weights, were computed. Elements were determined in conjunction with experts and subject matter specialists. The matrix utilized the proposed values for each factor on Saaty's scale of importance, as shown in Table 6. According to the

AHP computation results, NDVI contributes the most to DHI (42.9%), followed by LST (33.6%), NDMI (16.8%), and TWI (6.7%). Table 7 is a summary of the weights assigned to each component group and criterion.

Consistency Ratio is a  $CR$  used to construct matrices in AHP, which must be less than 0.1 to avoid reversing subjective judgments and weights. Table 8 shows the derived weights for the components, as well as the  $CR$ . These comparisons established that it is less than 0.1, with the method's upper limit indicating that Equation (13) is credible.

$$DHI = 0.429 NDVI_S \times 0.336 LST_S \times 0.168 NDMI_S \times 0.067 TWI_S \quad (13)$$

where  $DHI$ ,  $NDVI_S$ ,  $LST_S$ ,  $NDMI_S$ , and  $TWI_S$  denote Drought Hazard Index, Normalized Difference Vegetation Index score (Table 1), Land Surface Temperature score (Table 2), Normalized Different Moisture Index score (Table 3), and Topographic Wetness Index score (Table 4).

Table 5. Random Index (RI) Value (Saaty, 1980, 2008)

n	1	2	3	4	5	6	7	8	9
RI	0.00	0.00	0.58	0.90	1.12	1.24	1.32	1.41	1.45

Table 6. Scale for various elements comparison (Saaty, 1980, 2008)

Intensity	Definition	Explanation
1	Equal importance	Two element contribute equally to the goal
3	Moderate importance	Experience and judgement slightly favor one element over another
5	Strong importance	Experience and judgement strongly favor one element over another
7	Very strong importance	One element is favored very strongly over another, it dominance is demonstrated in practice
9	Extreme importance	The evidence favoring one element over another is of the highest possible order of affirmation
2,4,6,8	Can be used to express intermediate values	

Table 7. Matrix of pairwise comparisons of the criteria in relation to the goal

Parameter	LST	NDVI	NDMI	TWI	Weight
LST	1	1/2	3	5	0.336
NDVI	2	1	2	5	0.429
NDMI	1/3	1/2	1	3	0.168
TWI	1/5	1/5	1/3	1	0.067

Table 8. Parameter of Consistency Ratio

Parameter	Value
$\lambda_{max}$	4.131
n	4
Random Index (RI)	0.90
Mean Relative Error (MRE)	29.5%
GCI	0.17
Psi	8.3%
Consistency Index (CI)	0.37
Consistency Ratio (CR)	4.8%

The study's primary visualization result is shown in Figure 6. This was accomplished by combining the criteria weights from Equation (13) with some GIS-related operations such as layer overlay, raster conversion, and clipping. Figure 6 is classified into 5 classes based on the likelihood of DHI, namely very low, low, moderate, high, and very high. The Natural Breaks method was used to divide the space, which compiles similar values while minimizing class differences. A total of 106,797.42 ha, or 50.07% of the areas, were classified as having a very low or low drought hazard. A moderate drought hazard occupied up to 24.41% of the total area, while

only 21.66% had a high or very high drought hazard, as shown in Table 9. Low and moderate drought occurred in the northern part of the study area and partly spread to the south, dominated by forest areas. The high drought was found to be concentrated in the central part of Gorontalo Regency, mostly used for agricultural and economic purposes (Figure 7). Therefore, the area's development needs to be carefully planned to implement drought avoidance measures. It is specifically critical in drought-prone areas to define land use and develop human activities compatible with the region's capacity.

The created DHI is an invaluable resource for risk management, damage estimation, land-use zoning, life, and property insurance claim validation, land tax valuation, lifeline emergency services, and risk reduction efforts by planning agencies and local governments. Additionally, the technique used in this study is easily transferable to other regions capable of evaluating additional criteria in accordance with data availability.

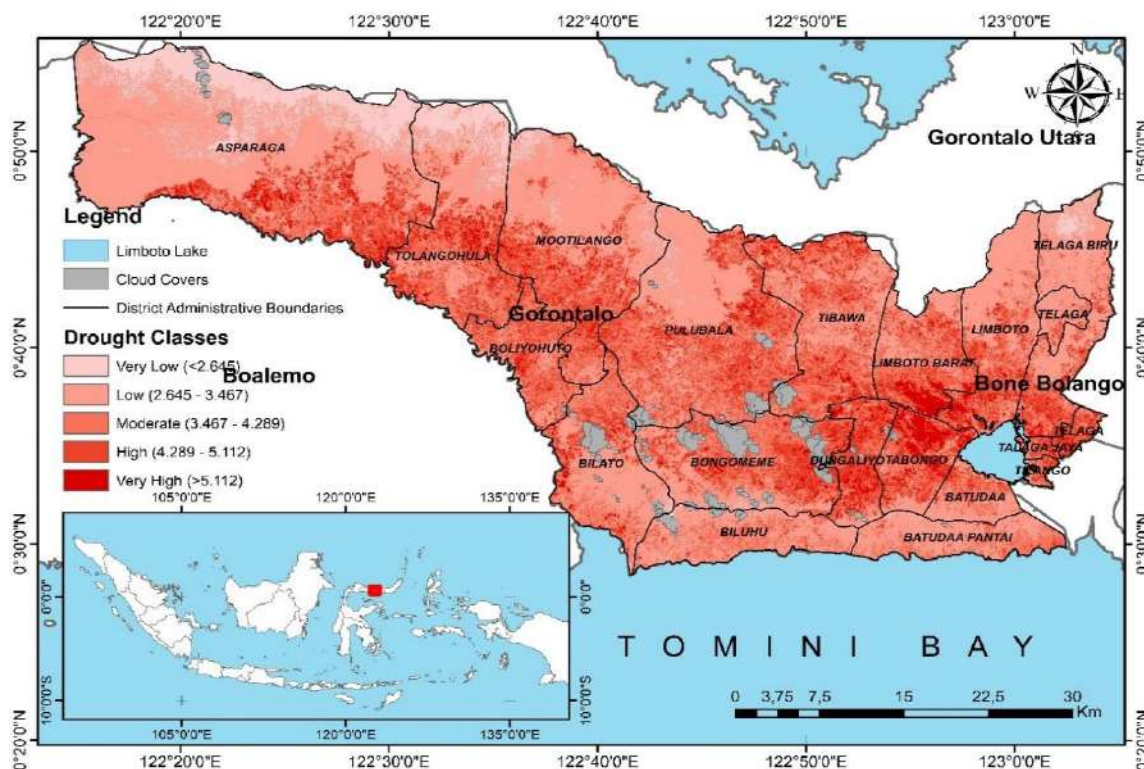


Figure 6. Distribution of drought hazard

Table 9. Distribution of Classes of DHI in Gorontalo Regency

Classes of Drought	Range Weight	Area (Ha)	%Area
Very Low	< 2.645	13,965.66	6.55
Low	2.645 - 3.467	92,831.76	43.53
Moderate	3.467 - 4.289	52,064.10	24.41
High	4.289 - 5.112	38,117.34	17.87
Very High	> 5,112	8,072.28	3.78
Limboto Lake	-	2,325.00	1.09
Cloud Cover	-	5,903.00	2.77
Total		213,279.14	100.00

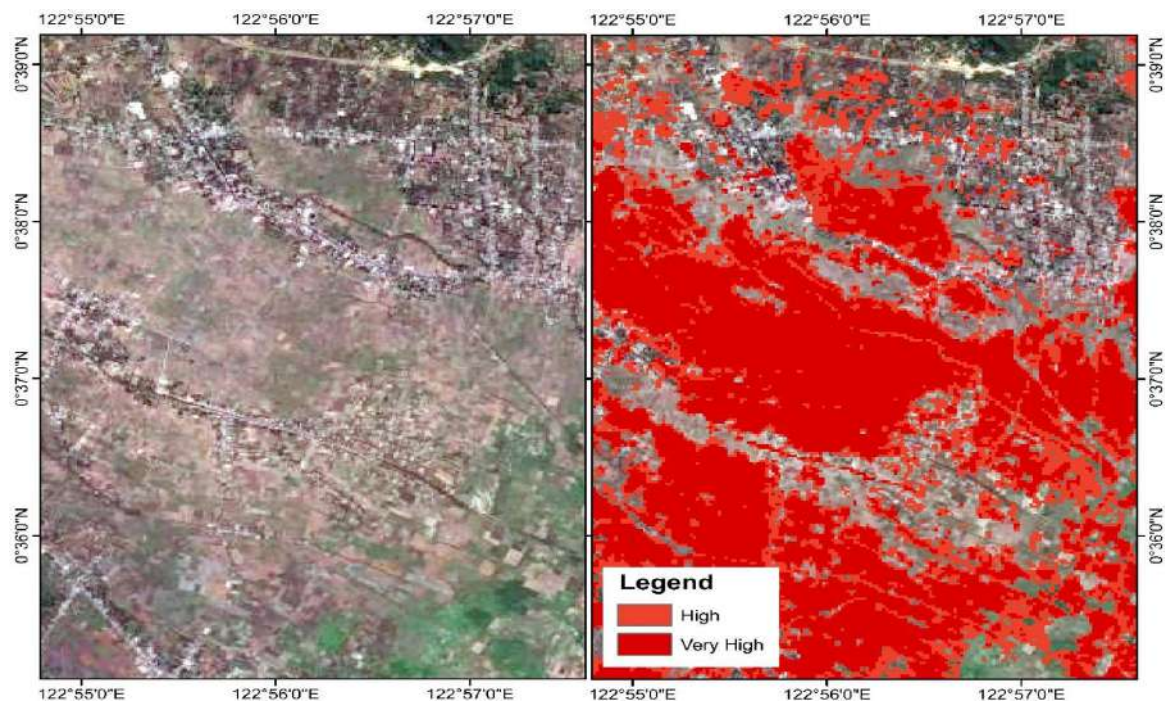


Figure 7. Comparing the distribution of high drought hazards with land use based on google earth

## 5 DISCUSSION

Several studies have been conducted on DHI in various regions around the world. However, none produced an integrated DHI map using Remote Sensing (RS), Geographic Information Systems (GIS), and Analytic Hierarchy Process (AHP). This is generally because the Indonesian National Aeronautics and Space Agency only uses a single variable, namely the Normalized Difference Vegetation Index (NDVI), and the SPI method to conduct DHI.

The method used in this study is consistent with the climatological and geomorphological parameters used in preliminary studies with the addition of Remote Sensing parameters such as LST, NDVI, and NDMI (Belal *et al.*, 2012; Wijitkosum and Sriburi, 2019; Cheng and Tao,

2010; Moghari *et al.*, 2017; Wijitkosum, 2018; Ekrami *et al.*, 2016). Numerous drought studies that utilize data derived from satellites have been conducted. The Temperature Condition Index (TCI) and Normalized Difference Vegetation Index (NDVI) were developed by combining reflectance in the visible, near-infrared, and thermal bands, thereby considerably improving early drought detection, monitoring, and forecasting of its consequences on agriculture (Gebrehiwot *et al.*, 2011; Belal *et al.*, 2012). Study carried out by (Belal *et al.*, 2012). successfully extended satellite data analysis to large-area vegetation monitoring and biomass productivity estimation using National Oceanic and Atmospheric Administration (NOAA) AVHRR data. Dutta *et al.* (2015) found that NOAA-

AVHRR NDVI derived VCI estimates can be useful for monitoring the onset, duration, and spatial-temporal extent of agricultural drought. Meanwhile, Roustia *et al.*, (2020) stated that MODIS NDVI-derived from VCI with precipitation and LST images are useful for monitoring drought in Afghanistan. The relationship was negative between all NDVI categories with extreme and moderate drought conditions (Roustia *et al.*, 2020). According to (Malik *et al.*, 2019) the relationship between LST and NDVI has shown a strong negative correlation in summer, rainy, and winter seasons ( $R^2 > 0.9$ ). The use of the NDVI threshold and the consideration of separating croplands from other land cover types reduces the inclusion of misclassified drought areas, thereby improving agricultural drought estimation (Faridatul & Ahmed, 2020). The combination of the NDVI and LST provides extremely useful information for agricultural drought monitoring and early warning systems for farmers with a high negative correlation (Sruthi & Aslam, 2015). This study found that NDVI significantly influences the DHI in Gorontalo (42.9%) and LST (33.6%) using 76.5% Landsat TM 8 OLI. According to Bajgiran *et al.* (2008), individual meteorological stations discovered substantial connections between NDVI levels and rainfall data in semiarid environments. These connections are because other local elements such as topography, soil characteristics, previous years' stress, and the area's land cover features need to be considered (Gebrehiwot *et al.*, 2011).

NDVI and NDMI are useful for detecting and observing a specific drought area. The vegetative stress, surface water, and poor soil moisture saturation are all significant indicators used by the NDI and NDMI to detect the severity of drought in a specific area (Bhattacharya *et al.*, 2021). These factors are useful for monitoring and assessing drought conditions in the vegetation and moisture aspects (Lin *et al.*, 2010; Lin *et al.*, 2011). TWI is used to confirm that hilltops are more susceptible to drought than lowlands in the catchment area, where water is more available as flow accumulates (Muukkonen *et al.*, 2015). Furthermore, high and low TWI values represent potentially wetter and drier converging and diverging terrains (Adams *et*

*al.*, 2014). Bennie *et al.* (2008) stated that fine-scale topographic diversity within an area influences spatial patterns of tree development and growth responsiveness to climate. Topography influences water and energy variations throughout complicated terrain, leading to top climatic conditions and topographic gradients. These include varying levels of temperature, evapotranspiration, soil moisture, and vegetation patterns on the landscape.

Several studies on general drought hazards in various locations have been conducted in Indonesia. However, none resulted in a comprehensive drought hazard map. Therefore, this study is the first to create a drought hazard map using the GIS-RS-AHP method in Indonesia. Furthermore, meteorological stations and networks in large countries are generally insufficient and underdeveloped. The spatial resolution of rainfall data derived from these weather stations has been estimated to be greater than 100 km<sup>2</sup> due to the sparse distribution and distance. Additionally, due to the sparse nature of infrastructure networks in major countries', continuous rainfall records are few or impossible to gather promptly. In addition, meteorological drought indices, e.g., SPI, RAI, and SPEI, have been commonly used and limited by the distribution of weather stations with the provision of only point data (Faridatul & Ahmed, 2020). Therefore, they failed to visualize the spatial detail with the inability to determine drought susceptibility across spatial units, thereby decreasing the reliability of the drought index. In contrast, RS-based indices facilitate multi-temporal drought vulnerability mapping on a regional scale. Therefore, utilizing GIS-RS-AHP to transform qualitative and quantitative factors in DHI maps was critical in fixing this issue. This is a promoting study with the ability to produce DHI maps when expanded to encompass a wider portion of the country. However, it is difficult to obtain clean data due to cloud cover, which can reduce the accuracy of the results. Therefore, a longer time span of satellite data is needed to obtain more reliable results. This means the study was unable to compare the results obtained with the drought that occurred in the field due to the

absence of real drought disaster information. Hence, it only compared the results with google earth (Figure 7) and the drought hazard map obtained from <https://inarisk.bnpb.go.id/>. This map is prepared using the SPI method and divides the hazard level into 3 classes: low, medium, and high. Based on this method, Gorontalo Regency is dominated by a high level of drought hazard, which is spread in almost all regions.

## 6 CONCLUSION

In conclusion, the AHP computation results show that *NDVI* is the most important contributing factor to DHI, accounting for 42.9%, followed by *LST* (33.6%), *NDMI* (16.8%), and *TWI* (6.7%), at CR value of 0.048. Areas with low, high, and very high DHI are 43.53% (9831.76 ha), 17.87%, and 3.78% of the total landmass.

Remote Sensing methods that give improved real-time and spatially continuous data usable for conducting rigorous drought risk assessments across wide areas are beneficial to a country with a big land area, such as Indonesia. Satellite data can also be used to monitor droughts, provide early warnings, and mitigate the impacts of drought. In line with this, the local government or other stakeholders need to utilise a huge database to ascertain the spatial diversity of drought in the Gorontalo Regency. Additionally, these findings showed that extensive regional study is beneficial in appropriately identifying and regionalizing the drought phenomenon.

Therefore, policymakers will have evidence to develop drought management policies that are suited for local conditions. This study is also expected to highlight the critical role of satellite-derived data in measuring the severity of droughts in the tropics and the tool's utility in supporting policymakers in guiding practical measures for drought hazard reduction.

## DISCLAIMER

The authors declare and attest that this study is solely for academic purposes.

## AVAILABILITY OF DATA AND MATERIALS

All data are available from the authors.

## AUTHOR CONTRIBUTION STATEMENTS

Olii, M.R. developed the Drought Hazard Index (DHI) model using the Analytical Hierarchy Process (AHP). Olii, A., and Pakaya, R. used Remote Sensing and Geographic Information System to conduct an analytical analysis of the DHI factors. All authors made significant contributions to the discussion of the results and the writing of the manuscript.

## ACKNOWLEDGMENTS

The authors are grateful to all the organizations mentioned in this study for providing the necessary data and the Engineering Faculty of Universitas Gorontalo for providing financial support through study funding

## REFERENCES

- Adams, H.R., Barnard, H.R. & Loomis, A.K., 2014. Topography alters tree growth-climate relationships in a semi-arid forested catchment. *Ecosphere*, 5(11), pp.1–16.
- Akbar, T.A., Hassan, Q.K., Ishaq, S., Batool, M., Butt, H.J. & Jabbar, H., 2019. Investigative spatial distribution and modelling of existing and future urban land changes and its impact on urbanization and economy. *Remote Sensing*, 11(2).
- Alavipanah, S.K., Mogaddam, M.K. & Firozjaei, M.K., 2017. Monitoring spatiotemporal changes of heat island in Babol City due to land use changes. In: *International Archives of the Photogrammetry, Remote Sensing and Spatial Information Sciences*. Tehran, Iran.pp.17–22.
- Amalo, L.F., Ma'Rufah, U. and Permatasari, P.A., 2018. Monitoring 2015 drought in West Java using Normalized Difference Water Index (NDWI). *IOP Conference Series: Earth and Environmental Science*, 149(1), pp.1–7.
- Arnfield, A.J., 2003. Two decades of urban climate research: A review of turbulence, exchanges of energy and water, and the urban heat island. *International Journal of Climatology*, 23(1), pp.1–26.
- Bajgiran, P.R., Darvishsefat, A.A., Khalili, A. and

- Makhdoum, M.F., 2008. Using AVHRR-based vegetation indices for drought monitoring in the Northwest of Iran. *Journal of Arid Environments*, 72(6), pp.1086–1096.
- Barsi, J.A., Schott, J.R., Hook, S.J., Raqueno, N.G., Markham, B.L. and Radocinski, R.G., 2014. Landsat-8 thermal infrared sensor (TIRS) vicarious radiometric calibration. *Remote Sensing*, 6(11), pp.11607–11626.
- Belal, A.A., El-Ramady, H.R., Mohamed, E.S. and Saleh, A.M., 2012. Drought risk assessment using remote sensing and GIS techniques. *Arabian Journal of Geosciences*, 7(1), pp.35–53.
- Bennie, J., Huntley, B., Wiltshire, A., Hill, M.O. and Baxter, R., 2008. Slope, aspect and climate: Spatially explicit and implicit models of topographic microclimate in chalk grassland. *Ecological Modelling*, 216(1), pp.47–59.
- Beven, K.J. and Kirkby, M.J., 1979. A physically based, variable contributing area model of basin hydrology. *Hydrological Sciences Bulletin*, 24(1), pp.43–69.
- Bhattacharya, S., Halder, S., Nag, S., Roy, P.K. and Roy, M.B., 2021. Assessment of Drought Using Multi-parameter Indices. In: P.K. Roy, M.B. Roy and S. Pal, eds. *Advances in Water Resources Management for Sustainable Use*, 1st ed. Singapore: Springer Singapore. pp.243–255.
- Chakraborty, A. & Joshi, P.K., 2016. Mapping disaster vulnerability in India using analytical hierarchy process. *Geomatics, Natural Hazards and Risk*, [online] 7(1), pp.308–325. Available at: <<https://doi.org/10.1080/19475705.2014.897656>>.
- Chang, D.Y., 1996. Applications of the extent analysis method on fuzzy AHP. *European Journal of Operational Research*, 95(3), pp.649–655.
- Chen, K., Blong, R. and Jacobson, C., 2003. Towards an Integrated Approach to Natural Hazards Risk Assessment Using GIS: With Reference to Bushfires. *Environmental Management*, 31(4), pp.546–560.
- Cheng, J. & Tao, J.P., 2010. Fuzzy comprehensive evaluation of drought vulnerability based on the Analytic Hierarchy Process- An empirical study from Xiaogan City in Hubei Province. *Agriculture and Agricultural Science Procedia*, 1, pp.126–135.
- Dutta, D., Kundu, A., Patel, N.R., Saha, S.K. and Siddiqui, A.R., 2015. Assessment of agricultural drought in Rajasthan (India) using remote sensing derived Vegetation Condition Index (VCI) and Standardized Precipitation Index (SPI). *Egyptian Journal of Remote Sensing and Space Science*, [online] 18(1), pp.53–63.
- Ekrami, M., Marj, A.F., Barkhordari, J. & Dashtakian, K., 2016. Drought vulnerability mapping using AHP method in arid and semiarid areas: a case study for Taft Township, Yazd Province, Iran. *Environmental Earth Sciences*, 75(12), pp.1–13.
- Faridatul, M.I. & Ahmed, B., 2020. Assessing agricultural vulnerability to drought in a heterogeneous environment: A remote sensing-based approach. *Remote Sensing*, 12(20), pp.1–17.
- Gao, B.C., 1996. NDWI A Normalized Difference Water Index for Remote Sensing of Vegetation Liquid Water From Space. *Remote Sensing of Environment*, 58, pp.257–266.
- Gebrehiwot, T., van der Veen, A. and Maathuis, B., 2011. Spatial and temporal assessment of drought in the Northern highlands of Ethiopia. *International Journal of Applied Earth Observation and Geoinformation*, [online] 13(3), pp.309–321. Available at: <<http://dx.doi.org/10.1016/j.jag.2010.12.002>>.
- Goepel, K.D., 2013. Implementing the Analytic Hierarchy Process as a Standard Method for Multi-Criteria Decision Making in Corporate Enterprises – a New AHP Excel Template with Multiple Inputs. In: *International Symposium on the Analytic Hierarchy Process*.
- Gulácsi, A. & Kovács, F., 2015. Drought Monitoring With Spectral Indices Calculated From Modis Satellite Images In Hungary. *Journal of Environmental Geography*, 8(3–4), pp.11–20.
- Hais, M., Hellebrandová, K.N. & Šrámek, V., 2019.

- Potential of Landsat spectral indices in regard to the detection of forest health changes due to drought effects. *Journal of Forest Science*, 65(2), pp.70–78.
- Haq, M., Akhtar, M., Muhammad, S., Paras, S. and Rahmatullah, J., 2012. Techniques of Remote Sensing and GIS for flood monitoring and damage assessment: A case study of Sindh province, Pakistan. *Egyptian Journal of Remote Sensing and Space Science*, [online] 15(2), pp.135–141. Available at: <<http://dx.doi.org/10.1016/j.ejrs.2012.07.002>>.
- Jin, M., Li, J., Wang, C. and Shang, R., 2015. A practical split-window algorithm for retrieving land surface temperature from Landsat-8 data and a case study of an urban area in China. *Remote Sensing*, 7(4), pp.4371–4390.
- Karnieli, A., Agam, N., Pinker, R.T., Anderson, M., Imhoff, M.L., Gutman, G.G., Panov, N. and Goldberg, A., 2010. Use of NDVI and land surface temperature for drought assessment: Merits and limitations. *Journal of Climate*, 23(3), pp.618–633.
- Lin, M.L., Chu, C.M. & Tsai, B.W., 2011. Drought risk assessment in western inner-mongolia. *International Journal of Environmental Research*, 5(1), pp.139–148.
- Lin, M.L., Wang, Q., Sun, F., Chu, T.H. and Shiu, Y.S., 2010. Quick spatial assessment of drought information derived from MODIS imagery using amplitude analysis. *World Academy of Science, Engineering and Technology*, 43(7), pp.628–632.
- Loon, A.F.V., Stahl, K., Baldassarre, D.G., Clark, J., Rangelcroft, S., Wanders, N., Gleeson, T., Dijk, A.I.J.M.V., Tallaksen, L.M., Hannaford, J., Uijlenhoet, R., Teuling, A.J., Hannah, D.M., Sheffield, J., Svoboda, M., Verbeiren, B., Wagener, T. and Van Lanen, H.A.J., 2016. Drought in a human-modified world: reframing drought definitions, understanding, and analysis approaches. *Hydrol. Earth Syst. Sci.*, 20, pp.3631–3650.
- Malik, M.S., Shukla, J.P. and Mishra, S., 2019. Relationship of LST, NDBI and NDVI using landsat-8 data in Kandaihimmat watershed, Hoshangabad, India. *Indian Journal of Geo-Marine Sciences*, 48(1), pp.25–31.
- McKee, T.B., Doesken, N.J. and Kleist, 1993. The relationship of drought frequency and duration to time scales. In: *Proceedings of the Eighth Conference on Applied Climatology*. Boston: American Meteorological Society. pp.179–184.
- Moghari, S.M.H., Araghinejad, S. & Azarnivand, A., 2017. Fuzzy analytic hierarchy process approach in drought management: Case study of Gorganrood basin, Iran. *Journal of Water Supply: Research and Technology - AQUA*, 66(3), pp.207–218.
- Muukkonen, P., Nevalainen, S., Lindgren, M. and Peltoniemi, M., 2015. Spatial occurrence of drought-associated damages in Finnish boreal forests: Results from forest condition monitoring and GIS analysis. *Boreal Environment Research*, 20(2), pp.172–180.
- Olii, M.R., Olii, A. & Pakaya, R., 2021. The Integrated Spatial Assessment of The Flood Hazard Using AHP-GIS: The Case Study of Gorontalo Regency. *Indonesian Journal of Geography*, 53(1), pp.126–135.
- Patel, D.P. & Prashant, S.K., 2013. Flood Hazards Mitigation Analysis Using Remote Sensing and GIS: Correspondence with Town Planning Scheme. *Water Resources Management*, 27, pp.2353–2368.
- Prasad, A.S., Pandey, B.W., Leimgruber, W. and Kunwar, R.M., 2016. Mountain hazard susceptibility and livelihood security in the upper catchment area of the river Beas, Kullu Valley, Himachal Pradesh, India. *Geoenvironmental Disasters*, 3(3), pp.1–17.
- Prasetya, T.A.E., Munawar, Taufik, M.R., Chesoh, S., Lim, A. and McNeil, D., 2020. Land Surface Temperature Assessment in Central Sumatra, Indonesia. *Indonesian Journal of Geography*, [online] 52(2), pp.239–245. Available at: <<http://marefateadyan.nashriyat.ir/node/150>>.
- Rahmati, O., Kalantari, Z., Samadi, M., Uuemaa, E., Moghaddam, D.D., Nalivan, O.A., Destouni, G. and

- Bui, D.T., 2019. GIS-based site selection for check dams in watersheds: Considering geomorphometric and topo-hydrological factors. *Sustainability (Switzerland)*, 11(20).
- Rousta, I., Olafsson, H., Moniruzzaman, M., Zhang, H., Liou, Y.A., Mushore, T.D. and Gupta, A., 2020. Impacts of drought on vegetation assessed by vegetation indices and meteorological factors in Afghanistan. *Remote Sensing*, 12(15), pp.1–21.
- Saaty, T.L., 1980. *The Analytic Hierarchy Process*. New York: McGraw Hill. International.
- Saaty, T.L., 2008. Decision making with the analytic hierarchy process. *International Journal Services Sciences*, 1(1), pp.83–98.
- Sheffield, J. & Eric, F.W., 2011. *Drought: past problems and future scenarios*. London, Washington D.C.: Eartscan.
- Sholihah, R.I., Trisasongko, B.H., Shiddiq, D., Iman, L.S., Kusdaryanto, S., Manijo and Panuju, D.R., 2016. Identification of Agricultural Drought Extent Based on Vegetation Health Indices of Landsat Data: Case of Subang and Karawang, Indonesia. *Procedia Environmental Sciences*, 33, pp.14–20.
- Sruthi, S. X & Aslam, M.A.M., 2015. Agricultural Drought Analysis Using the NDVI and Land Surface Temperature Data; a Case Study of Raichur District. *Aquatic Procedia*, [online] 4, pp.1258–1264. Available at: <<http://dx.doi.org/10.1016/j.aqpro.2015.02.164>>.
- Sun, D. & Pinker, R.T., 2003. Estimation of land surface temperature from a Geostationary Operational Environmental Satellite (GOES-8). *Journal of Geophysical Research: Atmospheres*, 108(11), pp.1–15.
- Tucker, C.J., 1979. Red and photographic infrared linear combinations for monitoring vegetation. *Remote Sensing of Environment*, 8(2), pp.127–150.
- Tucker, C.J. & Choudhury, B.J., 1987. Satellite remote sensing of drought conditions. *Remote Sensing of Environment*, 23(2), pp.243–251.
- USGS, 2019. *Landsat 8 Data Users Handbook*. 5th ed. [online] USGS, United State: USGS. Available at: <<https://landsat.usgs.gov/documents/Landsat8DataUsersHandbook.pdf>>.
- Voogt, J.A. & Oke, T.R., 2003. Thermal remote sensing of urban climates. *Remote Sensing of Environment*, 86(3), pp.370–384.
- Wang, F., Qin, Z., Song, C., Tu, L., Karnieli, A. and Zhao, S., 2015. An improved mono-window algorithm for land surface temperature retrieval from landsat 8 thermal infrared sensor data. *Remote Sensing*, 7(4), pp.4268–4289.
- Weng, Q., 2009. Thermal infrared remote sensing for urban climate and environmental studies: Methods, applications, and trends. *ISPRS Journal of Photogrammetry and Remote Sensing*, [online] 64(4), pp.335–344. Available at: <<http://dx.doi.org/10.1016/j.isprsjprs.2009.03.007>>.
- Wijitkosum, S., 2018. Fuzzy AHP for drought risk assessment in lam Ta Kong watershed, the north-eastern region of Thailand. *Soil and Water Research*, 13(4), pp.218–225.
- Wijitkosum, S. and Sriburi, T., 2019. Fuzzy AHP integrated with GIS analyses for drought risk assessment: A case study from Upper Phetchaburi River Basin, Thailand. *Water (Switzerland)*, 11(5).
- Wu, J., Lin, X., Wang, M., Peng, J. and Tu, Y., 2017. Assessing agricultural drought vulnerability by a VSD Model: A case study in Yunnan Province, China. *Sustainability*, 9(6), pp.1–16.
- Yang, L., Chen, L. and Wei, W., 2015. Effects of vegetation restoration on the spatial distribution of soil moisture at the hillslope scale in semi-arid regions. *Catena*, [online] 124, pp.138–146.

## Organic Removal Treatment Using Microbubble Generator (MBG) in Eutrophic Disorder Condition

Tri Yulianti<sup>1,\*</sup>, Sri Puji Saraswati<sup>1</sup>, Johan Syafri Mahathir Ahmad<sup>1</sup>, Wiratni Budhijanto<sup>2</sup>

<sup>1</sup> Department of Civil and Environmental Engineering, Universitas Gadjah Mada, Yogyakarta, INDONESIA,  
Jalan Grafika No 2 Yogyakarta

<sup>2</sup> Department of Chemical Engineering, Universitas Gadjah Mada, Yogyakarta, INDONESIA,  
Jalan Grafika No 2 Yogyakarta

\*Corresponding authors: [triyulianti@mail.ugm.ac.id](mailto:triyulianti@mail.ugm.ac.id)

SUBMITTED 27 June 2021 REVISED 18 October 2021 ACCEPTED 26 October 2021

**ABSTRACT** The *Techno Park* basin, built as an extension of a small tributary of the Code River primarily acts as a retention basin for runoff during the rainy season. It improves the quality of water that has been degraded by domestic wastewater discharge from the surrounding community. Therefore, this study aims to assess the extent to which water quality of the basin can be improved with aeration technology. The aeration technology is a Microbubble Generator (MBG) built using a 100 Watts submersible pump with three horizontal nozzles at a depth of 40 cm from the water surface. Furthermore, the profiles of dissolved oxygen (DO) concentration were measured at the basin's inlet and outlet, as well as the depths of 1 m below surface water and the bottom of the basin. Diurnal DO was measured to investigate the causes of supersaturation. The aeration performance was also determined from the COD parameters at the inlet and outlet. Discharge measurements were then conducted on the tributary/drainage channel to the inlet basin. The result showed that the DO supersaturation concentration has been attributed to the contribution of photosynthesis from phytoplankton such as algae. Furthermore, no change in DO concentration was observed in a range of 1 m depth from the surface of the water to the bottom (0.3 - 0.14 mg-DO/l). In this eutrophic state, DO increased exponentially during the daytime hours and then decreased during the night. The daily measurement showed an increase in the average DO of 2.31 mg/l (standard deviation of 1.56 mg/l), with average COD<sub>inlet</sub> fluctuations of 18.79 mg/l (standard deviation of 13.56 mg/l) and average COD<sub>outlet</sub> of 14.38 mg/l (standard deviation 2.94 mg/l). Due to additional DO concentration coming from eutrophication during daylight, it was not possible to make a precise assessment of the effectiveness of the MBG aerator.

**KEYWORDS** Aerator; DO Concentration; Eutrophic Condition; Microbubble Generator; Organic Load (COD).

© The Author(s) 2022. This article is distributed under a Creative Commons Attribution-ShareAlike 4.0 International license.

### 1. INTRODUCTION

The *Techno Park* has two retention basins built in-line with a tributary of the Code River in the area of the Gadjah Mada University (UGM) Faculty of Engineering. Primarily, this basin functions as a container for grey water from people living around the tributary or drainage channel. During the first observation, the current was relatively the same every day, but the water quality status fluctuated. The water condition is poor and contains detergents or household soaps, resulting in bubbles, color, and odor, which are also indicative of excessive organic pollution. Furthermore, the tributary that flows into the Code River is influenced by the quality of the water flowing out of the basin.

The status of the Code River water quality has exceeded the class II standard in the downstream section based on the report of the 2018 Yogyakarta City Environment Service. A 98% of the pollution load comes from the domestic sector following the calculation of water quality parameters using the Storet Method. Sulistyono & Puji (2018) examined the water quality status of the Code River from 2007 to 2016 using the IP and Storet method. The results obtained classified the river as heavily polluted based on the class II Indonesia Government Regulation No. 82 of 2001. This organic load should be reduced to improve the water quality of the basin before entering the Code River.

The decrease in dissolved oxygen (DO) levels is one of the detrimental effects caused by the disposal of organic waste, with the concentration of DO being one of the most important indicators of self-purification of a water body (Huhnke, 2018). Furthermore, the rapid decline of oxygen will indirectly pose a threat to the life of flora and fauna in the water, and this type of condition is also a conducive place for bacterial growth. An increasing organic load in a body of water will be balanced by an increase in microorganisms to break down the organic content. However, oxygen will be consumed in the process, thereby decreasing the level of dissolved oxygen (DO) in the water (Dionisi, 2017).

Since organic load needs to be reduced to improve the water quality of the basin, the amount of DO in water should also be maintained. Oxygen in waters can be available through natural oxygen transfer processes (aeration), such as through increasing velocity flow to increase air contact with water, or through artificial reaeration. The natural aeration process was slow in the basin due to the reduced (laminar) flow of water. Therefore, reaeration should be conducted to increase the DO concentration, and in this study, the process was used as a diffuser aerator system in the form of a Microbubble Generator (MBG). It provided more oxygen for the microorganisms to decompose organic material, thereby increasing the water quality discharged into the Code River. Meanwhile, the MBG was applied as a solution to solve leachate in Sanitary Landfill and performed an efficient as well as less energy consumed technology. A pond with a volume of 75 m<sup>3</sup> discharged at 8 m<sup>3</sup>/hour performed effectively to increase the level of Dissolved Oxygen (DO) and to decrease the level of Chemical Oxygen Demand (COD) to about 15,3% and 16,2% respectively (Pradana *et al.*, 2016). Therefore, this study aims to analyze the extent to the MBG performance can increase DO concentration and reduce the concentration of organic pollutants in the basin.

## 2. METHODS

### 2.1 Installation of MBG aerator at the basin I

There are two basins built in the Engineering Faculty of Gadjah Mada University (UGM) area. The aim of the study and data collection was carried out at the first basin.

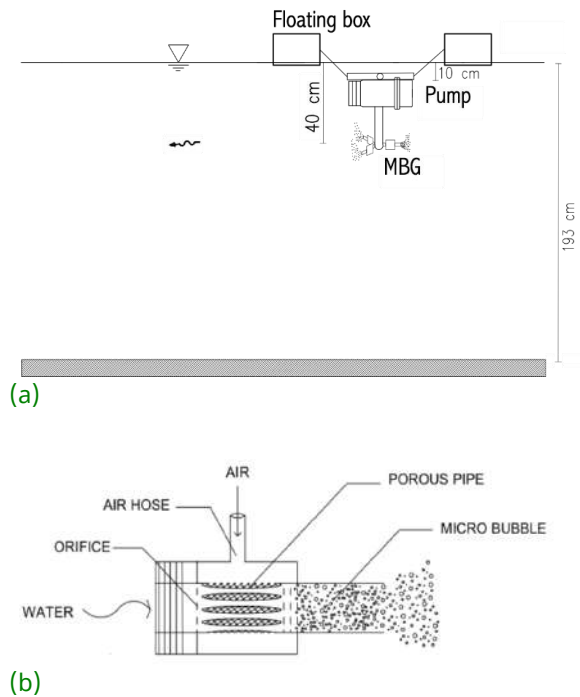


Figure 1. (a) Location of the measurement of discharge; (b) The position of the MBG from the longitudinal section of the basin; (c) MBG Nozzle

The surface area of the water basin was 950 m<sup>2</sup> with a volume of about 700 m<sup>3</sup> and the efficiency of reducing COD depends on the flow rate of the air sucked into the MBG. The smaller the air suction rate, the more effective COD removal. However, an extremely low suction rate can also make the MBG less stable (Budhijanto, *et al.*, 2015) due to the high collisions between the bubbles. The position of the MBG in the aerobic wastewater treatment pond should be designed to minimize the tendency of collisions between bubbles. Furthermore, the MBG was set at a depth of 40 cm in the middle of the basin to reduce the blockage of the pump filter by the large amount of waste entering the basin inlet as shown in Figure 1(a) (Kurniawan, 2019).

The submersible pump used was Lifetech SP608 with a pumping rate of 100 Watt, and the MBG aerator used was an ejector type with an inlet and outlet diameter of 25.4 mm (1 inch) and 15 mm (Figure 1b) respectively. The aerator has an air suction hole of 3 mm in diameter with a flow rate ranging from 0.1 – 0.6 l/min to generate microbubbles. The inner core comprised of a hollow porous pipe wrapped with gauze cloth and this allows the air entering through the suction hole to form small bubbles. Water pumped into the aerator will flow through a narrowing hole in the porous pipe to increase the speed of the flow and create negative pressure by decreasing the diameter. The presence of this negative pressure causes the air sucked through a porous hole to form microbubbles that dissolve into the water (Deendarlianto, *et al.*, 2015; Shalindry, *et al.*, 2015). In addition, the MBG used in this study had three nozzles.

## 2.2 Data collection

The study continued for 10 days from September 20, 2019 (dry season) and began when signs of algal growth appeared after 1.5 months of gray water flowing through the basin. A series of measurements were conducted each day between approximately 1:00 p.m. and 3:00 p.m., and it is considered as a continuation of a previous study (Yulianti *et al.*, 2019). Furthermore, data were collected to monitor the water quality changes as a result of re-aeration, and the MBG was operated continuously during the entire 10 days of data collection. In waters without eutrophic conditions, the maintenance-free MBG can only be operated for a maximum of 2 weeks. On the 11th day, one of the three installed MBG nozzles were reported to be clogged when the water turned eutrophic. The floc film was formed on the pump filter, and this was caused by a large number of suspended particles in the water following the increased turbidity, making it easy to cause blockages.

*In situ* measurements were made for discharge and DO concentrations. The discharge was measured at the outlets of the drainage channel from both Selokan Mataram and Kaliurang Street water sources. This was conducted using OTT C2

current meters based on the *Mean Area Method* (Lin, 2007); Indonesia National Standard (SNI) 8066: 2015 (Standard National Agency, 2015). In addition, the profile of DO stratification was measured by manually lowering down a probe connected to the meter (Lutron WA-2017SD) and recording a measurement every 1 m from the water surface to the basin floor. The DO was measured also at the basin inlet and outlet at a depth of 5 cm from the water surface. The results were plotted using the Surfer application to obtain a vertical DO distribution profile in the basin water.

Diurnal measurements were made on-site using the same DO meter type from the sixth day of the study for 5 days. The mass transfer reaction of DO in 24 four hours was described in a graph (shown at Figure 3).

- a. Each ascending part curve indicates the aeration of MBG and the results of photosynthesis of algae were far greater than the oxygen requirements for organic decomposition (COD) and algal respiration.

$$\frac{dO_2}{dt} = \text{reoxygation} - \text{deoxygation} \quad (1)$$

$$\frac{dO_2}{dt} = (\text{MBG} + \text{algal photosynthesis}) - (\text{COD removal} + \text{algal respiration}) \quad (2)$$

- b. Each descending part of the curve shows oxygen consumption for organic decomposition (COD) and algal respiration greater than the amount of aeration of the MBG.

$$\frac{dO_2}{dt} = \text{reoxygation} - \text{deoxygation} \quad (3)$$

$$\frac{dO_2}{dt} = \text{MBG} - (\text{COD removal} + \text{algal respiration}) \quad (4)$$

These automatically logged measurements only monitored DO concentrations, and there were no COD records in the field. The decrease in DO (downward curve) cannot be viewed in terms of the quantity of oxygen needed for depletion by microorganisms or plant respiration. Meanwhile, the measure of the oxygen used to decompose organic and inorganic matter chemically in

wastewater was COD. Water samples were taken at the basin inlet and outlet and were analyzed in the Laboratory of Sanitary Engineering DTSL FT UGM to determine COD based on Indonesia National Standard (SNI) 06-6989.22-2004 (Standard National Agency, 2004). Subsequently, in situ DO data and COD analysis at the inlet and outlet were represented in graphical form in Excel.

### 3. RESULTS AND DISCUSSIONS

#### 3.1 DO Stratification

Initially, DO measurements were obtained after the aerator has worked for 24 hours. Data retrieval was conducted once a day and the depth of the basin measured in the field was 1.90 m. The DO stratification from the surface to the bottom was calculated close to the MBG as shown in Figure 2.

Two different regions were evident; First, at depths less than 1 m, there was no systematic change in oxygen levels throughout the study. A range of increased DO was observed, from supersaturation at the surface ( $> 8$  mg/l) down to a depth of approximately 80 cm with aerobic condition (DO levels  $> 2$  mg/l) in the second

region. This can be explained by assuming that the cause of increased DO of the water was eutrophication since algae or another chlorophyll aquatic plant only float down to a certain depth about 60 cm below the surface of the water, where there is still intensity of sunlight (Lin, 2007).

This anoxic state (DO concentration  $< 2$  mg / l) requires further evaluation concerning the use of MBG. Even though the aerator was operated continuously for 24 hours, it was not sufficient to increase DO concentration in the depth of the water compared to that of the basin (1,93 m). Continuation of this condition can dramatically decrease the ability of aerobic bacteria to break down organic load (in terms of aerobic treatment). The aerobic microorganisms may die in very low DO conditions that can lead to anaerobic processes and cause odor in the water. The DO level sufficient for bacterial survival depends on the type of microorganism and temperature. Heterotrophic bacteria can survive in very low DO (0.1 - 0.7 mg/l) while autotrophic bacteria cease their activities when DO is below 1.5 mg/l. Therefore, DO concentrations in waters should be above 2 mg/l (Winkler, 1981) to maintain aerobic conditions.

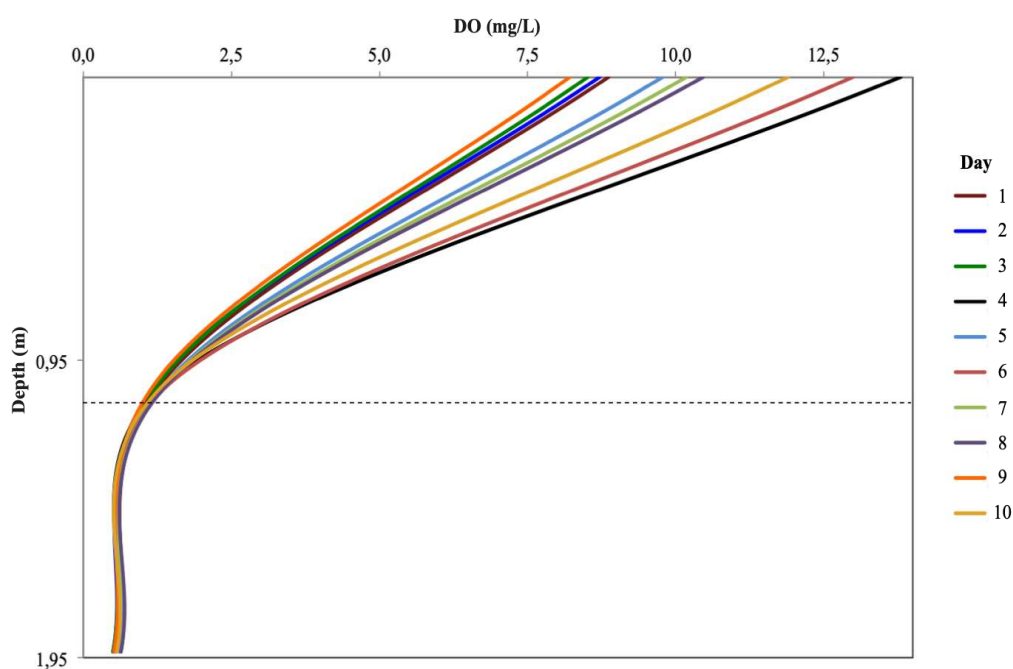


Figure 2. DO stratification measured

### 3.2 DO Diurnal Variation

Figure 3 showed the diurnal variation of DO concentration, where the levels may reach supersaturation at certain times of the day. Furthermore, the measured DO curve showed the result of the mass transfer reaction for 5 days in the basin water. The aim of the measurement, which lasted up to day 11, was to monitor the concentration without interrupting the apparatus for measuring the area and the vertical OD around the MBG of the previous days.

As an indication of eutrophication, the observation of an increase in the oxygen content during the day with high light intensity can be interpreted in contrast to the marked decrease at night. Eutrophication is caused by the growth of phytoplankton (micro-sized water plants containing chlorophyll) such as moss or algae, which utilize high-intensity light in a digestion process (photosynthesis) (Lin, 2007). Meanwhile, oxygen as a byproduct of photosynthesis increases the level of DO independent of the MBG. The absence of sunlight at night halts photosynthesis but phytoplankton and bacterial activity in the sediments still need oxygen for respiration. This is because high respiration levels relative to the oxygen supply from the MBG result in the night time decrease of DO concentration as seen in Figure 4.

The three main processes causing fluctuations in DO concentrations are photosynthesis, respiration, and reaeration (Correa-Gonzales, *et al.*, 2014; Boyd, 2018).

These conditions need to be considered for the operation of the MBG in the basin. The use of an aerator unit with 3 MBG nozzles with 100 watts of electricity cannot increase or maintain DO concentration during the night and in the lower depths of the basin water. Furthermore, dissolved oxygen input should be greater than the amount required for respiration by the water reservoir's nighttime biota activity to avoid anoxic conditions. For this, additional aerators can be added to increase DO, and in return, the electrical power required will be increased.

An alternative to increasing the number of aerators is to counter-intuitively turn off the MBG at night. As a result, the oxygen supply is interrupted and the respiration process of the aquatic plants is disturbed, which leads to a reduction in reproductive activities. Aerobic bacteria can then be developed since the aquatic plants use less nighttime oxygen. One additional advantage of this method is that the nitrification-denitrification process improves by alternately creating aerobic and anaerobic conditions of the basin. This process produces a stable N product that can evaporate into the air to reduce the nitrogen content in the water and indirectly limit eutrophication. Running the MBG aerator for a long duration can form flocks that block the MBG nozzle filter. Therefore, it should be operated on/off only in periods of 30 minutes to minimize this effect (Pradana *et al.*, 2016). This means that when the MBG is turned off at night, the device should be cleaned more frequently.

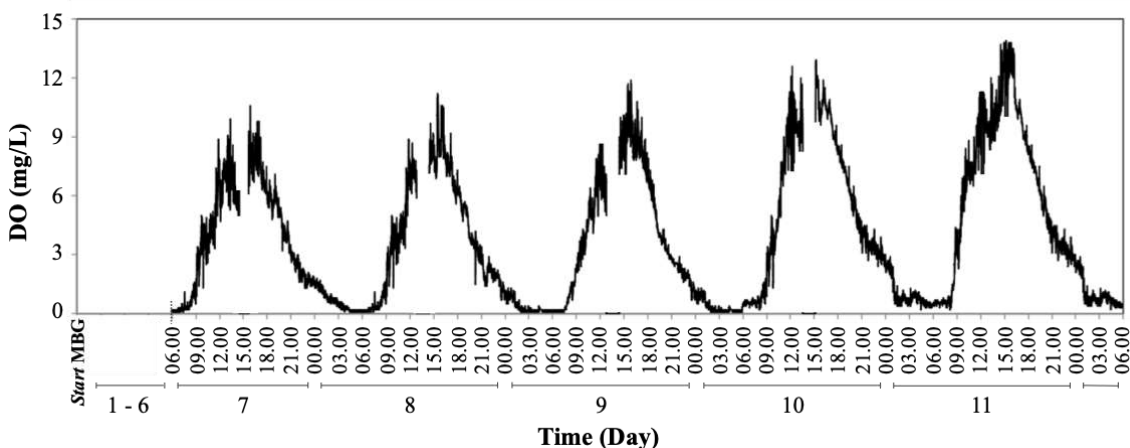


Figure 3. Changes in diurnal DO concentration

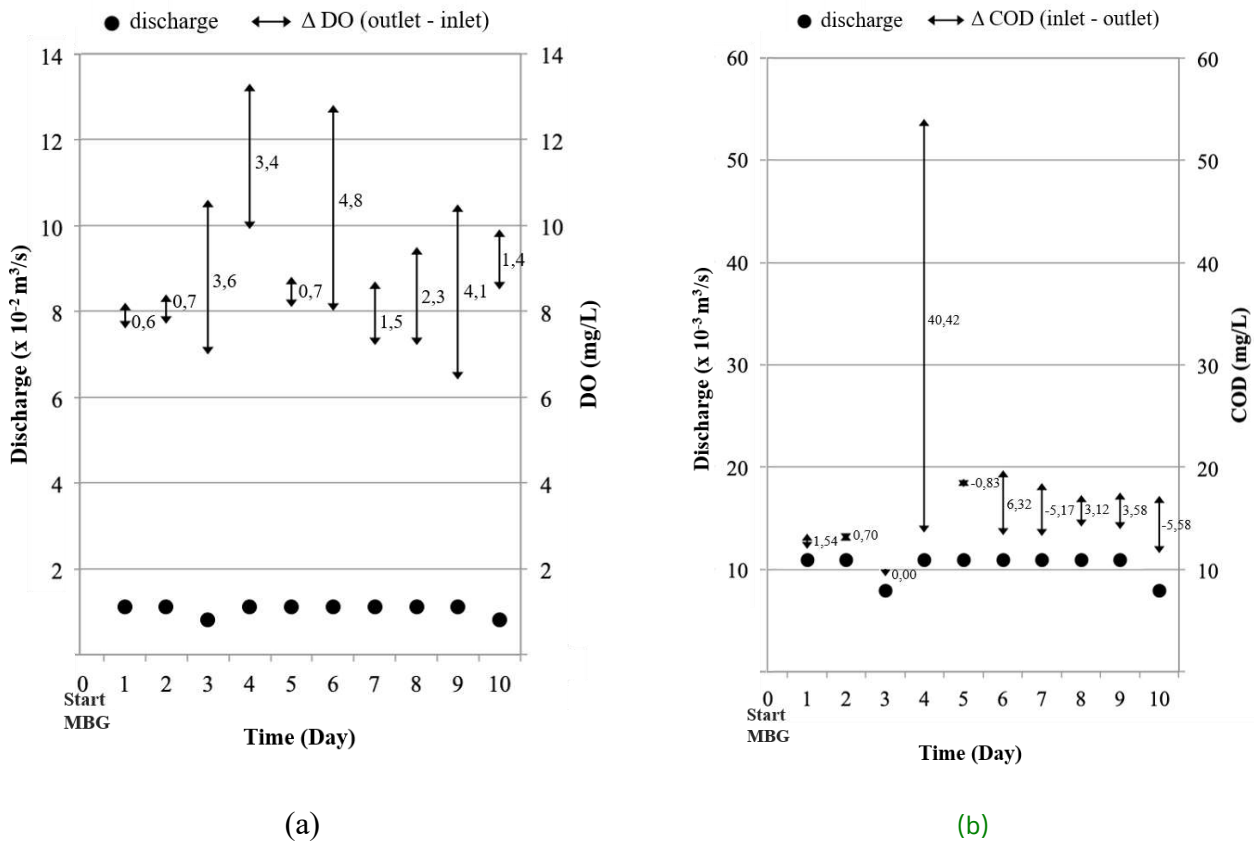


Figure 4. (a) Changes in DO concentration at the inlet and outlet; (b) The COD changes at the inlet and outlet

### 3.3 DO and COD Concentration at the Basin's Inlet and Outlet

Previous studies showed that an average increase in DO concentration at around 1 mg/l (standard deviation of 0.30 mg/l) and 30% of the COD was removed during the first week of using the MBG. The initial COD concentration in the inlet of the basin was 33.33 mg/l, and the concentration of COD (organic load) entering the pond will not directly affect the growth of aquatic plants. However, the concentration of organic load contributed to the increase in aerobic bacteria, and this caused high COD removal efficiency. The results of the decomposition of organic loads will increase the level of CO<sub>2</sub> in the water which is indirectly used by phytoplankton to grow and conduct photosynthesis. To a certain extent, algae have developed rapidly in water bodies and with high adaptability to the basin environment. Furthermore, the algae will continue to develop well on daylight to enable eutrophication (Yulianti *et al.*, 2019).

These eutrophication conditions cause variation of DO and COD concentrations at the inlet in the range of 6.4 mg/l - 9.9 mg/l and 9.57 mg/l - 54.04 mg/l respectively. Meanwhile, the resulting fluctuations for DO and COD removal were measured at the outlet as 7.89% - 64.04% and 0% - 74.80% (Figure 4). The DO concentrations in the water basin were sufficient for the removal of COD. However, the opposite case was also observed with an increase in COD concentration at the outlet. The COD analysis over the test period showed that there were several days when increased levels of DO is not necessary for decomposing the organic load. For example, on the 3<sup>rd</sup> day of measurement, when the change in DO concentration was high there was no change in COD at the outlet from the inlet. The COD removal cannot be predicted as the increase in DO concentration is also unpredictable. In addition, the organic load was more concentrated and very difficult to degrade due to decreased discharge from 0.025 to 0.011 m<sup>3</sup>/s over 10 days of measurements. This can also cause an indirect decrease in the ability of COD removal in water. The declining effectiveness of

COD removal with increased DO supersaturation can be explained from the results study of Handayani (2016). Furthermore, the interaction of aerobic bacteria in microalgae ponds (chlorophyll aquatic plants) was identified with indicators focusing on the relationship between levels of COD and DO. It has been explained that aerobic bacteria and aquatic plants can exist in symbiosis during the day. This is because chlorophyll plants and/or algae use light and carbon dioxide to photosynthesize and produce oxygen used by bacteria to oxidize organic compounds and produce carbon dioxide. Algae will continue to thrive in a pond that they have adapted to the local environment even with a low organic load. Meanwhile, this resulting DO concentration during the day can be very high, and at night the water may still become anoxic. This is because there is no ongoing photosynthesis process since aquatic plants need oxygen to respire.

Since DO concentrations of the surface water at night were measured to be anoxic (Figure 4), the lower depths of the basin were likely in anaerobic conditions while the aerobic bacteria cannot survive there. This is one of the factors leading to the decreasing organic decomposition observed; despite the increase in DO from the MBG aeration process, the non-availability of bacteria that have died before can decrease COD removal (Handayani, 2016). The death of many bacteria in the waters has contributed to the amount of decomposed organic load. Therefore, on the fourth day, the COD removal was high while the concentration was reduced to 40.42 mg/l. This was the result of the accumulation of dead bacteria from previous days.

#### 4. CONCLUSION

The condition of the basin showed the onset of eutrophication within just 1.5 months without additional maintenance. This has an impact on the fluctuation of COD removal and DO diurnal concentration. Furthermore, the basin water gets additional DO from the photosynthesis of algae during the daytime. However, since the respiratory processes of all the biota are increased at night following the uptake of MBG,

the OD level will be drastically reduced to anoxic conditions. By turning the MBG off at night, plant respiration and the nitrification-denitrification processes can be disrupted to also reduce energy usage. Meanwhile, turning the aerator off for more than 30 minutes can cause the formation of filming in the nozzle. This will result in a blockage, leading to an increased frequency of cleaning MBG.

These measurements showed a precise assessment of the effectiveness of the aeration system by MBG in removing organic pollutants due to eutrophication. Oxygen is supplied from other sources (such as eutrophication), but this will depend on the amount of discharge water entering the basin. During the study, the slow water flow increased eutrophication and DO concentration.

#### DISCLAIMER

The authors declare no conflict of interest.

#### AVAILABILITY OF DATA AND MATERIALS

All data are available from the author.

#### AUTHOR CONTRIBUTION STATEMENTS

Author Wiratni B provided the MBG aerator and equipments' needed for the research. Author Tri Y set up and carried out the experimental test, collected and analyzed field sample collection, while all authors analyzed the data result, contributed on discussing the result and drafting the manuscript.

#### ACKNOWLEDGMENTS

The authors are grateful to the Chemical Engineering Department of the Faculty of Engineering Gadjah Mada University for the procurement of MBG aerators and the licensing of the Faculty of Engineering in conducting the study at the Techno Park basin.

#### REFERENCES

APHA, 2005. *Standard Method for the Examination of Water and Wastewater, 21st Edition*. s.l.:American Public Health Association (APHA)..

Boyd, C., 2018. *Dissolved oxygen dynamics*, s.l.: Global Aquaculture Advocate.

BSN, 2004. *Water and Wastewater - Part 22: How to Test the Permanganate Value by Titrimetry*. SNI 06-6989.22-2004. s.l.:Indonesia National Standard Agency (BSN).

BSN, 2015. *Procedures for Measurement of River Flow Discharge and Open Channels Using Flow and Buoy Measuring Devices*. SNI 8066: 2015. s.l.:Indonesia National Standardization Agency (BSN).

Correa-Gonzales, J., Chavez-Parga, M., Cortes, J. & Perez-Munguia, R., 2014. Photosynthesis, Respiration and Reaeration in a Stream with Complex Dissolved Oxygen Pattern and Temperature Dependence. *Ecological Modelling*, Volume 273, pp. 220-227.

Deendarlianto, W., Tontowi, A., & Indarto, A., 2015. The Implementation of a Developed Microbubble Generator on The Aerobic Wastewater Treatment. *International Journal of Technology*, Volume 6, pp. 924-930.

Dionisi, D., 2017. *Biological Wastewater Treatment Process. Mass and Heat Balances*. s.l.:CRC Press, Taylor and Francis Group.

Handayani, E., 2016. *Liquid Waste Management with Microalgae Pond Systems: Effect of COD concentration on the Oxygen Supply Adequacy*. Yogyakarta: Gadjah Mada University.

Lin, S., 2007. *Water and Wastewater Calculations Manual 2 nd- Edition*. s.l.: McGraw-Hill.

Pradana, M., Fitriyadi, N., Hans, A., & Dridya, M.A., 2016. *Testing the Capability and the Energy Consumption of Micro-Bubble Generators in the Leachate of Wastewater Treatment Process at TPST Piyungan, Bantul, Yogyakarta*. Yogyakarta, Department of Mechanical and Industrial Engineering, Engineering Faculty, UGM, pp. 166-171.

Sawyer, C., McCarty, P. & Parkin, G., 2003. *Chemistry for Environmental Engineering and Science 5 th Edition*. s.l.:McGraw-Hill.

Winkler, M., 1981. *Biological Treatment of Waste-Water*. s.l.: Ellis Horwood.

# Factors Affecting Cyclist Behaviours in the Special Region of Yogyakarta

Danang Febrianto\*, Dewanti, Imam Muthohar

Department of Civil and Environmental Engineering, Universitas Gadjah Mada, Yogyakarta, INDONESIA  
Jalan Grafika No 2 Yogyakarta

\*Corresponding authors: [danangfbrnto@mail.ugm.ac.id](mailto:danangfbrnto@mail.ugm.ac.id)

SUBMITTED 28 July 2021 REVISED 19 October 2021 ACCEPTED 26 October 2021

**ABSTRACT** Bicycle-riding/cycling has reportedly become a new trend in various cities of Indonesia, as well as the Special Region of Yogyakarta, amidst the social restriction applied by the Government to decrease the spreading rate of the COVID-19 virus. This is observed to be a healthier effort in strengthening the immune system during the pandemic. However, the positive growth of this trend is proportional to the increasing data on bicycle accidents. This was due to the increased rate of injured and dead victims from 2017 to 2020. The human behavior factor is also one of the factors causing the high rate of these bicycle accidents. Therefore, this study aims to analyze the factors affecting the behavior of cyclists in the Special Region of Yogyakarta, to reduce the continuous increase of accidents. The data used in this study were the result of the Cyclist Behavior Questionnaire (CBQ) on the Yogyakarta riders. The samples were obtained through the purposive sampling method, using an online questionnaire with a google form and acquiring 362 respondents. Furthermore, the analytical method used was the structural equation modeling (SEM), through the AMOS 22.0 software. The results indicated that the regulation scale directly affected risk perception and cyclist behaviors (risky and positive). However, age only affected their behaviors, which did not directly affect the accidents. The regulation scale then directly affected the risky behavior of cyclists, with risk perception observed as the mediator, implying that the cyclists' knowledge of road safety regulations influenced individual behaviors. In conclusion, these results are expected to be one of the considerations in the policy of the government, to carry out the overall development of transportation, especially bicycles.

**KEYWORDS** Behavior; Cyclist; Traffic Safety; Structural Equation Modelling; AMOS.

© The Author(s) 2022. This article is distributed under a Creative Commons Attribution-ShareAlike 4.0 International license.

## 1 INTRODUCTION

The World Health Organization (WHO) reportedly determined that the Coronavirus Disease 2019 (COVID-19) was a new variant of an unknown virus on March 11<sup>th</sup>, 2020, which led to its declaration as a pandemic (World Health Organization, 2020). This caused the government to restrict mobility and traveling, as well as enforce the closure of school/business facilities, to accelerate the management of COVID-19 (Ministry of Health of RI, 2020). Amidst these social restrictions, a significant increase in the use of bicycles is being observed in Indonesia, especially the Specific Region of Yogyakarta (Yunianto, 2020). This location is popularly known as the city of bicycles, due to the increased previous and present use of these vehicles as a mode of transportation (Yogyakarta Government Tourism Office, 2019; Kompas.com, 2020). Besides the positive impact of this trend, a

subsequent increase in the data of cyclist accidents within Indonesia has been observed (Bike to Work Indonesia, 2020), as shown in Figure 1.

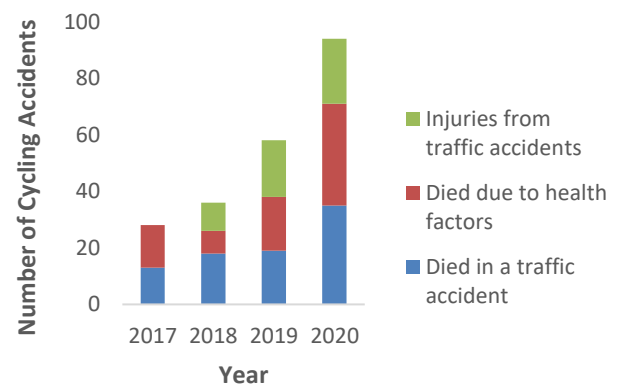


Figure 1. Cycling Accident Data in 2017-2020 (Bike to Work Indonesia, 2020)

This indicates that further study is needed in increasing the safety behaviour of cyclists, which is one of the crucial aspects in improving precautionary measures (Arifin *et al.*, 2018). Several previous studies have reportedly been conducted on bicycle-riding in Indonesia, based on the path designs and waiting rooms. However, only a few have focused on the factors affecting the safety behaviors of cyclists while on the road. Therefore, this present study is necessarily conducted based on supporting the safety of cyclists.

Several differences have also been observed between this study and previous ones. This includes the study on the behavior of cyclists, which is still very few in Indonesia. Due to the lack of sources, study experts are still in the stage of adopting questionnaires from similar foreign reports, with some character adjustments in Indonesia. Direct field observation is also being added in this study, with respondents' ages being limited to a minimum of 12 years. Furthermore, the analysis is being carried out using Excel, SPSS, and AMOS programs, respectively. Based on the previously described background, the high number of accidents is largely influenced by a cyclist's behavior, whose study is still observed to be very minimal. Therefore, this study aims to analyze the behavior of cyclists in Yogyakarta as an effort to support safety, to reduce the high rate of accidents.

## 2 LITERATURE REVIEW

### 2.1 Cyclist Behaviour

According to Arifin (2015), human behavior was the result of all kinds of environmental experiences and interactions, which were manifested in the form of knowledge, attitudes, and actions. The study of Useche (2018b) regarding the influence of gender on behavior also stated that age led to dangerous masculine characteristics, where young men are more likely to have risky driving attitudes than women. Meanwhile, the intense level of cycling affected both sexes. For risk perception, both genders had a significant effect on positive behavior. This indicated that higher risk perception led to a

greater level of positive behavior. Based on Kummeneje (2020), risk perception was an important factor in the occurrence of conflicts when cycling, regarding the attitudes and perspectives of uncertainty among regular cyclists in Norway. This showed that an individual's attitude was directly proportional to the perception of risk. When this perception is poor, an attitude is likely to occur in the cycling skills of a bad rider. Besides these two factors, other indicators are also recognized, such as concerns, tolerance, and priorities, as well as the location of origin from the urban and rural areas.

### 2.2 The Effect of Perception on Cyclist Behaviour

According to Saputra (2017), the most dominant factor causing traffic accidents in Indonesia was humans or HR (human resources). Moreover, Kummeneje and Rundmo (2020), stated that in line with a safe driving attitude, the perceptions of risk and worry were sources of major concerns, as both were related to the risk-taking behavior of an individual. The study of Rundmo (1996), also explained that the relationship between perceptions, behaviors, and accidents, was a complex matter, indicating that there were at least 3 approaches to observe these associations, namely,

1. Accidents lead to the perception of risk,
2. Perceived risk lead to accidents,
3. Perception of risk and accident/safety are endogenous variables.

According to Lawson *et al.* (2013), the safety perception of cyclists in Dublin city was observed, where respondents cycled an average of 9.54 and 6.85 km on weekdays and weekends, respectively. The behavioral model of this study showed that the use of safety accessories was not related to the self-confidence of cyclists. This was because cyclists using these accessories were more obedient to the rules on the road. The compliance with these rules described the experience and confidence level of the cyclist, as the purpose of the trip was not related to safety. The results also showed that Dublin motorcyclists were very ignorant and careless on the aspect of safety. Although the perception of cyclists was divided

into ages under and above 25 years, their use of safety accessories indicated that cycling was still dangerous than driving a car in Dublin. Also, the attitude of careless car drivers in this city was very risky. Therefore, the cycling experience affected the perception of safety.

### 3 METHODS

#### 3.1 Questionnaire Design

The questionnaires that were digitally disseminated in the Indonesian language consisted of four sections.

Section 1: This contained individual and demographic variables, such as gender, age, occupation, and education.

Section 2: This consisted of self-reported risky cycling behavior, which used the raw data of the Cyclist Behavior Questionnaire (CBQ) (Useche et al., 2018c). The aspect of this questionnaire contained 44 items, which were divided into three factors through the Likert's Scale, namely Violations (V; 16 items), Errors (E; 16 items), and Positive Behaviors (PB; 12 items). Also, the total score of Risky Behavior was obtained from Violations and Errors (Useche dkk., 2018b). In addition, this questionnaire used five levels of scaling, namely 1 = never, 2 = rarely, 3 = sometimes, 4 = often, 5 = always.

Section 3: This encompassed the Cyclist Risk Perception and Regulation Scale (RPRS) used to measure the perception and knowledge of riders, regarding the policy of cycling. This consisted of 14 items (9 for perception and 5 for knowledge on regulation), where scales 1 and 5 = the lowest and highest for the regulation knowledge/risk perception, respectively (Useche *et al.*, 2018a).

Section 4: This included the cyclists' characters, to observe the aim of using bicycles, intensity, and experience on encountered accidents.

#### 3.2 Sample

This study used online questionnaires through a google form, with the purposive sampling technique, which helped in selecting the target samples that conceived specific characteristics, based on the pre-determined criteria. Also, the use of online dissemination techniques considered the pandemic period limitations, to reduce direct interaction with other people. The selected respondents were cyclists with previous cycling experiences in the Special Region of Yogyakarta, the age range of these respondents was between 12 years old and above. This was because road cycling was not recommended for children below the age of 12 years (VicRoads, 2018). The respondent data recapitulation is shown in Table 1.

According to Sugiyono (2007), the minimum number of respondents used was 349 when the total population was uncertain. In this present study, 362 of 377 Yogyakarta cyclists filled the disseminated questionnaire after reducing the incomplete data. The results showed that 78 and 22% of these respondents were male and female, respectively. Furthermore, the cyclists between the age of 17-35 years dominated this study, with most being employees and students. The results also indicated that 70, 29, and 1% of the total population had higher, secondary, and elementary educations, respectively. In addition, 90% of the bicycles used were for sports, as 17% of the respondents reported that they had been in accidents. Based on age, the data on the respondents with accident experiences are shown in Table 3.

Table 1. Data tabulation of gender vs respondent intensity vs age

Gender	Cycling Intensity (hours)	Age							Total
		Early adolescence	Late adolescence	Early adulthood	Late adulthood	Early old age	Late old age	Elderly	
Male	<1	0	11	5	2	2	0	0	20
	1 - 5	0	49	44	21	6	5	3	128
	6 -10	2	27	37	22	5	1	1	95
	11 - 15	0	9	9	6	1	1	1	27
	16 - 20	0	4	0	1	1	0	0	6
	21 - 25	0	0	2	1	0	0	0	3
	>25	0	1	3	0	0	0	0	4
Male total		2	101	100	53	15	7	5	283
Female	<1		7	2	1	1	0		11
	1 - 5		22	11	4	4	2		43
	6 -10		11	2	3	2	0		18
	11 - 15		3	3	0	0	0		6
	16 - 20		0	0	1	0	0		1
	>25								
Female total			43	18	9	7	2	0	79

Table 2. Data tabulation of age vs accident vs cycling intensity

Age	Accident	Intensity (hour/week)							Total
		<1	1- 5	6 - 10	11 - 15	16 - 20	21 -25	> 25	
Early adolescence 12 - 16 years	Yes			2					2
	No			0					0
Late adolescence 17 - 25 years	Yes	2	11	8	5	1		0	27
	No	16	60	30	7	3		1	117
Early adulthood 26 - 35 years	Yes	0	8	8	6		0	0	22
	No	7	47	31	6		2	3	96

Table 3. Continuation of data tabulation of age vs accident vs cycling intensity

Age	Accident	Intensity (hour/week)							Total
		<1	1- 5	6 - 10	11 - 15	16 - 20	21 -25	> 25	
Late adulthood 36 - 45 years	Yes	0	4	3	1	0	0		8
	No	3	21	22	5	2	1		54
Early old age 46 - 55 years	Yes	1	1	1	0	1			4
	No	2	9	6	1	0			18
Late old age 56 -65 years	Yes								0
	No		7	1	1				9
Elderly > 65 years	Yes		1	0	0				1
	No		2	1	1				4
Total									362

### 3.3 Statical Analysis

To observe the correlation effect among dimensions, the model testing was conducted through the Structural Equation Modelling (SEM), with the initial step using the Confirmatory Factor Analysis (CFA). This CFA test was performed to acquire the fit or significant variable to be used in the complete structural equation model. Also, the attempt to understand the latent variable eventually produced a conceptual definition known as a construct. This variable operational definition was created for the unobserved abstract construct to be measured through dimensions and indicators. Furthermore, the significance test was performed to empirically measure the previously tested latent variable. When the  $p\text{-value} = \leq 0.05$  or  $C.R. \geq 1.967$  ( $C.R. = t_{count}$ ), the indicator or dimension was significantly determined, with continuity to the validity test. However, this indicator/dimension should be removed when the result is insignificant. The validity test was performed through the observation of the loading factor standard of each indicator or dimension. This indicated that when the standard is  $\geq 0.5$ , the result was validly determined. Meanwhile, the related indicator/dimension should be removed in the subsequent analysis when the result is invalid (Haryono, 2016).

The dimension reliability test used the CR (Construct Reliability) method, where assessments were carried out through the previously analyzed loading factor standard. According to the method, the score obtained from the analysis should be  $\geq 0.7$  or acceptable between 0.6 – 0.7 (Hair Jr *et al.*, 2010). A goodness of fit index test was also used to acquire a complete significant structural equation. Therefore, the assessments of statistical chi-square ( $X^2$ ), significance probability ( $p$ ), the goodness of fit index (GFI), Adjustment Goodness of fit index (AGFI), comparative fit index (CFI), Tucker-Lewis Index or non-normed fit index (TLI or NNFI), root mean square error of approximation (RMSEA), and root mean square residual (RMSR or RMR), were used to analyze the significance between the model and the data (Haryono, 2016).

## 4 RESULTS

The data analysis in this study was performed by examining each item, to determine when the results should be used as measuring instruments. Using the AMOS software, the validity test was conducted through convergent analysis. This indicated that the condition for the loading factor value stated that the score should be greater than 0.5. Moreover, reliability was tested by calculating the CR value, with conditions stating that the acceptable score should be greater than 0.6 (Ghozali, 2008). After the data were validated by removing the insignificant loading factor values, the reliability test was carried out. Using the CR method, the values of the reliability test indicated the results greater than 0.6, which were 0.9 and 0.7 each for risky and positive behaviors, as well as risk perception and regulation scale, respectively. After the dimension test using the CFA, the next analytical step was the formulation of the model structure.

This model was arranged from 3 exogenous variables, namely age, cycling intensity, and regulation knowledge (regulation scale). Also, the risk perception in this model functioned as the mediator, as three endogenous variables were observed, namely positive and risky behaviors, as well as accidents. The risky behavior variable was subsequently reflected by two factors, namely violations and errors. The indicator data in this model referred to previously analyzed information, through the confirmatory factor analysis. This showed that the loading factor values should be significant or greater than 0.5 and 0.6 in the validity and construct reliability tests, respectively. Therefore, each model was made as a unit and arranged according to the previously obtained theories. The initial GOF test showed a massive likelihood chi-square, as the significance values ( $p$ ) were still insignificant, i.e., below 0.05. The values of GFI, CFI, AGFI, and TLI were also yet to exhibit fit values, i.e., below 0.09. Meanwhile, the RMSEA and RMR values were 0.056 and 0.321, which were categorized decent

due to being above 0.05. A fit structural model result was subsequently acquired after the modification indices stage, which was conducted by eliminating insignificant indicators based on the recommendation of AMOS. The chi-square value was categorized as good at 142.291, which was lower than the t-table value (407.366). The significance value (p) of 0.384 was also categorized as good, due to being greater than 0.05. The GFI, AGFI, CFI, and TLI at 0.950, 0.932, 0.996, and 0.996 respectively, were further found

to be good based on exceeding 0.09. In addition, the RMSEA and RMR values were good at 0.016 and  $0.011 \leq 0.08$  and 0.05, respectively. Using AMOS 22.0, Table 3 presented the direct effect of a construct towards others, while Table 2 showed the amount of the effect. With the standardized value of a coefficient parameter (p) being below  $\alpha = 0.05$ , the study hypothesis was supported by the data (significant) while the estimations showed the amount of effect.  $p < 0,05 = \text{significant}$

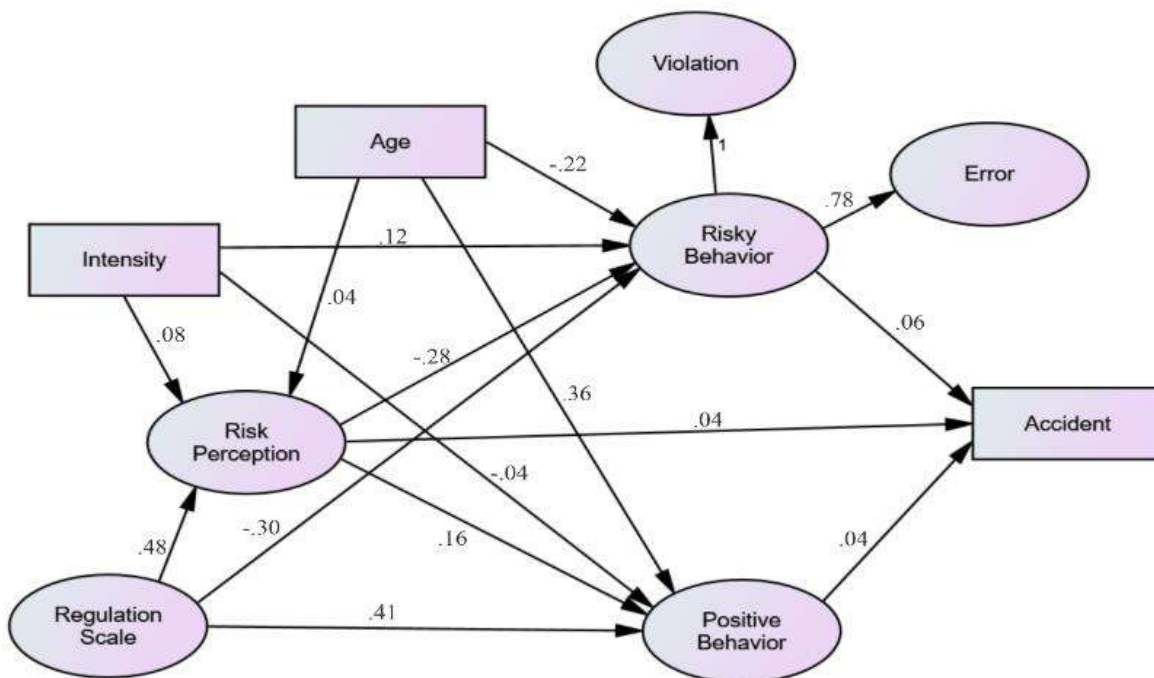


Figure 2. Standardized parameter estimates.

Table 4. Standardized direct effect

	<i>Intensity</i>	<i>Age</i>	<i>Regulation Scale</i>	<i>Risk Perception</i>	<i>Risky behaviour</i>	<i>Positive behaviour</i>
<i>Risk Perception</i>	0,081	0,040	0,479 (p = ***)			
<i>Risky behaviour</i>	0,106	-0,222 (p = ***)	-0,298 (p = 0,004)	-0,281 (p = 0,002)		
<i>Positive behaviour</i>	-0,043	0,359 (p = ***)	0,411 (p = ***)	0,115		
<i>Accident</i>				0,040	0,062	0,042

The analytical results showed that age ( $p=0.529$ ), intensity ( $p=0.177$ ), and regulation knowledge of the cyclists (regulation scale) did not significantly affect risk perception. This was because the  $p$ -value was still above 0.05. However, the regulation knowledge positively affected risk perception at 0.479. This indicated that better regulation knowledge highly affected cyclists. According to Kummeneje, *et al.* (2020), age had no significant effect on the risk perception of Norwegian cyclists. Meanwhile, Useche (2018b) stated that intensity had a significant influence on risk perception in Latin and North America, as well as Europe. This was not in line with the present study due to insignificant results. Differences in the study locations were likely to be a factor in these distinguished results. However, Useche (2018b) was in line with the study, based on having a significant positive effect on risk perception.

Based on the cyclists' risky behaviors, the results showed that the values of risk perception, age, and regulation knowledge (regulation scale) had significant and negative impacts at -0.281, -0.222, and -0.298, respectively. This showed that better risk perception improved with age, leading to adequate safety regulation knowledge. These were in line with Useche (2018b), which showed significant results regarding the effects of age, risk perception, and regulatory knowledge, on the unsafe behavior of cyclists. However, different results were obtained on the intensity construct of both studies. This was because intensity had significant and insignificant ( $p = 0.088$ ) effects on risky behavior, in Useche (2018b) and this present study, respectively. These results indicated that intensity level did not influence the risky behavior of cyclists. For positive behavior, no significant effect was observed with the values of risk perception and intensity at 0.411 and 0.359, respectively. This was not in line with Useche (2018b), which stated that risk perception and

intensity had a positive significant effect on the safety behavior of cyclists. However, similar results were observed for safety regulatory knowledge and age, which had a significant effect on positive behavior. This signified that good regulatory knowledge improved with older age, leading to a positive effect on road safety behaviors.

Based on the accident factor, significant impacts were not observed for the values of risk perception, as well as positive and risky behaviours. This was not in line with Useche (2018d), which showed significant results for both accident constructs. The low rate of accident victims among the respondents affected the results of this study, leading to the observed estimated differences with other reports. According to Table 4, the indirect relationship of the model was described using the Sobel Test method, to observe the significance value ( $p$ -value). Several calculations were also performed using the Sobel Test Calculator (Preacher & Leonardelli, 2010), which showed that only the regulation scale had a significant effect ( $p = 0.007$ ) at -0.135. This implies that the regulation scale affected risky behavior.

The better the regulatory knowledge of cyclists, the lesser the chances of exhibiting dangerous behaviors. The results obtained from this study should be a further recommendation in the decision-making policy of the government, which indirectly shows that safety regulatory knowledge influences dangerous behavior. This suggests that the government should continue to socialize and provide guidance regarding cyclists' road safety regulations, for them to be properly educated. Therefore, the recapitulation of the factors directly/indirectly affecting the behaviours of cyclists in Yogyakarta is shown in Table 6 as follows.

Table 5. Standardized indirect effect

	<i>Intensity</i>	<i>Age</i>	<i>Regulation Scale</i>	<i>Risk Perception</i>	<i>Risky behaviour</i>	<i>Positive behaviour</i>
<i>Risk Perception</i>						
<i>Risky behaviour</i>	-0,023	-0,011	-0,135 (p = 0,007)			
<i>Positive behaviour</i>	0,009	0,005	0,055			
<i>Accident</i>	0,007	0,002	0,012	-0,013		

Table 6. Recapitulation of direct and indirect influences

Effect	Factor		Value	Result	
<i>Direct</i>	<i>Risk perception</i>	<---	<i>Regulation Scale</i>	0.479	Significantly positive
		<---	<i>Risk Perception</i>	-0.281	Significantly negative
	<i>Risky behaviour</i>	<---	<i>Age</i>	-0.222	Significantly negative
		<---	<i>Regulation Scale</i>	-0.298	Significantly negative
	<i>Positive behaviour</i>	<---	<i>Age</i>	0.359	Significantly positive
		<---	<i>Regulation Scale</i>	0.411	Significantly positive
<i>Indirect</i>	<i>Risky behaviour</i>	<---	<i>Regulation Scale</i>	-0.013	Significantly negative

## 5 DISCUSSION

The direct effect showed that the regulation scale directly and positively affected the perception of risk in behaving, indicating that a better understanding of safety led to a greater assessment of uncertainties. Also, the regulation scale affected both positive and risky behaviors (cyclist behaviours). In addition, this safety regulation indirectly and negatively affected risky behaviour, indicating that better knowledge of rules led to more negligence in unsafe behaviors. In this study, the regulation scale significantly contributed to risk perception and behaviour, indicating the concern to be addressed in making future policies. The socialization regarding safety rules and information should also be continuously conducted through the effectiveness of community forums, based on the existence of several bicycle utilization, such as sports equipment, regular use, hobby, short-

## 6 CONCLUSION

The use of bicycles as a tool for exercise was in line with government regulations, which

distance travel, and profession. Reaching out to all types of bicycle use is realistically difficult, although it should be continuously conducted to educate cyclists. Moreover, the Government of the Special Region of Yogyakarta should continuously improve in providing safe and comfortable infrastructures for cyclists. This involved the provision of a bicycle path and routes, safe intersection design, signs, parking areas, and the integration with public transportations. In addition, proper infrastructures indirectly attract the interest of cyclists to use bicycles as their daily mode of transportation. These results are expected to complement several studies on bicycles in Indonesia. Therefore, further studies should be developed through the observation of more effective factors in the bicycle user environment. Several interesting future parameters should be related to the dominant male cyclists, factors causing an accident, or regular cycling interests.

continuously provided information on the importance of immunity and distance maintenance during the pandemic. These results

supported the government's program in promoting sports activities, based on the regular maintenance of self-immunity (Deniati & Annisa, 2021). As a sporting tool, the use of bicycles focused on the non-closure of users (Ika, 2020). The number of growing communities was also a forum for the government to socialize in building new habits of cycling, as a means of transportation. This specified that the government should build a safe and comfortable infrastructure for cyclists. As a mode of transportation, the factors affecting the government's decision to convert casual cyclists into regular ones include, (1) building environmental factors (mileage, bicycle parking, road surface quality, and seasonal changes), (2) socio-economic features (age, gender, vehicle ownership), (3) psychological factors (habits, attitudes, norms), and (4) factors related to cost, travel time, comfort, and safety (Heinen, *et al.*, 2010).

Based on the factors affecting cyclists' safety behaviours, this study showed that the regulation scale directly and indirectly affected risk perception and unsafe attitude. Therefore, the government should continue the socialization on road safety rules, with the expectation that cyclists should improve their knowledge and safety behaviors. Future studies is then recommended to focus on experienced accident-based cyclists, to obtain more significant results. These results were in line with Useche (2018d), regarding the effect of the regulation scale on cyclists' accidents in Europe and Latin America. Furthermore, the knowledge of traffic rules affected safety behaviors when cycling. These results are expected to assist the Indonesian government in making policies regarding the use of bicycles.

#### DISCLAIMER

The authors declare no conflict of interest.

#### AVAILABILITY OF DATA AND MATERIALS

All data are available from the author.

#### AUTHOR CONTRIBUTION STATEMENTS

Danang F and Dewanti conceived of the presented idea. Danang F developed the theory and performed the computations. Dewanti and Imam M verified the analytical methods. Dewanti and Imam M encouraged Danang F to investigate a specific aspect and supervised the findings of this work. All authors discussed the results and contributed to the final manuscript.

#### ACKNOWLEDGMENTS

The authors are grateful to the bicycle communities in the Special Region of Yogyakarta, for their participation and support in this study.

#### REFERENCES

- Arifin, M. Z., Wicaksono, A. & Permata, N. D., 2018. *Kajian Strategi Penanganan Program Keselamatan Pesepeda*. Malang, Prosiding Simposium Forum Studi Transportasi antar Perguruan Tinggi ke-21 Universitas Brawijaya.
- Bike to Work, 2020. <https://www.b2w-indonesia.or.id/>. [online] Available at: [https://docs.google.com/spreadsheets/d/e/2PACX-1vTaLpFotxAoQN\\_ljx3GXkoakMJpesxwSTk-3EfQnPD\\_mpDNzoMKeZn5671M7atI1cdbk7S1DHYqsbi8/pubhtml](https://docs.google.com/spreadsheets/d/e/2PACX-1vTaLpFotxAoQN_ljx3GXkoakMJpesxwSTk-3EfQnPD_mpDNzoMKeZn5671M7atI1cdbk7S1DHYqsbi8/pubhtml) [Accessed 22 November 2020].
- Deniati, E. N. & Annisaa, 2021. Hubungan Tren Bersepeda dimasa Pandemi Covid-19 dengan Imunitas Tubuh Lansia. *Sport Science and Health*, 3(3), pp. 125-132.
- Ghozali, I., 2008. *Model Persamaan Struktural, Konsep dan Aplikasi dengan Program AMOS 16.0*. Semarang: Badan Penerbit Universitas Diponegoro.
- Haryono, S., 2016. *Metode SEM Untuk Penelitian Manajemen dengan AMOS, LISREL, PLS*. Bekasi: PT. Intermedia Personalia Utama.
- Heinen, E., van Wee, B. & Maat, K., 2010. Commuting by Bicycle: An Overview of The Literature. *Transport Review*, 30(1), pp. 59-96.
- Ika, 2020. *Universitas Gadjah Mada*. [online] Available at: <https://ugm.ac.id/id/berita/19632->

pakar-ugm-jelaskan-cara-aman-bersepeda-di-tengah-pandemi-corona [Accessed 6 May 2021].

Kementerian Perhubungan RI, 2020. *PM 59 Tahun 2020 Tentang Keselamatan Pesepeda di Jalan*. Jakarta: s.n.

Kompas.com, 2020. *Ramai Pesepeda di Perempatan Tugu Yogya, Bagaimana Penjelasannya?*. [Online] Available at : <https://www.kompas.com/tren/read/2020/07/12/151000165/ramai-pesepeda-di-perempatan-tugu-yogyakarta-bagaimana-penjelasannya> [Accessed 26 November 2020].

Kummeneje, A.-M. & Rundmo, T., 2020. Attitudes, risk perception and risk-taking behaviour among regular cyclists in Norway. *Transportation Research*, 69, pp. 135-150.

Lawson, A. R., Pakrashi, V., Ghosh, B. & Szeto, W., 2013. Perception of Safety of Cyclists in Dublin City. *Accident Analysis and Prevention*, 50, pp. 499-511.

Mandic, S., Flaherty, C., Pocock, T., Kek, C. C., McArthur, S., Ergler, C., ChilLón, P., Bengoechea, E. G., 2018. Effect of Cycle Skill Training on Children's Cycling-Related Knowledge, Confidence and Behaviour. *Journal of Transport & Health*, 8, pp. 271-282.

Ministry of Health of RI, 2018. *Directorate of Health Promotion and Community Empowerment*. [online]. Available at: <https://promkes.kemkes.go.id/content/?p=8807> [Accessed 15 July 2021].

Preacher, K. J. & Leonardelli, G. J., 2010. *Calculation for the Sobel Test*. [Online] Available at: <http://quantpsy.org/sobel/sobel.htm> [Accessed 9 June 2020].

Rundmo, T., 1996. Associations Between Risk Perception and Safety. *Safety Science*, 24 (3), pp. 197-209.

Sugiyono, 2007. *Statistika Untuk Penelitian*. 12th ed. Bandung: Alfabeta.

Useche, S. A., Alonso, F., Montoro, L. & Esteban, C., 2018d. Distraction of Cyclists: How Does It Influence Their Risky Behaviours and Traffic Crashes?. *PeerJ Journal*, 6, pp. 1-25.

Useche, S. A., Montoro, L. & Alonso, F. M. T., 2018b. Does gender really matter? A structural equation model to explain risky and positive cycling behaviours. *Accident Analysis and Prevention*, 118, pp. 86-95.

Useche, S. A., Montoro, L., Tomas, J. M. & Cendales, B., 2018c. Validation of the Cycling Behaviour Questionnaire: A tool for measuring cyclists' road behaviours. *Transportation Research*, 58, pp. 1021-2030.

Useche, S., Montoro, L., Alonso, F. & Oviedo-Trespalacios, O., 2018a. Infrastructural and Human Faktors Effecting Safety Outcomes of Cyclist. *Sustainability*, 10 (2), pp. 299..

VicRoads, 2018. *A Family Guide to Bike Ed*. [Online] Available at: <https://www.vicroads.vic.gov.au/safety-and-road-rules/cyclist-safety/learning-to-ride> [Accessed 19 April 2021].

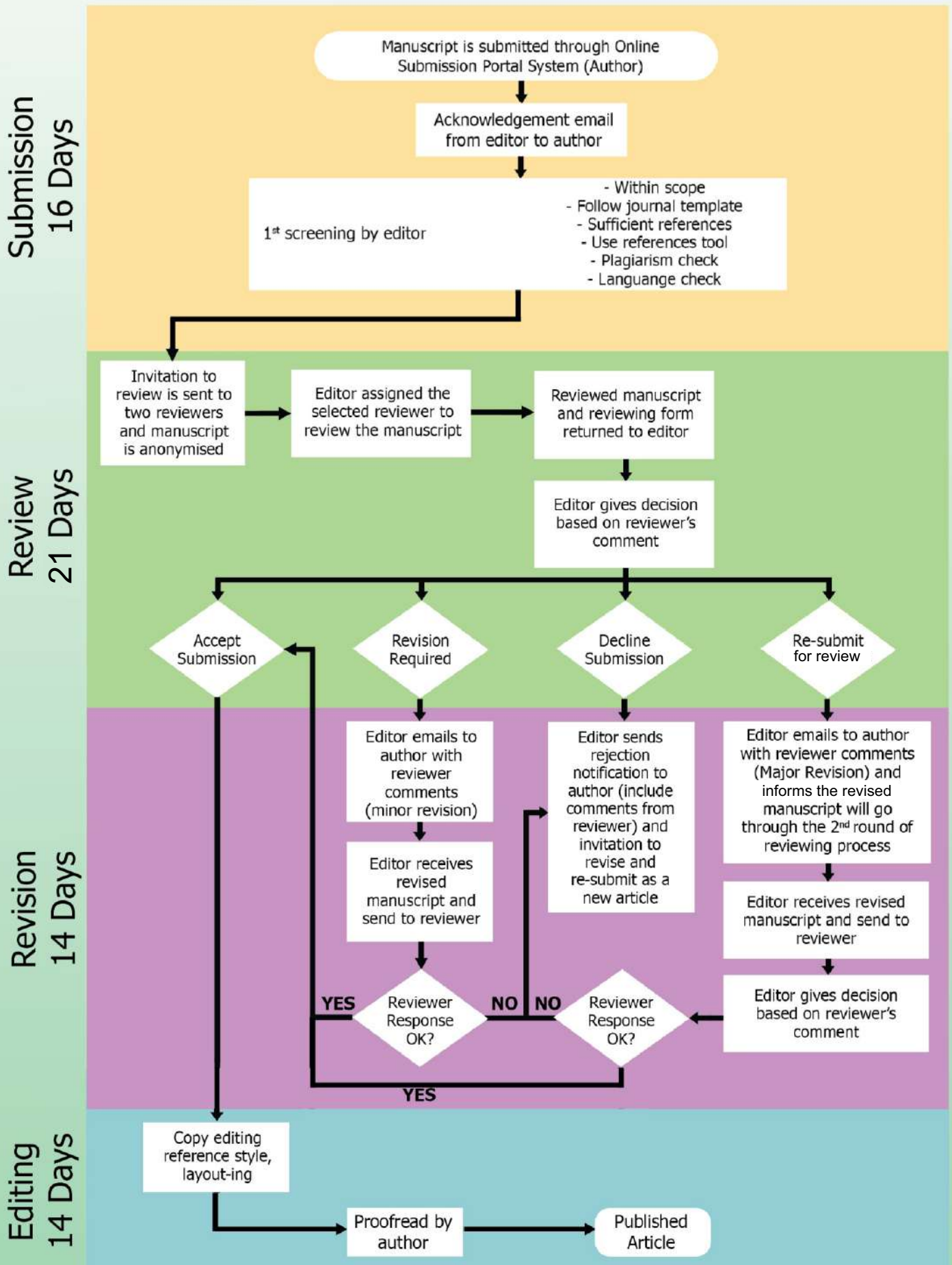
World Health Organization , 2020. *World Health Organization (WHO)*. [Online] Available at: <https://www.who.int/director-general/speeches/detail/who-director-general-s-opening-remarks-at-the-media-briefing-on-covid-19---11-march-2020> [Accessed 21 November 2020].

Yogyakarta Government Tourism Office, 2019. *DI Yogyakarta Tourism Statistics*. Yogyakarta: Yogyakarta Government Tourism Office.

Yunianto, P., 2020. *Webinar Keselamatan Pesepeda di Jalan*. Jakarta, Kementerian Perhubungan RI.

# FLOWCHART

## PUBLICATION PROCEDURE IN JCEF



In cooperation with:



## JOURNAL OF THE CIVIL ENGINEERING FORUM

Four Monthly Journal

Publisher Department of Civil and Environmental Engineering  
Faculty of Engineering Universitas Gadjah Mada  
Address Jl. Grafika No.2 Kampus UGM, Yogyakarta 55281  
Telephone +62274 - 545675  
Fax +62274 - 545676  
E-mail [jcef.ft@ugm.ac.id](mailto:jcef.ft@ugm.ac.id)  
Website <https://jurnal.ugm.ac.id/jcef>

ISSN 2089-5631



20895631050300919